TÉCNICO LISBOA

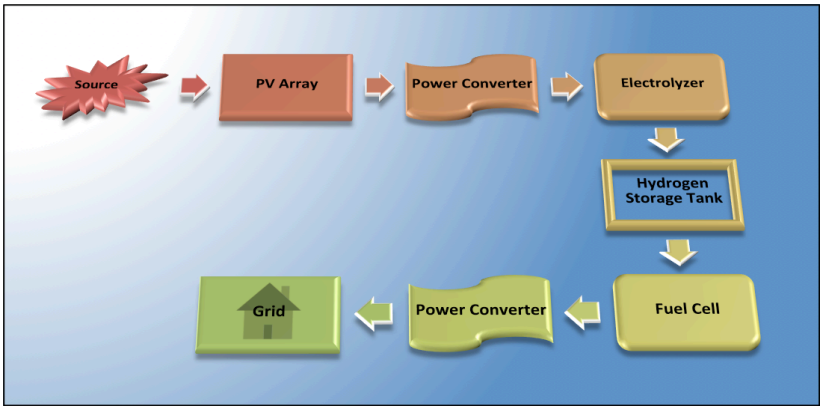


# Hydrogen Storage for Intermittent Power Sources
## Automation a Solar-Hydrogen Prototype Power Plant

**Pedro Maria de Bivar Black Henriques**

Thesis to obtain the Master of Science Degree in
**Physics Engineering**

**Examination Committee**

Chairman: Professor Luís Filipe Moreira Mendes
Supervisor: Professor Horácio João Matos Fernandes
Member of the Committee: Doutor Rui Pedro da Costa Neto

**October 2012**

# Abstract

The advent of a new Era of sustainable energy systems is upon us. The huge ecological footprint related to our energy consumption has long taken its toll on pollution and environmental changes. The reserves of conventional energy sources are running out and will soon not be able to satisfy the energy needs of an ever-growing global population. The urge to solve these grievous problems is the driving force behind intense research efforts that are being put into the alternative energy field. However, renewable energy sources are prone to availability fluctuations dependent on weather conditions. So, in order to find actual substitutes for fossil fuels, we still need to develop and mature solutions that can grant us stable and reliable renewable energy systems. A very promising solution is the buffering of harvested energy into electrical energy storage systems, so that it can later by used in a more controlled fashion – *Timeshifting*. The purpose of this work is to build a Prototype Photovoltaic Power Plant that stores energy in the form of Hydrogen (produced from electrolysis and reconverted by a Fuel Cell) and develop a control system that enables its automation, so that it can later be integrated in a remotely controlled laboratory.



**Keywords**: Renewables, Photovoltaic energy, Hydrogen fuel, Energy storage, Fuel Cell, Automation

# List of Figures

Figure 1.1 – (a) Evolution of energy consumption from 1970-2010 (b) evolution of fossil fuel consumption (c) distribution by source in 2010. The data used in these charts was provided by [1] .....2
Figure 1.2 – Solar Spectral Irradiance at sea level and at the top of the atmosphere [3].....4
Figure 1.3 – Yearly sum of global irradiation incident on optimally inclined photovoltaic modules [6] .....4
Figure 1.4– Evolution of energy supply by energy source in Portugal [7].....5
Figure 1.5 – Evolution of Photovoltaic Installed Capacity in Portugal, since 2003 [9] .....6
Figure 1.6 – Load Profiles for (a) a winter day, 21.01.11 (b) a summer day, 28.07.11 [8].....7
Figure 1.7 – Power delivered on 02.10.12 by (a) Wind, (b) Photovoltaic and (c) Hydro Plants [www.ren.pt] .....8
Figure 1.8 – Operational Results of constant output control in Futamata Wind Power Plant [11] .....9
Figure 1.9 – Schematic of the prototype Photovoltaic Power Plant .....10
Figure 2.1 – Review of various methods used to produce Hydrogen .....14
Figure 2.2 – Hydrogen phase diagram. Notice that liquid phase only exists between 13.84K–33.20K (triple and critical point) .....16
Figure 2.3 – Schematic of individual Fuel Cell .....17
Figure 2.4 – The first Fuel Cell: Grove's 1842 "gas battery" chain that used energy produced from recombination of and to perform electrolysis .....18
Figure 2.5 – Operation of a (a) PEM Electrolyser and a (b) PEM Fuel Cell [14] .....20
Figure 2.6 – Polarization curve of a low temperature Fuel Cell .....22
Figure 2.7 – I-V curves of the electrolyzer (a) theoretical (b) experimental results [14] .....25
Figure 2.8 – Effect of (a) membrane thickness and (b) operating temperature on PEM Electrolyzer Efficiency [15]26
Figure 3.1 – Band structure of (a) an isolator (b) a semiconductor and (c) a metal .....28
Figure 3.2 – The PN junction at equilibrium .....28
Figure 3.3 – Closed circuit flow of electrons in an illuminated PN Junction. .....29
Figure 3.4 – I-V characteristics of an illuminated PN Junction .....30
Figure 3.5 – The effects of (a) Irradiance and (b) Temperature on I-V characteristics .....31
Figure 3.6 – DC efficiency vs. Irradiance .....32
Figure 3.7 – Spectral Responses of different PV Cell types .....32
Figure 4.1 – Block Diagram of a PV Power Plant that stores energy in the form of Hydrogen .....33
Figure 4.2 – Intensity spectrum and look angle of high brightness (a) Red – 629nm (b) Green – 525nm (c) Blue – 465nm LEDs .....34
Figure 4.3 – Linear Regulator. The transistor Q is in the linear region, thus acting as a variable resistor, controlled by gate-to-source voltage. .....36
Figure 4.4 – Comparison of efficiencies of Switch and Linear regulators as a function of output current for conditions $\mathrm{Vin} = 3.6\ \mathrm{V}$ and $\mathrm{Vout} = 1.5\ \mathrm{V}$. .....37
Figure 4.5 – (a) Buck Converter schematic (b) ON state (c) OFF state .....37
Figure 4.6 – Continuous Conduction Mode .....38

Figure 4.7 – Discontinuous Conduction Mode .....39
Figure 4.8 – Boundary between CCM and DCM .....40
Figure 4.9 – Current in the Inductor .....41
Figure 4.10 – Output voltage ripple in a step-down converter. Note that $iC = CdvCdt$.....42
Figure 4.11 – 2nd Order Low Pass Sallen-Key Filter .....43
Figure 4.12 – (a) Butterworth step response (b) Bessel step response .....45
Figure 4.13 – Design and dimensioning of the Power Conversion Unit .....46
Figure 4.14 – NE555 oscillator its Astable mode of operation and its typical output .....48
Figure 4.15 – Cylindrical Capacitor.....49
Figure 5.1 – *SolidWorks 2012* 3D representation of the prototype.....51
Figure 5.2 – *SolidWorks 2012* design of the acrylic casing for the electrolyzer membrane.....52
Figure 5.3 – *OrCAD Capture* schematics of the Power Converter Module .....53
Figure 5.4 – *PSpice* simulation result. The blue line is the current in the inductor and the yellow line is the current in the load.....54
Figure 5.5 – *PSpice* simulation result. Red is the input voltage, green is the load voltage and yellow is the voltage in the Sallen-Key Filter .....54
Figure 6.1 – I-V Characteristics of the Solar Cell.....57
Figure 6.2 – Total Power output of the PV array as a function of load resistance .....57

# List of Tables

Table 1.1 – Heat of Combustion for some common fuels [2].....3

Table 1.2 – Portuguese Generation Equipment (a) in December 2004 and December 2005 (b) in December 2011 and August 2012 [8] .....6

Table 2.1 – Comparison of Fuel Cell technologies.....19

# Table of Contents

ABSTRACT ..... III
LIST OF FIGURES ..... V
LIST OF TABLES ..... VII
TABLE OF CONTENTS ..... IX

**1 INTRODUCTION ..... 1**
1.1 HYDROGEN ..... 2
1.2 SOLAR RADIATION ..... 3
1.3 THE PORTUGUESE ENERGY LANDSCAPE ..... 5
1.4 MOTIVATION ..... 9
1.5 DISSERTATION STRUCTURE ..... 11

**2 HYDROGEN TECHNOLOGIES ..... 13**
2.1 HYDROGEN PRODUCTION ..... 13
2.2 HYDROGEN STORAGE ..... 14
2.3 HYDROGEN AS FUEL ..... 16
2.3.1 Origin of the Fuel Cell ..... 17
2.3.2 Fuel Cell Technologies ..... 18
2.3.3 The PEM Fuel Cell ..... 19
2.3.4 The PEM Electrolyzer ..... 25

**3 PHOTOVOLTAIC TECHNOLOGIES ..... 27**
3.1 CELL STRUCTURE ..... 27
3.1.1 Semiconductors ..... 27
3.1.2 PN Junction ..... 28
3.1.3 Illuminated PN Junction ..... 29
3.2 I-V CHARACTERISTICS ..... 29
3.2.2 Irradiance Temperature effects ..... 31
3.2.3 Cell Efficiency ..... 31
3.2.4 Spectral Response ..... 32

**4 SCALED POWER PLANT DESIGN ..... 33**
4.1 LIGHT SOURCE ..... 33
4.2 PV ARRAY ..... 34
4.3 POWER CONVERTER ..... 35
4.3.1 Continuous Conduction Mode (CCM) ..... 38
4.3.2 Discontinuous Conduction Mode (CCM) ..... 39
4.3.3 Mode boundary ..... 40
4.3.4 Inductance and Capacitance ..... 41
4.3.5 Current and Voltage Measurement ..... 43
4.3.6 Power Converter Dimensioning ..... 46
4.3.7 Control Algorithm ..... 47
4.4 HYDROGEN STORAGE ..... 47
4.5 GRID ..... 50

**5 ENGINEERING DEVELOPMENT TOOLS ..... 51**
5.1 3D MECHANICAL MODELLING ..... 51
5.2 SOFTWARE DEVELOPMENT ..... 52
5.3 CIRCUIT TESTING ..... 53
5.4 PCB DESIGN ..... 55

**6 RESULTS AND DISCUSSION ..... 57**
6.1 CALIBRATIONS ..... 59
6.2 MEASUREMENTS ..... 61

**7 CONCLUSIONS ..... 65**

BIBLIOGRAPHY ..... 67
APPENDIX A – THE PROGRAM FOR THE MICROCONTROLLER ..... 69
APPENDIX B – PCB LAYOUTS ..... 77

# 1 INTRODUCTION

"*I will get right to the point*", declared Nobel laureate Richard Smalley, speaking before the American Congress. "*Energy is the single most important problem facing humanity today. We must find an alternative to oil. We need to somehow provide clean, abundant, low-cost energy to six billion that live on the planet today and 10-plus billion that are expected by the middle of the century.*"

Richard Smalley's bluntness before congress reflects the urgency of the matter he was dealing with. In these simple few words one of the biggest problems humanity is facing in the turn of this new century was exposed: we need a new "*clean, abundant, low-cost*" energy source.

While many of us may argue whether the current alternatives to fossil fuels – oil, coal and natural gas – have yet reached maturity regarding production, storage and distribution; none of us questions that without viable alternatives, our increasing energy demands will not be met, as fossil fuels are limited and will reach their production peak. As Smalley shrewdly acknowledged "*We must find an alternative to oil"*. If these weren't good enough reasons to abandon fossil fuels, we can't forget that their combustion has a devastating impact on environment since it emits carbon dioxide (CO2) and other air contaminants like nitrogen oxides, sulphur dioxide and volatile organic compounds. These gases play a major role in the greenhouse effect, contribute to global warming and generate acid rains and smog.

Earth's biosphere, in which living beings have their sustenance, has a perfectly balanced composition to ensure healthy life to all of them. Pollution is the introduction of contaminants with which we generate disorder, instability and harm to many ecosystems and living species, such as our own. We come to an inevitable conclusion: without renewable energies, our evolution is simply not sustainable.

a)

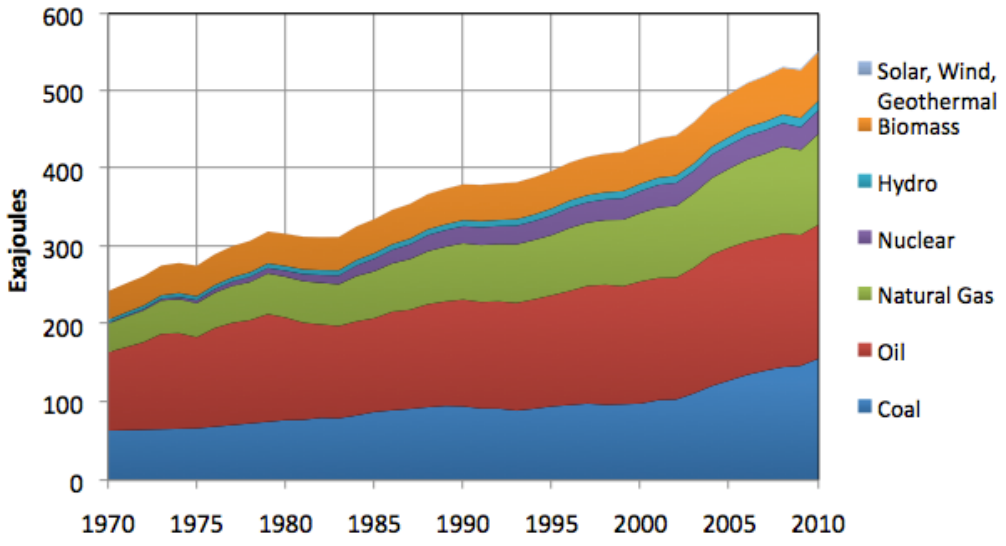

b) c)

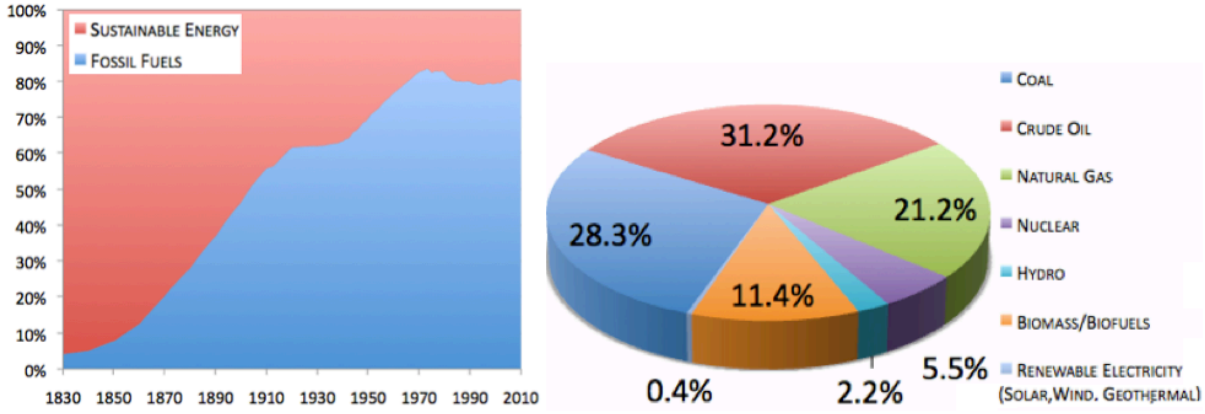


**Figure 1.1 – (a) Evolution of energy consumption from 1970-2010 (b) evolution of fossil fuel consumption (c) distribution by source in 2010. The data used in these charts was provided by [1]**

The statistical data used to create these charts was taken from the on-line periodical *The Oil Drum*, published by the non-profit corporation *Institute for the Study of Energy and Our Future* (ISEOF). Figure 1.1a) shows an almost exponential growth in energy demand, caused mainly by population growth in the last forty years. As we can see from figure 1.1c), fossil fuels still represent 80.7% of our overall energy consumption. Finally in picture 1.1b) one can take notice that fossil fuel consumption has had two exponential growth periods. The first one starts with the industrial revolution and corresponds to coal exploitation, and the second to the beginning of oil production in the turn the nineteenth century. Concerns linked to the oil crisis of the nineteen seventies, led to initial investments on research and development of new sustainable energy technologies, in order to try and reduce our dependence on non-sustainable forms of energy. Ever since, the continuing appeal of renewables is also related to their environmental benefits. This state of global awareness is represented by the lowered plateau in the last thirty years of the graph 1.1b).

This work will focus on two particular renewable sources of energy – Hydrogen and Solar Radiation.

## 1.1 Hydrogen

Hydrogen is the lightest element and by far the most abundant in the Universe, constituting roughly 75% of its elemental mass (not counting dark matter). As shown in table 1.1, it is also the most energetic molecule, having higher heat of combustion than gasoline, diesel, coal and natural gas. These characteristics make Hydrogen a suitable candidate for substituting fossil fuels.

One important distinction is that, unlike Coal, Oil and Gas, Hydrogen is not a primary source of energy, meaning it does not exist in a natural state in Nature. It is always mixed with other elements. So to use it, one has to produce it first. Hydrogen is thusly characterised as an *Energy Vector*, because it is an energy carrier. It can be produced in many different ways, using a wide range of technologies, which we will study in more detail in the subsequent chapters. Some of these involve established industrial processes while others are still at the laboratory stage.

**Table 1.1 – Heat of Combustion for some common fuels [2]**

| Fuel | kJ/g |
|---|---|
| Hydrogen | 141.9 |
| Gasoline | 47.0 |
| Diesel | 45.0 |
| Ethanol | 29.7 |
| Propane | 49.9 |
| Butane | 49.2 |
| Wood | 15.0 |
| Coal (Lignite) | 15.0 |
| Coal (Anthracite) | 27.0 |
| Natural Gas | 54.0 |

Developing safe, reliable, compact and cost-effective hydrogen storage technologies is one of the most technically challenging barriers to the widespread use of hydrogen as a form of energy. As evidenced by table 1.1, hydrogen has a very high energy content per mass (about three times more than gasoline), but on the down side, its energy density per volume, even in the liquid state, is very low, thus posing a challenge to its compact storage.

Hydrogen storage is common practice in industry, where it works safely and provides the service required. Also, hydrogen can easily be stored at large scale in vessels or in underground caverns. The problem is that across all industries, from automobiles to computers, modern products tend to have very demanding size and weight constraints, so for these applications, a breakthrough in on hydrogen storage technology is still required.

Significant research and development is under way, with new systems in demonstration. Different new approaches are now being tested. Some of them will be discussed en the following chapter.

## 1.2 Solar Radiation

The electromagnetic radiation from the Sun incident in the earth's surface is its most important source of energy. This radiation has its origin in the thermonuclear fusion reactions that are constantly taking place inside the nucleus, transforming hydrogen atoms into helium atoms. But the radiation that leaves the sun is not the same that reaches the surface of the earth. For most part of the way it travels through vacuum, suffering no losses. But roughly for the last one hundred kilometres, it travels through the atmosphere being subjected to such phenomena as reflection, dispersion (by dust particles and pollution) and absorption (by ozone, steam, oxygen, carbon dioxide). This effect is clearly depicted in the difference between the yellow and red spectra in figure 1.2. Notice that the spectral distribution of irradiance at the top of the atmosphere shows close resemblances to one emitted by a black body with the dimension of the sum at a temperature of 6000K. The maximum spectral irradiance takes place in the visible spectrum at 474nm, which corresponds to Blue.

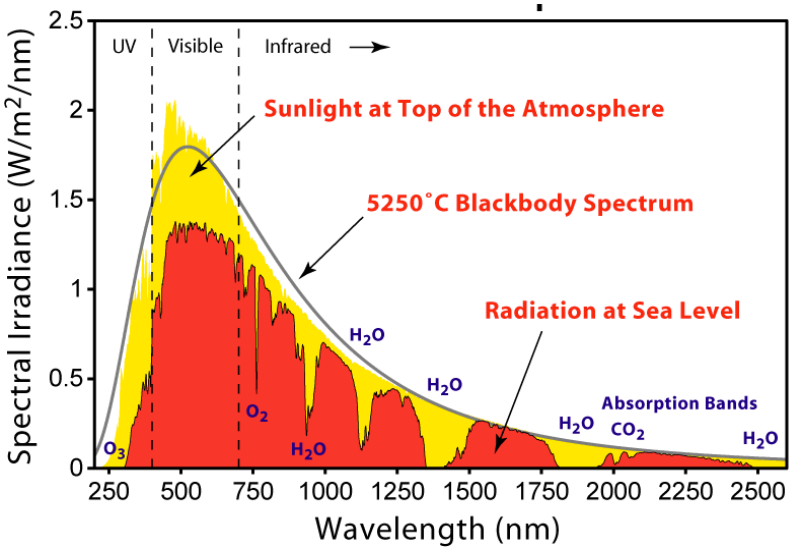


**Figure 1.2 – Solar Spectral Irradiance at sea level and at the top of the atmosphere [3]**

Although the value for the total irradiance (the integral of the spectra in figure 1.2) at the top of the atmosphere is a constant – called the *solar constant*, equal to 1366 $Wm^{-2}$; its value at sea level depends on the weather conditions and on the latitude (radiation reaching the equator has shorter optical trajectory inside the atmosphere comparing to radiation reaching the north pole). These values vary from roughly 1000 $kWh.m^{-2}$on the poles to 2500 $kWh.m^{-2}$ near the equator.

As demonstrated by figure 1.3, Portugal is a country with great solar irradiance, when comparing to other European countries. For instance, Germany is one of the world's leading countries in PV installed power (about 28,000MW), and has much smaller values of irradiation than Portugal (figure 1.3). We come to the conclusion that Portugal has great potential to explore PV energy solutions. On the next section we study the current state of Portuguese energy system in order to gain a wider insight on what are the investment tendencies and opportunities.

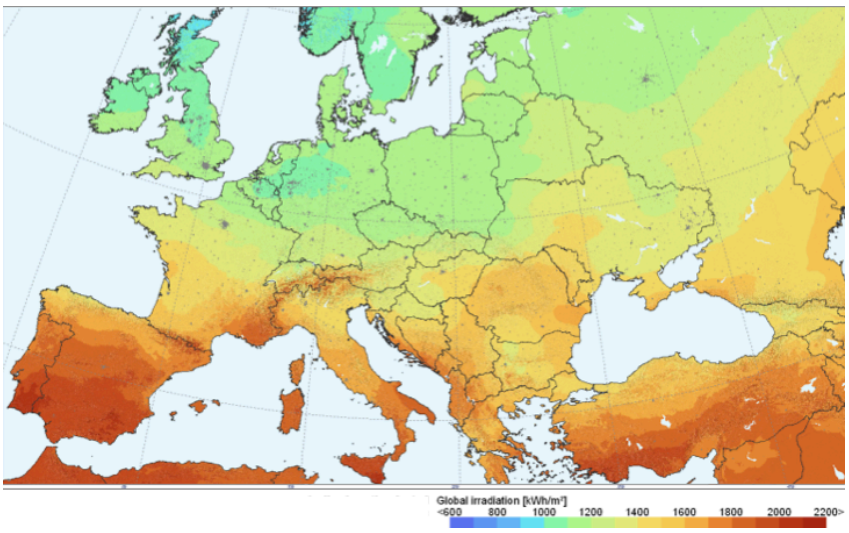


**Figure 1.3 – Yearly sum of global irradiation incident on optimally inclined photovoltaic modules [6]**

## 1.3 The Portuguese Energy Landscape

According to the data presented by REN (Rede Eléctrica Nacional), the annual electrical energy consumption in Portugal in 2011 was 50,5 TWh. This was 3.2% less than the previous year (or 2.3% with the correction for the effect of temperature and working days), which is the largest annual decline ever to occur in the country. This decline (shown in figure 1.4) was motivated by an increase of the tax for electricity fro 13% to 23%.

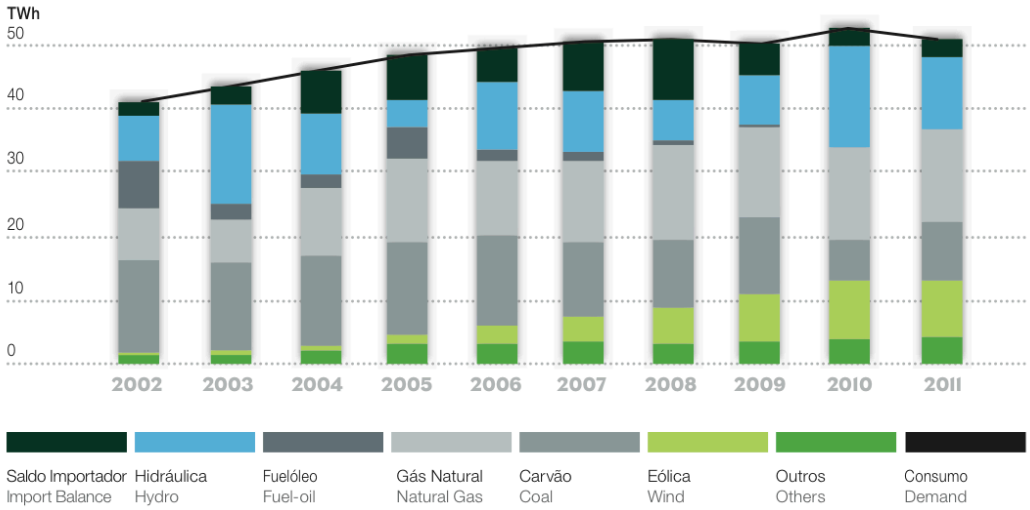


**Figure 1.4– Evolution of energy supply by energy source in Portugal [7]**

Electrical energy in Portugal has essentially thermal origin, produced from the burning of fossil fuels – Oil, Coal, Natural Gas (54% of energy production in 2011) and Hydro origin, produced from the potential energy stored in Lagoons and Rivers (22% of energy production in 2011).

We can see that Hydro and Wind (18% of energy production in 2011) are responsible for most of the renewable energy production in Portugal. The problem with the generation of hydroelectricity is that it is dependent on the big annual variation of rainfall. This instability is represented in figure 1.4 by the large oscillations of the blue bar. Furthermore, Portugal has invested largely in Wind Farms scattered all over the country in the last few years, passing from an Installed Capacity (maximum power that can be delivered) of 474 MW in 2004 to more than 4,100 MW in 2012. This is represented by the steady growth of the light green bar in figure 1.4.

A new Portuguese market liberalization policy has divided electricity production in two different regimes:

- **Ordinary Status Generation** (OSG) – traditional non-renewable thermal sources and big hydroelectric complexes. Essentially performed by three major companies – EDP, Turbogas, Tejo Energia.
- **Special Status Generation** (SSG) – endogenous and renewable sources.

This policy's primary objective is to promote and facilitate energy production. To abandon paradigm of centralized production by big plants, and promote private initiative, heading towards a liberalized market. This has had a major impact on the Portuguese energy market: Since 2004 the total Installed Capacity of SSG producers has changed from 1,854 MW to 6,549 MW in August 2012 – 253.2% growth; while for OSG the change was merely

from 9,893MW to 11,682MW – 18.1% growth. All the values related to Installed Capacity were taken from table 1.2 (a) and 1.2 (b).

**Table 1.2 – Portuguese Generation Equipment (a) in December 2004 and December 2005 (b) in December 2011 and August 2012 [8]**

| MW | Dez 2005 | Dez 2004 | Var. |
|---|---|---|---|
| POTÊNCIA INSTALADA SEP / SENV | 10 434 | 9 893 | 541 |
| Centrais Hidroeléctricas | 4 582 | 4 386 | 196 |
| Albufeiras | 2 403 | 2 207 | 196 |
| Fios de Água | 2 179 | 2 179 | 0 |
| Centrais Térmoeléctricas | 5 852 | 5 507 | 345 |
| Carvão | 1 776 | 1 776 | 0 |
| Fuel | 1 476 | 1 523 | -47 |
| Fuel / Gás natural | 236 | 236 | 0 |
| Gasóleo | 197 | 197 | 0 |
| Gás natural | 2 166 | 1 774 | 392 |
| POTÊNCIA INSTALADA P. R. E. | 2 360 | 1 854 | 506 |
| Produtores Térmicos | 1 142 | 1 049 | 93 |
| Produtores Hidráulicos | 340 | 331 | 9 |
| Produtores Eólicos | 877 | 474 | 404 |

| [MW] | ago 2012 | dez 2011 | Var. |
|---|---|---|---|
| POTÊNCIA INSTALADA | 18 230 | 18 897 | -667 |
| Centrais Hidroelétricas P. R. O. | 4 985 | 4 980 | 5 |
| Albufeiras | 2 397 | 2 397 | 0 |
| Fios de Água | 2 588 | 2 583 | 5 |
| Centrais Termoelétricas P. R. O. | 6 697 | 7 407 | -710 |
| Gás Natural CC | 3 829 | 3 829 | 0 |
| Carvão | 1 756 | 1 756 | 0 |
| Fuelóleo | 946 | 1 657 | -710 |
| Gasóleo | 165 | 165 | 0 |
| P. R. E. (1) | 6 549 | 6 510 | 38 |
| Produtores Térmicos | 1 846 | 1 863 | -17 |
| Produtores Hidráulicos | 415 | 412 | 3 |
| Produtores Eólicos | 4 109 | 4 081 | 28 |
| Produtores Fotovoltaicos | 179 | 155 | 24 |

After the strong investment in Wind Farms, in the last few years, Photovoltaic plants have also attracted much interest, having been elected by the Portuguese government [10] as the technology with biggest potential of development in the next decade in Portugal. In January 2007 the county's first photovoltaic plant started operations with only 8MW. Since then many more have been created, and we table 1.2 (b) shows that as of August 2012 there were 179MW of Photovoltaic produced electricity connected to the national grid. The government's National Strategy for Energy [10] has announced the goal of reaching 1500MW until 2020, almost ten times the current value. The evolution of PV installed capacity in Portugal is depicted in figure 1.5

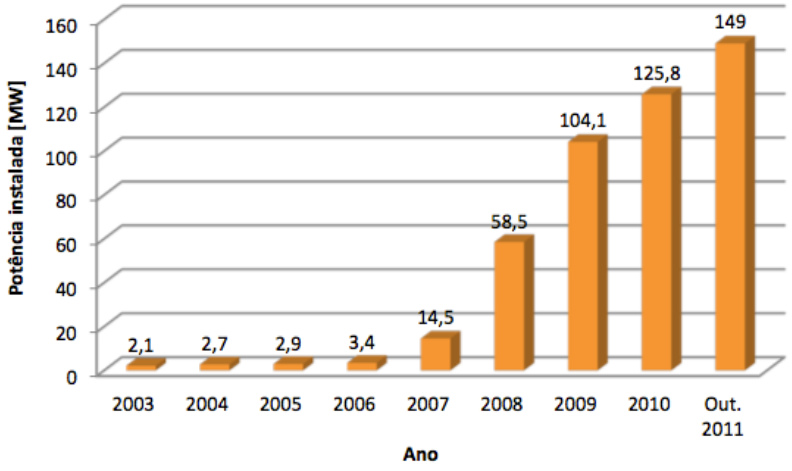


**Figure 1.5 – Evolution of Photovoltaic Installed Capacity in Portugal, since 2003 [9]**

One of the most significant contributions to the Installed Capacity of photovoltaic producers was the construction of the Amareleja Power Station in 2008, which was, at the time, the world's biggest of its kind at 46MW.

The power requested from the grid by the equipment used by the various consumers (domestic, industrial, etc.) changes over the different times of the day, month or year, depending on climatic conditions (wind, rain, irradiance, etc.), on the activities preformed. This is measured in Load Profiles.

Managing the grid's Generating Equipment to meet the energy demands imposed by these Load Profiles is a permanent challenge faced by the entity responsible for the system. To do this, one has to take in to account the characteristics of the Power Plants available, such as dispatchability (the ability to change output quickly on demand), variability (the extent to which the Plant may exhibit undesired or uncontrolled changes in output), pollution, electricity cost. For instance, the activity of Fuel Oil Plants is avoided unless strictly necessary because Oil is highly pollutant and very expensive. Coal is the cheapest form of producing electricity, but its Power Plants are non-dispatchable. This makes Coal Power Plants suitable for assuring base production – demand during the off-peak, or night-time, that is constant all through the day. Other non-dispatchable forms of energy are used for base production such as Wind and Photovoltaic, but the fact that they have some variability (depend on wind and irradiance conditions respectively) makes their output almost unpredictable, which raises some difficulties in matching demand. Dispatchable sources like Hydro can be turned on and off quickly, so they are used in times of high demand – peaks. Natural Gas Plants are both dispatchable and non-variable, so they can be used to meet base production or peaks, depending on the needs. For instance, Hydro has great variability as was already discussed above, so in rainy months, Hydro Plants can operate continuously, thus contributing to base production. In this case, peaks are met by Natural Gas [8]. This situation is illustrated in figure 1.6 (a)

Figure 1.6 shows two Load Profiles: one of the annual peak on the 21st January 2011 – a winter day; the other of the 28th of July.

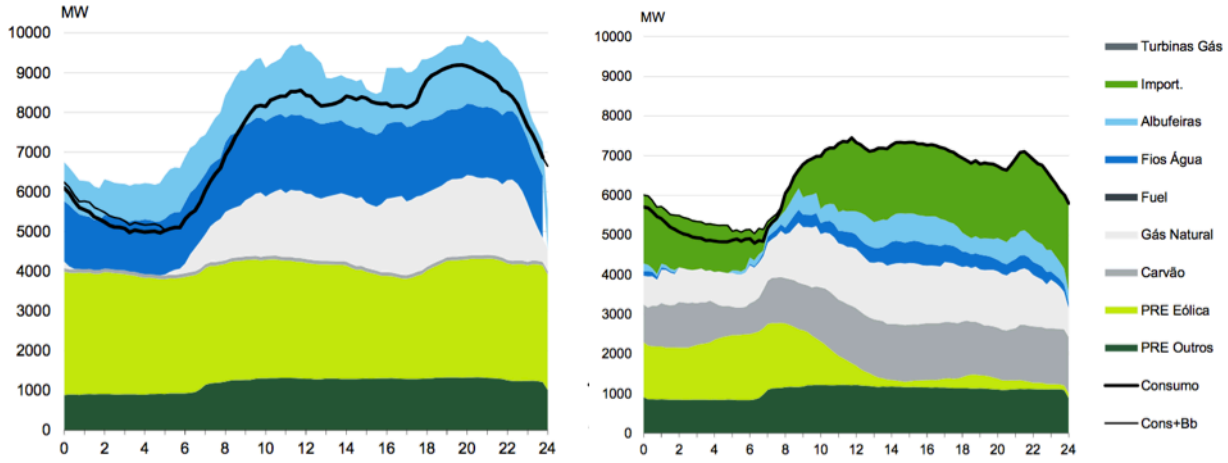


**Figure 1.6 – Load Profiles for (a) a winter day, 21.01.11 (b) a summer day, 28.07.11 [8]**

A close analysis reveals that off-peak period is between 0:00-7:00 in both cases, but the maximum peak in the winter is around 19:00–20:00 while in the summer is around 11:00–12:00. These values are related to the energy expenses related to heating and cooling respectively.

The 21st of January was had exceptional weather conditions, as evidenced by figure 1.6 (a). This profile shows a great contribution of Wind and other sources in Special Status Generation, and a continuous activity in hydroelectricity production sites. This is the situation discussed above, were the peak is met by Natural Gas Power Plants. There was an excess of production so exportation balance was positive that day. Almost all energy was produced by renewable sources and the only fossil fuel used was the less pollutant one. An almost ideal scenario.

On the 28th of July, things were not that easy. In the summer there is typically worst wind conditions, and this is depicted in figure 1.6 (b). There was some Wind in off-peak period but it dwindled in the afternoon. This is where hydro came to the rescue. But rain is also scarce in the summer so the lagoons where not very full nor did the rivers have sufficient discharge to meet peak demand, even with Natural Gas and Coal Plants working to satisfy base demand. With Fuel Oil being less and less a viable option for generating electricity because of its price and pollution, as the countries Generating Equipment was not able to satisfy the Energy demand, the only solution was to import energy. All through the day importation values where high.

This is the typical situation in the summer, and has become worse, as energy expenses related to cooling in this period tend to rise every year. The need for a Renewable Energy source that is more abundant in the summer (as opposed to Water) and available at peak hours (as opposed to Wind – figure 1.7(a)) becomes obvious. The simplest answer is the radiance of the Sun.

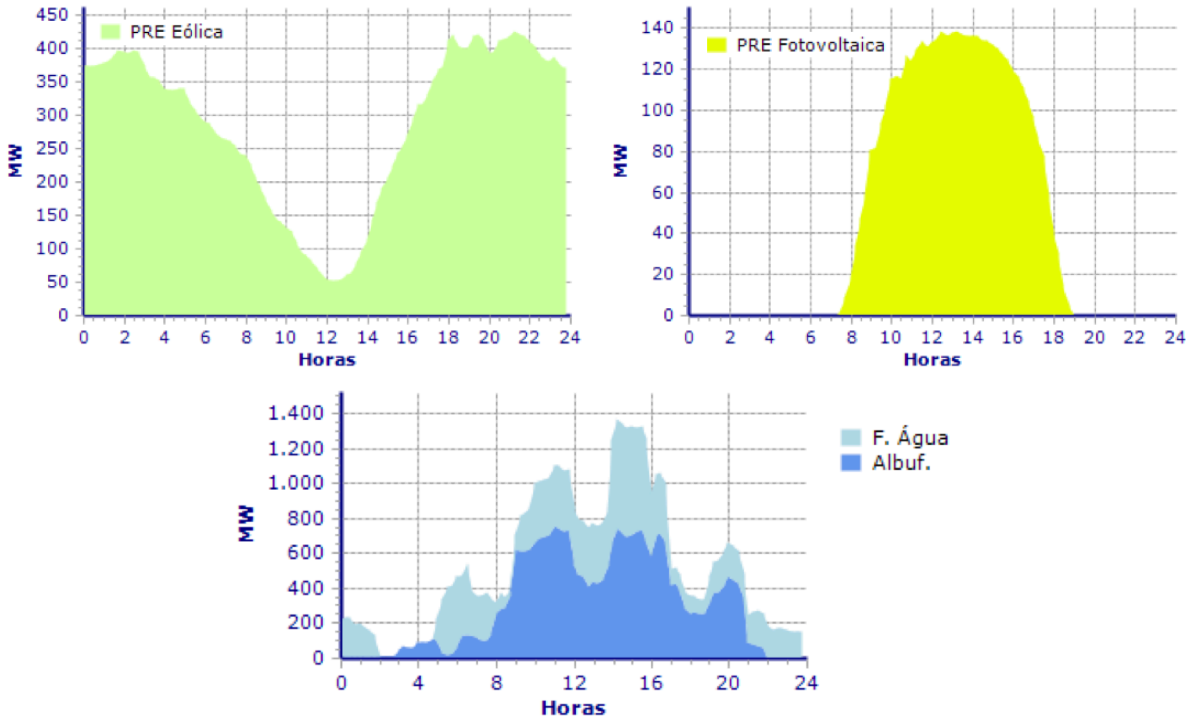


**Figure 1.7 – Power delivered on 02.10.12 by (a) Wind, (b) Photovoltaic and (c) Hydro Plants [www.ren.pt]**

If the national energy strategy is followed, then in ten years time, Photovoltaic installed power will has increased to ten times its current value (as was discussed above). That means that, based on figure 1.7 (b), on a summer day, PV Plants will be able to deliver almost 1400MW of power to the grid during peak hours. Well, this is a value in the order of the power delivered by Hydro Pants (figure 1.7 (c)). This means that by investing in PV, Hydro Plants would be able to slow production in the summer, which would reflect in a rise of lagoon water levels always so low in this time of year.

## 1.4 Motivation

Even in countries with so much solar irradiance as Portugal, there are some technical limitations to the widespread of Photovoltaic technologies. The fact is that renewable sources are intermittent – their availability is subjected to weather fluctuations. **If we want to produce Renewable Energy in large-scale, a solution will have to be developed in order to minimize the effect of production fluctuations**. A simple, but not at all ideal solution, would be make hybrid Plants, where fossil fuels would be burned in the times of day with less irradiance, to smoothen the variations. Another would be to improve prediction of production in order to plan ahead. But the most studied and promising solution, thus the one I will be focusing on in this work, is **Energy Storage** or ***Buffering***: **By storing the generated energy that is not immediately consumed, typically during times of lower demand, one can use it latter to fill the voids created by the fluctuation of renewable sources, thus smoothing production variations and increasing the reliability of these Power Plants – this is called *Timeshifting*.**

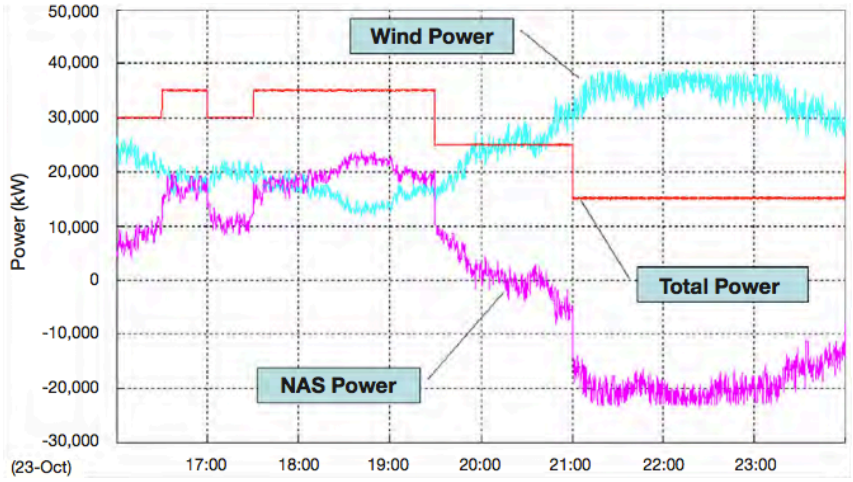


**Figure 1.8 – Operational Results of constant output control in Futamata Wind Power Plant [11]**

In June 2008 Futamata Wind Power Plant started operation in Japan. This generation facility is equipped batteries. It consists of 51MW of wind turbines and 34MW of NaS Batteries. By using the battery, the total power output of the facility is smoothed and the peak output is controlled to always stay bellow 40MW. Figure 1.8 shows the results of this control.

The most relevant electric energy storage systems are divided in three types. Mechanical (pumped hydro and compressed air), Electrochemical (batteries) and Chemical (hydrogen). Today, pumped hydro storage (PHS) plants represent nearly 99% of worldwide electrical storage installed capacity, which is about 3% of global generation

capacity [11]. The roundtrip efficiency of these plants is in the range of 70%-80%, and it has a long lifetime and practically unlimited cycle stability. The main drawbacks of this storage method are the dependence on topological conditions, large footprint area, very low energy density and water losses due to evaporation. Batteries have good roundtrip efficiencies (65%-75%), but they can't store for long periods of time (optimized for 6-8h), have lower cycle lifetimes. They may be viable solutions in specific low power applications (like Futamata Wind Power Plant in Japan), but their characteristics render them impractical for utility-scaled applications. Hydrogen roundtrip efficiencies range from 35%-50%, which is very low, but on the other hand has the very high energy density, which allows for massive amounts of energy stored.

The National Renewable Energy Laboratory has developed a study on lifecycle cost of Hydrogen versus other technologies for Electrical Energy Storage [12]. The study concluded that Hydrogen for energy storage is potentially cost competitive with battery systems and could be competitive with compressed air systems and pumped hydro in locations that are not favorable for these technologies.

Hydrogen Storage has gained interest in the last few years is now the focus of intensive researches aiming to assess the viability of this technology to substitute the established ones. Also, for reasons mentioned above, PV power plants are an important solution to explore in upcoming years. Having both these trends in the field of Renewable Energy in mind, my work will consist of the construction and automation of a prototype Photovoltaic Power Plant shown in figure 1.9 in schematic form.

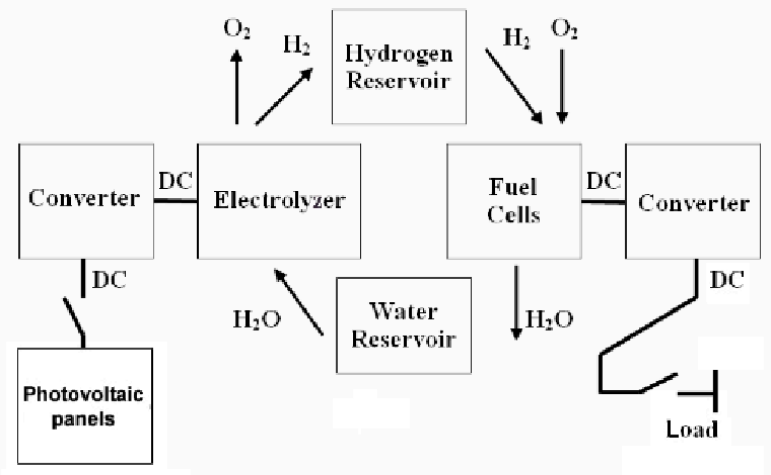


**Figure 1.9 – Schematic of the prototype Photovoltaic Power Plant [13]**

The viability of a solar-hydrogen power system has been tested in experimental works such as the one by Shapiro et al. [18] who built a prototype stand-alone power system with a PEM fuel cell and electrolyzer, high-pressure hydrogen tank and PV panel. The aim was to test stand-alone power system performance, viability of hydrogen as seasonal energy storage and to investigate the experimental electrolyzer and its performance when combined with a PV panel. The overall performance was found to be promising: "*This system could be grid-coupled to supply premium power needs for high-reliability, high-quality backup power, or integrated with a photovoltaic array to serve remote locations*."

The plant consists of a Photovoltaic Cell, connected to an Electrolyser (to convert electrical energy to hydrogen) by means of a DC-to-DC converter, a hydrogen and water reservoir, and a fuel cell (to reconvert

hydrogen to electricity) connected to a final load by means of another DC-to-DC converter. The plant will be delivering the energy to a variable load, which will be mimicking the grid's variable demand. The goal is to produce photovoltaic energy and demonstrate the simplicity of the concept behind hydrogen storage, studying the efficiencies of these processes.

The prototype will be automated so that it can integrate the e-Lab – a remotely controlled laboratory located in the campus of IST (Instituto Superior Técnico) composed of various automated experiences showing different concepts in the field of physics, offering the possibility for students to complement their theoretical knowledge with real time practical applications, by simply using their computers.

## 1.5 Dissertation Structure

There will be seven chapters in this dissertation. Chapter one introduces the main topics of discussion, and presents the motivations for the present work. Chapter 2 unravels the state of the art in Hydrogen industry, from production to storage and consumption. Chapter 3 explains the operation o PV Cells. Chapter 4 contains a detailed explanation of each component of the scaled power plant, and its design. Chapter 5 describes the software tools used in the design and construction of the automated prototype. Chapter 6 presents the experimental results. Chapter 7 announces the conclusions of the work and pointers for directions of future work. Finally, the references are presented under the title Bibliography. Appendix A has the C program for the microprocessor, and Appendix B the schematics of PCS layouts.

# 2 HYDROGEN TECHNOLOGIES

## 2.1 Hydrogen Production

Hydrogen can be produced from a variety of different methods. Each of them is in different stages of development, and each offers unique opportunities, benefits and challenges. The choice of a particular method depends on the application. There are three major forms through which hydrogen can be produced:

- **Thermochemically** – when hydrogen is produced from gas or liquid fuel, typically Oil or Natural Gas, the process is called *Reforming*. There are three reforming techniques:
    - Steam Reforming – Endothermic reaction that uses a mixture of fuel and water to produce hydrogen and carbon monoxide.

$$CH_4 + H_2O + heat \rightarrow CO + 3H_2 \qquad (2.1)$$

    - Partial Oxidation – Exothermic reaction that uses air, or oxygen in particular, to oxidize the fuel, generating hydrogen and carbon monoxide

$$CH_4 + \tfrac{1}{2}O_2 \rightarrow CO + 2H_2 + heat \qquad (2.2)$$

    - Autothermal Reforming – Consists of a combination of the other two, in order to achieve a reaction with neutral energy balance.

  Hydrogen can also be produced from Coal, called *Gasification*. It's a much more complex process so the cost is higher. The problem with all these processes is that they emit carbon monoxide, which is hazardous to PEM cells.

- **Electrochemically** – Through the process of electrolysis, water uses electric energy to produce pure hydrogen and oxygen without parasitic carbon emissions.

$$H_2O(l) + Electrical\ \ Energy \rightarrow H_2(g) + \frac{1}{2}O_2(g) + heat \qquad (2.3)$$

  This method is especially attractive when the source of electrical energy necessary for the process is renewable. This way the overall process is completely clean. As this is the goal of the present work, the choice of production method fell in this category as will be presented in the following sections. The problem with this method is the 65%-75% range of efficiencies, which compared to the thermochemical processes, is lower.

- **Biologically** – Recent research has presented new options for renewable method for production of Hydrogen. For example, he gasification, pyrolysis or fermentation processes can convert biomass (e.g. ethanol, wood) into biogas containing hydrogen. Another example is the use of Algae's Photosynthesis, which produces oxygen, electrons and, to catalyze hydrogen production with the help of the enzyme Hydrogenase

$$H_2O \rightarrow 2H^+ + 2e^- + \tfrac{1}{2}O_2 \quad \& \quad 2H^+ + 2e^- \rightarrow H_2 \qquad (2.4)$$

These biological methods are very attractive as a means to handle organic residuals. The main challenge they face is the slowness of the processes.

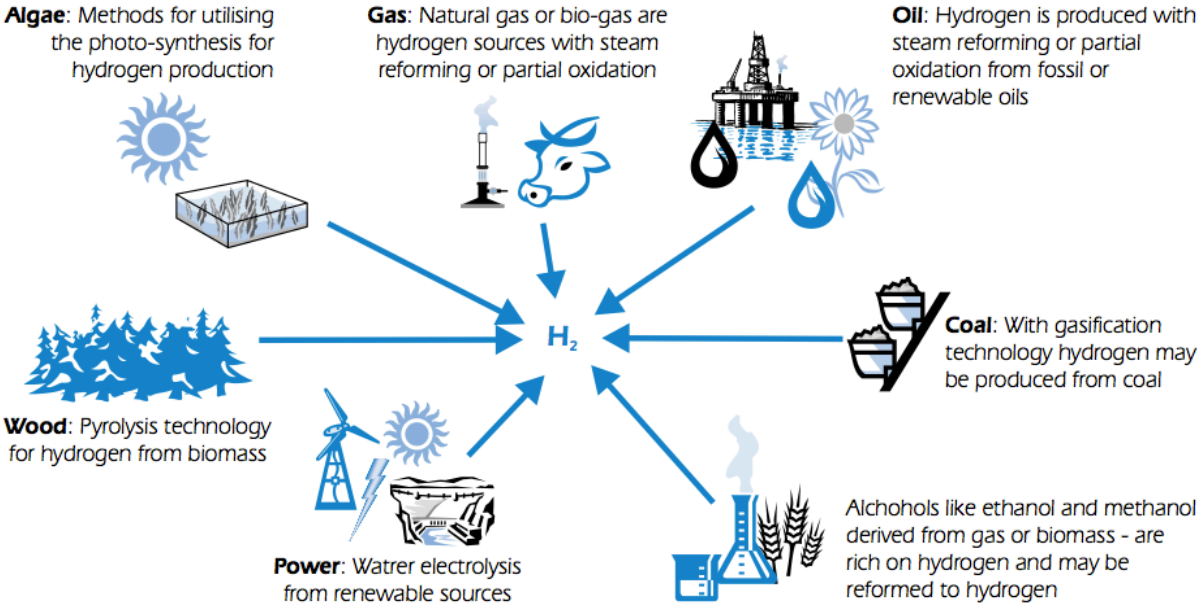


**Figure 2.1 – Review of various methods used to produce Hydrogen**

Several technologies are already available for the industrial production of hydrogen. The first commercial technology, dating from the late 1920s, was the electrolysis of water to produce pure hydrogen. In the 1960s, the industrial production of hydrogen headed slowly towards a fossil-based production, which is now the main source for hydrogen production. In this initial phase of the Hydrogen Economy pathway, in order to start building the market, it will be produced from the well-established energy systems based on electricity from fossil fuels. The long-term goal is to turn renewable energy sources the most important source for the production of hydrogen.

## 2.2 Hydrogen Storage

When Hydrogen is used in energy systems, it is intended to work as an energy vector, just like electricity. Today if we want electricity for mobile applications, in can be stored batteries, in a number of technologies. If Hydrogen is to become a realistic substitute (or complement) of electricity as an energy carrier, then some practical and feasible solutions for its storage have to be developed. As was presented in the first chapter, the storage of Hydrogen can be a daunting task, because of is low energy density per volume.

Let us take a more down-to-earth approach to this problem. A modern everyday car, with a range of 400 km, burns about 24 kg of petrol in a combustion engine. To cover the same range, 8 kg of hydrogen are needed for the combustion engine version or 4 kg hydrogen for an electric car with a fuel cell. Well, at room temperature and atmospheric pressure (1.013 bar), 4 kg of hydrogen occupy a volume of 45 $m^3$ or 45000 liters. This corresponds to a balloon of 5 m diameter — hardly a practical solution for a vehicle.

I will now present the most important solutions to the hydrogen storage problems, as was done in [19].

- **Compressed Gas** – The most obvious solution, hence the most matured one. The most common tanks of inexpensive steel are regularly filled up to 200 bar in most countries. At this pressure, storing our 4kg of hydrogen still requires 0.22 $m^3$(220 liters). The average fuel tank of compact cars is about 60-70 litres, to clearly still too much space for this application. That is why novel high-pressure tanks involving fiber-reinforced composite materials are being developed. These are tested up to 600 bar and filled up to 450 bar for regular use. But still, high-pressure vessels present a considerable risk and also the energy needed to compress the hydrogen, even for a relatively moderate pressure of 200 bar, its about 18% of its energy content.
- **Cryogenic Liquid** – In this method, hydrogen is stored in liquefied form. Liquid hydrogen has an over 800 times higher density than in its gaseous state. Therefore, liquefaction of hydrogen is particularly attractive from the point of view of improving the mass per volume ratio. However, the condensation temperature of hydrogen at atmospheric pressure is 19.33 K and the unavoidable heat transfer, even through a super-insulated container, leads directly to loss of hydrogen due to evaporation. These losses, estimated at roughly 1% per day after three days. Liquid Hydrogen storage units were developed and proven in space technology. Liquid hydrogen is a fuel in the launching process of the Space Shuttle.
- **Hydrides** – Another storage option is to chemically bond hydrogen in a solid material. Many metals and alloys are capable of reversibly absorbing large amounts of hydrogen. Molecular hydrogen is dissociated at the surface before absorption and recombine for desorption. Hydrogen is place in the form of atoms, never molecules, on interstitial sites of the host metal lattice. Metal-hydride systems can store more hydrogen than in liquid hydrogen in a safe and efficient way. However, those materials with good storage capabilities and reversibility only release hydrogen at relatively high temperatures, too high for fuel cell application. Also, the materials fitting these requirements are too heavy or too expensive for a commercial application. To overcome the disadvantages in conventional heavyweight metal hydrides, new materials using lighter elements have been investigated in the recent years.
- **Carbon Nanotubes** – There are also studies concentrating on storage in high surface area materials, such as carbon nanotubes. The absorption of a gas on a surface is a consequence of the filed force at the surface of the solid. The variation of attractive surface forces as a function of distance from the surface decides whether van der Waals-type absorption of hydrogen takes place. This method has shown great storage capabilities, however, it is still unpractical due to the limitation on mass production and utilization of carbon Nanotubes.

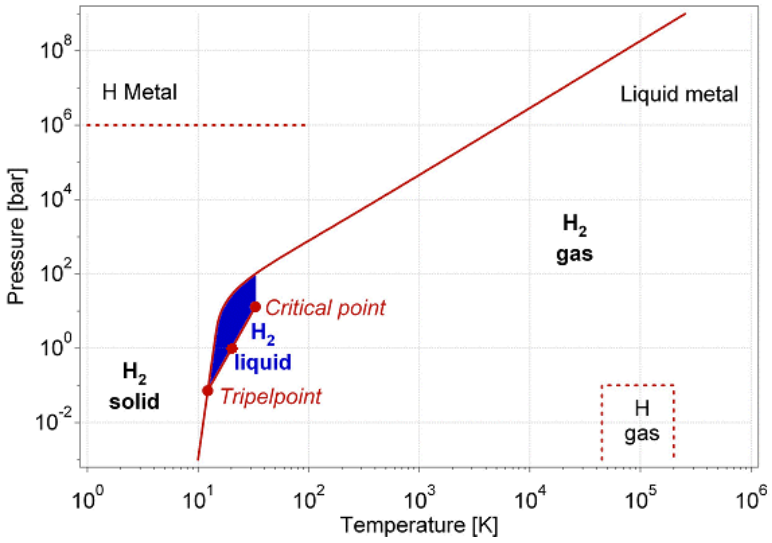


**Figure 2.2 – Hydrogen phase diagram. Notice that liquid phase only exists between 13.84K–33.20K (triple and critical point) [29]**

## 2.3 Hydrogen as Fuel

Hydrogen as fuel has been around for long. NASA has been using liquid hydrogen to propel space shuttles and other rockets into orbit since the 1970s. Hydrogen Internal Combustion Engines (H2ICE) have been patented in the 1970s, but only recently have any cars equipped with these engines became available to the market. However, there is a new and more efficient way to produce energy from hydrogen. It is called the Fuel Cell. Fuel cells convert fuel and air directly to electricity, heat and water in an electrochemical process.

At present, hydrogen and fuel cells do not offer sufficient short-term end-user benefits to justify their higher costs compared to conventional technologies. Therefore, the strategy should aim to identify pathways for increasing infrastructure and production volumes. In certain applications, such as portable power, emergency back-up power, and auxiliary power units, fuel cells may offer early customer benefits and attract premium prices. But moving from the fossil fuel economy to a new hydrogen and fuel cell-based economy will not happen overnight. While intensive research and development efforts are being put into making fuel cells a competitive technology, a strategy is required to maximize the benefits of transition technologies such as the above mentioned combustion engines.

As was discussed in the first chapter, the prototype Solar Power Plant stores energy in the form of hydrogen so it can perform energy Time Shift to better satisfy the needs of the grid. Hydrogen handled in the prototype will be produced from water through Electrolysis. It will be stored and then reconverted to electricity by a Fuel Cell.

A fuel cell is a device that converts directly the chemical energy stored in gaseous molecules of Fuel and Oxidant into electrical energy. The basic building block of a fuel cell consists of an electrolyte layer in contact with a porous anode and cathode on either side. A schematic representation of a fuel cell is shown in figure 2.3.

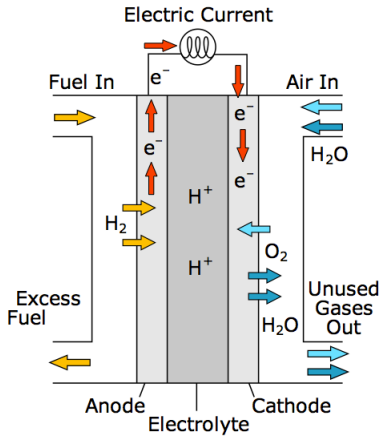


**Figure 2.3 – Schematic of individual Fuel Cell [30]**

In a typical fuel cell, gaseous fuels are fed continuously to the anode and an oxidant (oxygen from air) is fed continuously to the cathode; the electrochemical reactions take place at the electrodes to produce an electric current.

The operation of a Fuel Cell is very similar to that of an electrochemical battery, seeing that both promote a chemical reaction to create a potential difference in their electrodes. This generates a flux of electrons that perform electrical work. Their difference lies in the fact that in batteries the chemical energy is stored in the electrolyte and, once this energy is consumed, the battery has to be recharged. In Fuel Cells the energy comes from the fuel and Oxidant stored outside the unit. This gives Fuel Cells a much bigger storage capacity, only limited by external factors.

A fuel cell can be seen as a "chemical factory" that continuously transforms fuel energy into electricity as long as fuel is supplied. However, unlike internal combustion engines that can be regarded as factories as well, fuel cells rely on a chemical reaction involving the fuel, and not on its combustion.

During combustion the molecular bonds of the fuel are broken and electrons reconfigure so fast that they cannot be recovered to generate electricity directly. Their energy is then transformed into heat, which is transformed into mechanical energy and finally into electricity. These successive transformations impose strong limitations in the overall efficiency of the process. On the contrary, in a fuel cell, the electron transfer necessary to complete the bonding reconfiguration occurs over a much slower time base. This allows direct collection of electrons, which leads to overall efficiencies two or three times higher than in internal combustion engines (depending on the fuel cell technology).

The power produced by a fuel cell depends on cell type, size, temperature of operation, and pressure of supplied gases. A single fuel cell produces barely enough voltage for even the smallest applications. To increase the voltage, individual fuel cells are combined in series to form a stack.

### 2.3.1 Origin of the Fuel Cell

The history of Fuel Cell dates all the way back to the discovery of water Electrolysis in 1789. Adriaan Paets van Troostwijk (1752–1837), a merchant in Amsterdam, and his friend Johan Rudolph Deiman (1743–1808), a

medical doctor, used a friction based electrostatic machine to generate electricity and then discharged it into the electrodes of a Leyden jar (primitive for of capacitor) full of water. Based on their observations they shrewdly concluded that a 2:1 mixture of oxygen and hydrogen was produced.

Later, in 1838, William Robert Grove (1811 -1896), a Welsh lawyer turned scientist, won renown for his development of an improved battery. The "Grove cell," as it came to be called, used a platinum electrode immersed in nitric acid and a zinc electrode in zinc sulfate. Then, in 1939, Grove discovered that by arranging two platinum electrodes with one end of each immersed in a container of sulfuric acid and the other ends separately sealed in containers of oxygen and hydrogen, a constant current would flow between the electrodes. The sealed containers held water as well as the gases, and he noted that the water level rose in both tubes as the current flowed. He called this device the "gas battery". He soon realized that by combining several sets of these electrodes in a series circuit he might generate electricity. So, 1842 Grove connected a number of "gas batteries" together in series to form a "gas chain". He used the electricity produced from the "gas chain" to power an Electrolyzer, splitting water into hydrogen and oxygen – this was the first Fuel Cell. Figure 2.4 is taken from represents Gove's original 1842 paper, and represents the experiment.

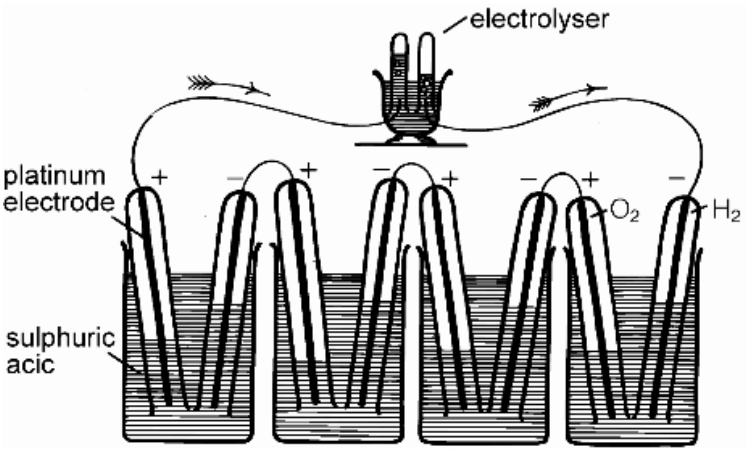


**Figure 2.4 – The first Fuel Cell: Grove's 1842 "gas battery" chain that used energy produced from recombination of $H_2$ and $O_2$ to perform electrolysis [31]**

## 2.3.2 Fuel Cell Technologies

There are many types of Fuel Cells, classified primarily by the type of electrolyte used, type of fuel, and operation temperature. The type of electrolyte determines the kind of chemical reactions that will take place inside the Cell. The most important Fuel Cell technologies are briefly presented next:

- **Alkaline** (AFC) – It's probably the most studied fuel cell technology and one of the first to be developed, beginning in 1960 with NASA's attempt to provide on-board electric power for the Apollo space vehicle. The problem with this technology is that $CO_2$ reacts with the electrolyte $KHO$ to form $K_2CO_3$ altering its composition, making this type of fuel cell only viable for Spatial or Submarine applications; never for Terrestrial applications. Its advantage lies on its reduced production costs and high efficiencies.
- **Polymer Electrolytic Membrane** (PEM) – Generate higher current densities therefore are more compact. This makes the technology suitable for mobile applications. The electrolyte is solid, so the only liquid in this cell is

water. This reduces corrosion problems. It works at low temperatures so the cell reaches its optimal performance temperature rather quickly. These characteristics make PEM Fuel Cells the best candidate for penetration into the Automobile Industry. Has the disadvantage that it is sensitive to fuel impurities like to $CO$.

- **Phosphoric Acid** (PAFC) – Operate at higher temperatures, 150º–200º. This enables the use of a Combined Cycle. Higher temperatures are also responsible for the higher tolerance to fuel impurities. The drawbacks are low current densities and long startup times, which renders them impractical for mobile applications
- **Molten Carbonate** (MCFC) – Operate at high temperatures, 600º-700º. They can be used with more than one fuel. Their cost of production is relatively low because they do not use noble material in their membranes. The high temperatures make it suitable for the use of combined cycles yielding efficiencies of almost 50%. The drawbacks are the long startup times, low power density and long exposure to high temperatures deteriorates the materials and shorten the cell's durability
- **Solid Oxide** (SOFC) – Operate at extremely high temperatures, 700º-1000º. Are used with a Combined Cycle the recycle the lost heat. These temperatures make them very efficient – can reach 60%. Another advantage is that the electrolyte is solid so it's more resilient and does require a lot of maintenance. Its drawbacks are very long startup times, low power density and shortened durability.

**Table 2.1 – Comparison of Fuel Cell technologies [28]**

| Fuel Cell Type | Common Electrolyte | Operating Temperature | Fuel | Efficiency | Applications |
|---|---|---|---|---|---|
| Polymer Electrolyte Membrane (PEM)* | Perfluoro sulfonic acid | 50-100°C<br>122-212°F<br>typically 80°C | $H^+$ | 60% transportation<br>35% stationary | • Backup power<br>• Portable power<br>• Distributed generation<br>• Transportation<br>• Specialty vehicles |
| Alkaline (AFC) | Aqueous solution of potassium hydroxide soaked in a matrix | 90-100°C<br>194-212°F | $OH^-$ | 60% | • Military<br>• Space |
| Phosphoric Acid (PAFC) | Phosphoric acid soaked in a matrix | 150-200°C<br>302-392°F | $H^+$ | 40% | • Distributed generation |
| Molten Carbonate (MCFC) | Solution of lithium, sodium, and/or potassium carbonates, soaked in a matrix | 600-700°C<br>1112-1292°F | $CO_3^-$ | 45-50% | • Electric utility<br>• Distributed generation |
| Solid Oxide (SOFC) | Yttria stabilized zirconia | 700-1000°C<br>1202-1832°F | $O_2^-$ | 60% | • Auxiliary power<br>• Electric utility<br>• Distributed generation |

### 2.3.3 The PEM Fuel Cell

The low operating temperatures and immobilized electrolyte membrane (that reduces corrosion, and provides

for longer cell and stack life) are the main features that position this cell as the most convenient in this work. This is why they will be one of the main targets of our attention. In the next few sections its operation and performances will be explained in detail, so as to gain a better insight into the operation of our Prototype Plant.

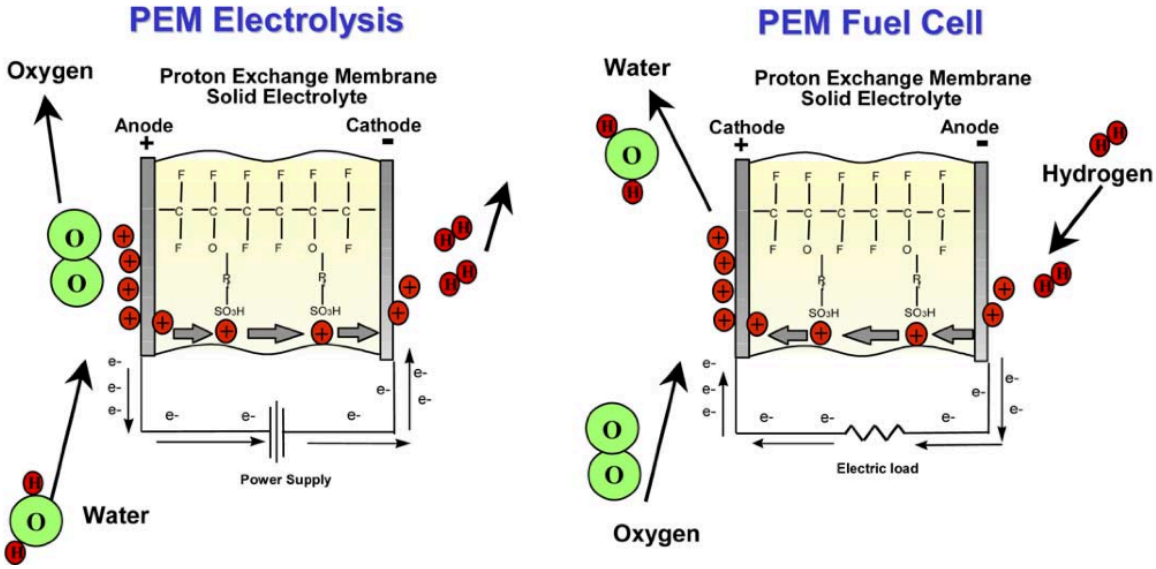


**Figure 2.5 – Operation of a (a) PEM Electrolyser and a (b) PEM Fuel Cell [16]**

In this type of fuel cell depicted in figure 2.5, hydrogen gas flows through channels to the anode, where a catalyst causes the hydrogen molecules to separate into protons and electrons. The membrane allows only the protons to pass through it. While the protons are conducted through the membrane to the other side of the cell, the anode collects the free electrons, forming a negatively charged stream that follows an external circuit to the cathode. This flow of electrons is electricity that can be used to do work, such as power a motor. The sub-reaction occurring in the anode is given by

$$H_2(g) \rightarrow 2H^+ + 2e^- \tag{2.5}$$

On the other side of the cell, air flows through channels to the cathode. When the electrons return from doing work, they react with oxygen in the air and the hydrogen protons (which have moved through the membrane) at the cathode to form water. The sub-reaction happening in the cathode is given by

$$\frac{1}{2}O_2(g) + 2H^+ + 2e^- \rightarrow H_2O(l) \tag{2.6}$$

This union is an exothermic reaction, generating heat that can be used outside the fuel cell.

If we sum both electrochemical reactions occurring at the anode and cathode we get a final overall reaction given by

$$H_2(g) + \frac{1}{2}O_2(g) \rightarrow H_2O(l) + Electrical\ \ Energy + Heat \tag{2.7}$$

Notice that the process of recombination of Hydrogen and Oxygen is produces electrical work. As it is not an ideal process, some heat is also exchanged. The reactions occurring in a PEM Electrolyzer are the reverse of those

we have just seen.

## Performance

In some electrical power-generating devices, it is very clear what form of energy is being converted into electricity. A good example is a wind-driven generator – the energy source is clearly the kinetic energy of the air moving over the blades. With a fuel cell, this is much more difficult to visualize. The energy of the chemical input and output is not so easily defined. This is where 'Gibbs free energy' comes in handy. It is defined as the "energy available to do external work, neglecting any work done by changes in pressure and/or volume'. In a fuel cell there is no pressure or volume changes, so all the work is external. This means that the Gibbs free energy is a measure of the maximum electrical work that can be extracted from a cell. This type of chemical energy is analogous to mechanical potential energy – it is the change in Gibbs free energy that gives us the released energy. I will use

$$\Delta\bar{g} = \bar{g}_{products} - \bar{g}_{reactats} \tag{2.8}$$

Where the $\bar{}$ sign indicates that it is the molar specific Gibbs free energy. So, for the reaction of formation of water by oxygen and hydrogen, presented above, this change is

$$\Delta\bar{g} = \bar{g}_{H_2O} - \bar{g}_{H_2} - \frac{1}{2}\bar{g}_{O_2} \tag{2.9}$$

The problem is this values changes with temperature. For example, for 25ºC it is $\Delta\bar{g}_{25^\circ} = -237.2\ kJmol^{-1}$ but for 80ºC it is lower $\Delta\bar{g}_{80^\circ} = -228.2\ kJmol^{-1}$. The values are negative which means the energy is released. For each water molecule formed, or hydrogen molecule used, two electrons are collected by the anode, so, for one mole of hydrogen, 2 $N_a$ electrons pass through the external circuit – where $N_a$ is Avogadro's number. If *–e* is the charge of one electron, then the total flowing charge is $-2\ N_a = -2F$, where F is Faraday's constant.

If $E$ is the voltage of the fuel cell, then the electrical work done moving this charge round the circuit is

*Electrical work done = charge x voltage =* $-2FE$

If the system is reversible (if there are no losses in the fuel cell), then this electrical work done will be equal to the released Gibbs free energy. So

$$\Delta\bar{g} = -2F \cdot E \Leftrightarrow \boxed{E = -\frac{\Delta\bar{g}}{2F}} \tag{2.10}$$

This is the reversible open circuit voltage of the hydrogen fuel cell. At room temperature, 25ºC, this value is $E = 1.48V$ if the product is liquid water, or $E = 1.23V$ if the product is steam.

The Fuel Cell is intended to be a Voltage source, so, as depicted in Figure 2.6, its ideal characteristic would be a constant output voltage, independent of the current. This voltage would be the reversible open circuit voltage of the hydrogen fuel cell that we just determined.

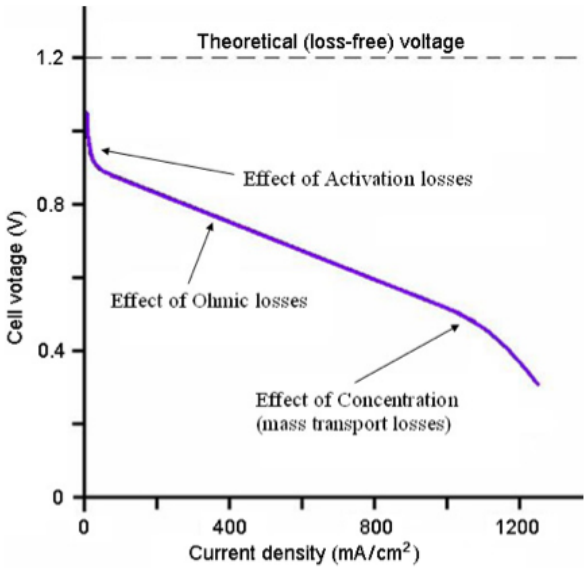


**Figure 2.6 – Polarization curve of a low temperature Fuel Cell [17]**

But what we studied so far was the ideal, or reversible case. No losses were assumed. Well, in reality things are not that simple. There are many irreversiblities associated with the operation of the cell, which in practice results in Voltage drop. I will present the most important losses:

- **Activation losses –** These are caused by the slowness of the reactions taking place on the surface of the electrodes. A portion of the voltage generated is lost in driving the chemical reaction that transfers the electrons to or from the electrode. This voltage drop is given by the Tafel Equation

$$\Delta V_{act} = \frac{RT}{2\alpha F}\ln\left(\frac{i}{i_0}\right) \tag{2.11}$$

Where $i$ is the current density, $i_0$ is the exchange current density and $\alpha$ is the *charge transfer coefficient* that is the proportion of the electrical energy applied that is harnessed in changing the rate of an electrochemical reaction. It varies from $0.0 - 1.0$. The equation is only valid for $i < i_0$. A rise of temperature will reduce activation losses, although this might seem counter-intuitive taking this equation into account. The fact is that $i_0$ is much more than linearly dependent on temperature, so its contribution mitigates the contribution of the linear term, imposing this reduction. This regime is represented in figure 2.6 by the initial steep non-linear slope for low currents.

- **Ohmic losses –** Ohmic losses occur because of resistance to the flow of ions in the electrolyte and resistance to flow of electrons through the electrode materials. The ohmic losses through the electrolyte, which are dominant, are reduced by decreasing the electrode separation and enhancing the ionic conductivity of the electrolyte. Because both the electrolyte and fuel cell electrodes obey Ohm's law, the ohmic losses can be expressed by the equation

$$\Delta V_{ohm} = ir \tag{2.12}$$

Where $i$ is the current density and $r$ is the area-specific resistance of the cell (which includes electronic, ionic and contact resistance). This regime is represented in figure 2.6 by the linear slope for the middle range currents.

- **Concentration losses –** If a great current is being drawn from the cell, then the rate at which the reactants are consumed will grow. This will originate a reduction in their concentration around the electrodes. If hydrogen (in the anode) or air (in the cathode) supplies do not meet this rate of consumption, then a concentration gradient will be formed. This will cause a reduction in the partial pressure of the reactants and, consequently, a voltage drop at the cell's terminals. However, it is generally agreed among fuel cell researchers that there is no analytical solution to the problem of modeling the changes in voltage, so the most common approach is entirely empirical with no claim for theoretical basis

$$\Delta V_{conc} = m \cdot \exp(ni) \tag{2.13}$$

Where $m$ and $n$ are fit constants. This regime is represented in figure 2.6 by the final right-most voltage drop, associated with large current densities.

- **Internal losses –** The internal current loss is due to the wasted fuel and oxidant that passes through the membrane and does not produce any useful work. In addition, the electron conduction in the membrane can lead to such losses. These affect the performance mostly at open circuit but can be negligible at higher currents, so they usually do not take part in the modeling.

The total losses are given by the sum of all these effects

$$V = E - \Delta V_{act} - \Delta V_{act} - \Delta V_{act}$$
$$\Leftrightarrow V = E - A_T \ln\left(\frac{i}{B_T}\right) - ir - m \cdot \exp(ni)$$
$$\Leftrightarrow V = E - A_T \ln(i) - A_T \ln(B_T) - ir - m \cdot \exp(ni)$$

Where $A_T$ and $B_T$ are fitting constants that depend on temperature. Seeing that $A_T ln(B_T)$ is a constant, we can postulate a *real open circuit voltage*

$$E_{oc} = E + A_T \ln(B_T)$$

Finally we have

$$\boxed{V = E_{oc} - ir - A_T \ln(i) - m \cdot \exp(ni)} \tag{2.14}$$

This equation is simple, yet has been found to give an excellent fit with the results of real fuel cells. The approach we have taken in considering these different losses has been moderately rigorous and mathematical, suitable for an initial understanding of the issues.

Up until now we noted that the change of Gibbs free energy in a chemical reaction varies with temperature. Equally important, though more complex, are the changes in Gibbs free energy with reactant pressure. *Nernst Equation* gives this dependence,

$$E = E^0 + \frac{RT}{2F}\ln\left(\frac{a_{H_2}\cdot\sqrt{a_{O_2}}}{a_{H_2O}}\right)$$

Where $E^0$ is the reversible voltage, and $a$ is the 'activity'. If, for instance, we chose the reaction were the product is stream, we can then assume that all the participants of the reactions are ideal gases and Nernst Equation takes a new form

$$E = E^0 + \frac{RT}{2F}\ln\left(\frac{p_{H_2}/p_0\cdot\sqrt{p_{O_2}/p_0}}{p_{H_2O}/p_0}\right) \tag{2.15}$$

It is now obvious, assuming that oxygen and water are at atmospheric pressure (as is usually the case), that pressurizing hydrogen improves the total power delivered to the load.

In the next section I will compare this model with the one for the PEM Electrolyzer.

## Efficiency

The total efficiency of a fuel cell is calculated as a product of three different efficiencies,

$$\eta_{FC} = \eta_{th}\times\eta_u\times\eta_i$$

Respectively, the Thermal Efficiency, the Voltage Efficiency and the Current Efficiency. The Thermal Efficiency is the efficiency of conversion of energy, so it is calculated as the ratio between the output electrical energy and the input energy (associated to the stored hydrogen).

$$\eta_{th} = \frac{E_{out}}{E_{in}} = \frac{P_{out}\cdot\Delta t}{\Delta H} \tag{2.16}$$

As was explained before, the operating voltage of a fuel cell is determined by the reversible open circuit voltage, reduced by the various loss voltages. The voltage efficiency is the ration between the operating voltage and the reversible open circuit voltage.

$$\eta_u = \frac{u}{U_{oc}} \tag{2.17}$$

Finally, the current efficiency is given by the product of the Faraday Efficiency, which is the ration between the real current and the theoretical current; and the hydrogen consumption factor, which accounts for the fact that there are some hydrogen molecules that pass through the membrane without reacting. This factor is calculated as the ration between the flow of hydrogen that reacts and the flow of hydrogen that is supplied.

$$\eta_i = \eta_F\times\mu_F = \frac{i}{n_e F\nu}\times\frac{reactant\ fuel}{total\ \ fuel} \tag{2.18}$$

Studies on PEMFC efficiency have been done by Teixeira J. [18] and Nunes G. [19], and their where able to achieve 43.8% and 42.4% electrical efficiency respectively. Teixeira J. further observed that in the range of $40 - 220\ mA\cdot cm^{-2}$ the values found for efficiency where all close to 40%.

### 2.3.4 The PEM Electrolyzer

As was discussed above, the electrolyzer is essentially the reverse process of the Fuel Cell. Its overall reaction is given by

$$H_2O(l) + Electrical\ \ Energy \rightarrow H_2(g) + \frac{1}{2}O_2(g) + Heat \qquad (2.19)$$

Its performance is conceptually similar to that of the PEMFC. It is affected by the same kind of loss phenomena. Figure 2.7 is a result of the experimental work performed by Ulleberg, Ø., [14], and shows the I-V characteristics of a PEM Electrolyzer and its dependence on temperature.

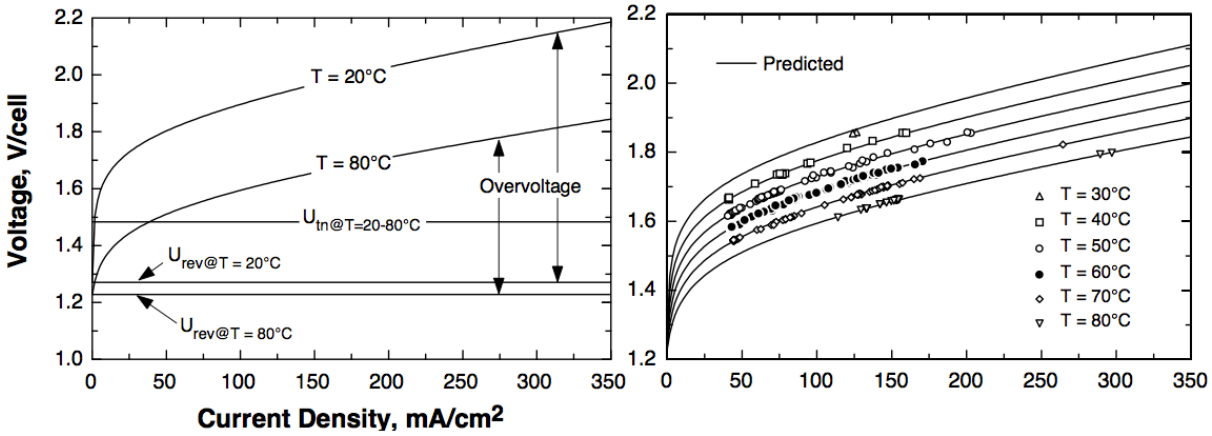


**Figure 2.7 – I-V curves of the electrolyzer (a) theoretical (b) experimental results [14]**

The results of Ulleberg's work in figure 2.7(b) were modelled by an empirical I-V characteristics equation

$$\boxed{V = E_{rev} + ir + A_T \ln(B_T i + 1)} \qquad (2.20)$$

Where m and n are fitting coefficients that depend on temperature. This equation has strongly resembles equation (2.10), it's equivalent for the fuel cell. The difference lies on the fact that power is now being fed into the system so the losses have a positive contribution. Also, for the same reason, the open circuit voltage (V for zero current density) is the reversible open circuit voltage. Notice that this model does not include the exponential contribution of concentration losses, as these are only effective at very high current densities, in the range of $1\ A \cdot cm^{-2}$. In our experimental setup that has a $25cm^2$ membrane, this would mean currents close to $25A$, which much more than our source can feed to the electrolyzer. So, in practical terms, we need not worry about this effect.

But there are some other important differences, especially in process efficiency. As discussed in the previous section, work performed by [18] and [19] collected clear evidences that the typical values for PEMFC efficiency

are around 40%. PEM Electrolyzers have much better performances, typically around 70% at room temperature as show in figure 2.8 taken from [15]. In this paper the authors studied the impact of different parameters on the efficiency of a PEM Electrolyzer. Two are presented here: the effect of temperature, and the effect of membrane thickness.

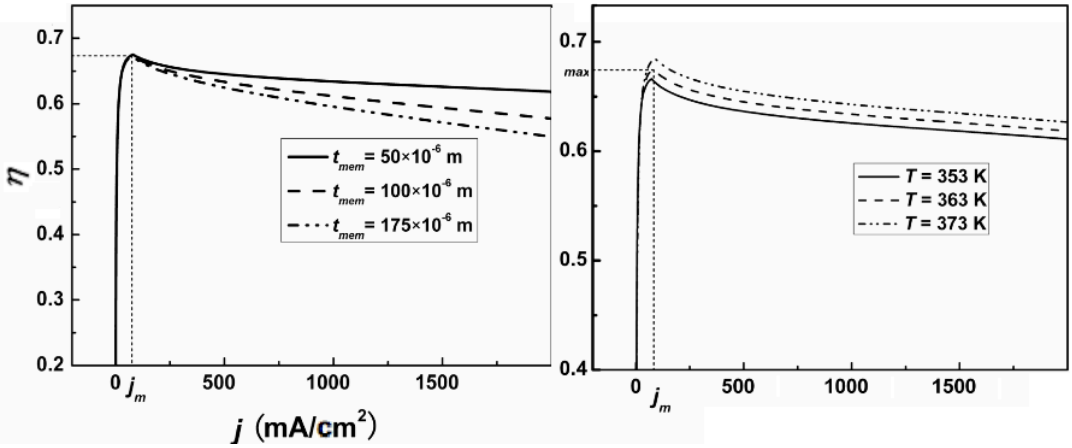


**Figure 2.8 – Effect of (a) membrane thickness and (b) operating temperature on PEM Electrolyzer Efficiency [15]**

With these typical values of efficiency for PEM fuel cell and electrolyzer (40% and 70% respectively), one can infer a rough estimate of 25-30% efficiency of the overall conversion and reconversion process, assuming no losses in hydrogen storage.

# 3 Photovoltaic Technologies

As was discussed in Chapter 1, PV technologies have been gaining relevance as 'green' energy producers. The key element in these systems is the PV Cell. These cells can directly convert solar energy into electricity. They are made of semiconductor materials, whose properties will be discussed shortly. In this chapter the basic principles of operation are explain and different technologies, in the market or still in a stage of development, are presented.

## 3.1 Cell Structure

### 3.1.1 Semiconductors

Semiconductors are solid materials, with crystalline or amorphous structure, that can be either be isolators or conductors, depending on their temperature and the height of their band gap. In a metal, electrons are considered to a good approximation to be 'free', meaning they are not immersed in any kind of potential. This model – *free electron Model*, is able to explain most of the physical properties of metals. But it proves inaccurate when dealing with semiconductors. To understand this apparent inconsistency, one first needs to get a firm grasp on what causes electrons in a metal to be 'free'. In fact, most of the differences between metals and semiconductors stem from the number of charge carriers. For the former, at room temperature, this quantity ranges between $10^{22} - 10^{29}\ cm^{-3}$, as for the latter, its typical values fall in the range of $10^{6} - 10^{14}\ cm^{-3}$. One can see that there are many orders of magnitude separating them. When a stationary point charge is embedded in a fluid of electrons, a phenomenon called *electrostatic screening* occurs – the electrons tend to gather around the charge, shielding its electric potential. Charles Kittel deduces in [23] that due to this effect, the electric field falls with a factor $1/r \cdot exp(-r/\lambda_s)$ , where $\lambda_s$ is the s*creening length* – a measure of the shielding distance. This factor is much faster than its vacuum equivalent $1\ /\ r$. Kittel also demonstrates that the factor is inversely proportional to the density of charge carriers. Consequently, the screening effect is much stronger in a metal than in a semiconductor. In fact, metals have $\lambda_s$ much smaller than the inter atomic distances in the cristal lattice, so the electron do not feel the potential unless they are at a distance in the order of $\lambda_s$ (which in this case is very small). In semiconductors the screening is not that strong because they have small intrinsic carrier densities, hence the electrons feel the interaction of the positive ion background lattice. By taking this potential into account, even in a simplified form such as the *Kronig-Penney Model*, also explained in [23], a hiatus between what is called the valence and conduction bands appears in the reciprocal space representation, its height being proportional to the strength of the lattice interaction potential.

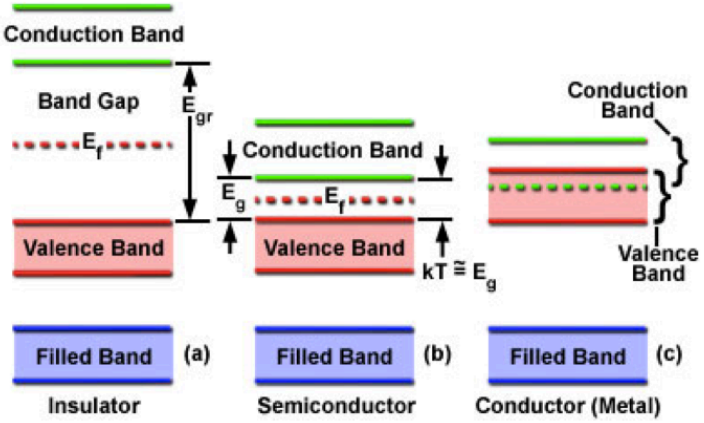


**Figure 3.1 – Band structure of (a) an isolator (b) a semiconductor and (c) a metal [32]**

If every energy band is completely full, the material is an isolator or a semiconductor. The difference being the band gap in an isolator cannot be surpassed. If a band is not fill, its a metal. This structure is depicted in figure 3.1.

In order to improve the conductivity properties of semiconductors, the concentration of charge carriers must be increased. This is possible by introducing impurities in the intrinsic semiconductor. This method is called *doping* and there are to kinds: On a *p-doped* semiconductor, the impurity has three valence electrons – one positive charge, or hole. Whereas on an *n*-doped semiconductor, the impurity has five valence electrons – one negative charge, or *electron*.

## 3.1.2 PN Junction

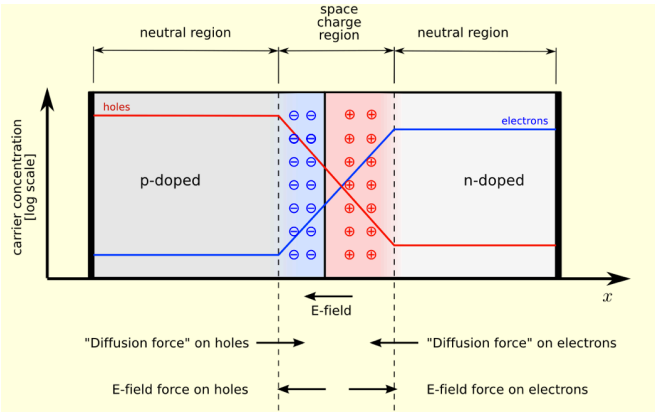


**Figure 3.2 – The PN junction at equilibrium [33]**

A PN Junction consists of *p*-type semiconductor material packed together with an *n*-type one. When joined, the excess holes in the *p*-type material flow by diffusion to the *n*-type material, while electrons flow by diffusion from the *n*-type material to the *p*-type material as a result of the carrier concentration gradients across the junction. The electrons and holes leave exposed charges behind near the junction. The middle region that is now striped of charge carriers is called the *depletion zone*. The positive fixed ions on the *n* side interact with the negative charged ones on the p side. As a consequence, an opposing electric field builds up in the depletion zone. This field will generate a drift of *minority carriers* back to where they where *majority carriers* – electrons back to the *n* side and holes back

to the *p* side. This opposing current quickly matches the diffusion current and the system reaches equilibrium. This electric field has the energy to produce electric current. All that needs are additional charge carriers to pump across the junction. So, a good way to generate new charge carriers would be to expose the materials to light. The electric field in the depletion region would do the rest.

### 3.1.3 Illuminated PN Junction

When light falls onto semiconductor material, photons with energy lower than the band gap energy ($E_{ph} < E_g$) interact only weakly with the semiconductor, passing through it as if it were transparent. However, photons with energy greater than the band gap energy ($E_{ph} > E_g$) interact with electrons in covalent bonds of the bulk material, and use their energy to break bonds and create *electron-hole pairs*. In other words, light generates an excess of minority carriers. However, some of them get recombined before they reach the depletion zone. In general, the closer the point of generation of the pair is to this zone, the better the chance of collection. As illustrated in figure 3.3, the electric field at the depletion region sweeps these additional electrons to the *n* side and holes to the *p* side. Consequently, now the drift current is bigger that the diffusion current, so there is a total net current – the junction falls out of equilibrium. Electrical power was created. This is the principle of solar cells.

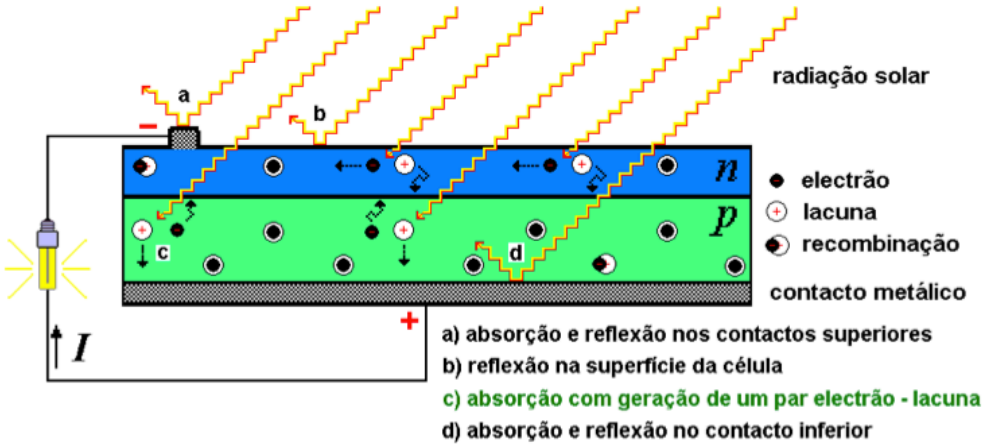


**Figure 3.3 – Closed circuit flow of electrons in an illuminated PN Junction [6]**

## 3.2 I-V Characteristics

A PV Cell can be fully characterized by its I-V characteristics. It is graphically represented in figure 3.4. Its analytical representation is the *characteristic equation*

$$I = I_0\left(e^{qV/k_BT} - 1\right) - I_L \qquad (3.1)$$

Where the first term is the so-called 'dark current' and $I_0$ is the saturation current. We want to reduce $I_0$ to as low a value as possible in order to be able to extract as much light generated current as possible. The second term, $I_L$, is the *light generated current*. From the analysis of the I-V characteristics one can extract important parameters that determine the quality of performance of the PV cell.

- *Open circuit voltage* – If an infinite load is connected to the cell then the carriers are not extracted. They accumulate on both sides of the junction and a potential difference builds up. In this case $I = 0$ so the characteristic equation yields

$$V_{OC} = \frac{nk_BT}{q}\ln\left(\frac{I_L}{I_0}+1\right) \approx \ln\left(\frac{I_L}{I_0}\right) \tag{3.2}$$

  Hence, $V_{OC}$ gives us information about the light generated current and the 'dark current'. Notice that $V_{OC}$ varies logarithmically with increased sunlight.

- *Short circuit current* – If the junction terminals are connected, then current will flow. As in this case $V = 0$, the characteristic equation yield

$$I_{SC} = -I_L \tag{3.3}$$

  Therefore the short circuit current is the light generated current. This makes the short circuit current very important because it tells us how much current generated light, which will be proportional to the number of incident photons with energy above the gap.

- *Maximum Power* – The operation point that delivers the maximum power. It is on important parameter because one can use it to adjust the load to receive this maximum amount of power.

- *Fill Factor* – It is related to the quality of the junction. Simply put, it is the measure of how ideal the I-V curve is.

$$FF = \frac{I_{mp}V_{mp}}{I_{SC}V_{OC}} \tag{3.4}$$

For the best performance one needs maximize the short circuit current, the open circuit voltage and the fill factor.

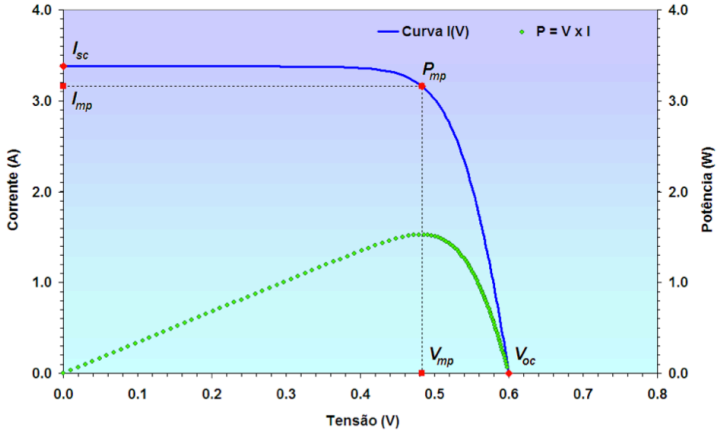


**Figure 3.4 – I-V characteristics of an illuminated PN Junction [6]**

### 3.2.2 Irradiance Temperature effects

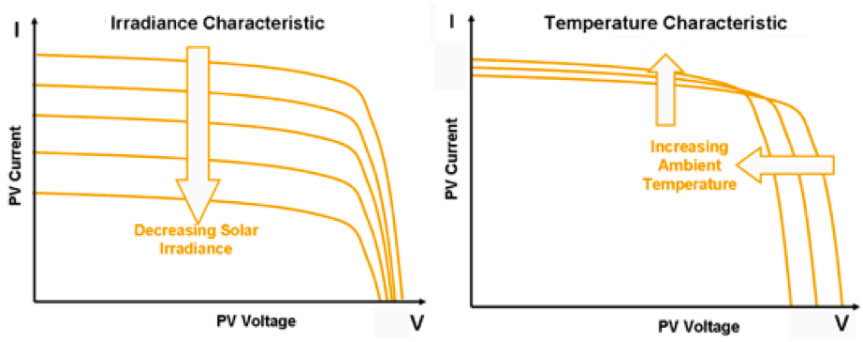


**Figure 3.5 – The effects of (a) Irradiance and (b) Temperature on I-V characteristics [34]**

The IV curve of a PV cell is a function of the incident solar irradiance an its operating temperature. The current generated is proportional to the number o incident photons with energy that surmounts the material's band gap. When the solar irradiance increases, so does the flux of photons meeting these requirements. So an increase in solar irradiance is reflected in an almost linear increase in $I_{SC}$ and small increase on $V_{OC}$ (because it depends logarithmically on irradiance as was explained in the previous section). This effect is illustrated in figure 3.5(a). Temperature is a very important factor because some of the energy brought by light is converted into heat, raising the temperature of the cell. As temperature increases, the semiconductor expands leading to a weaker interaction potential, which leads (as discussed in the previous section) to the shrinking of the band gap. Now more photons can be absorbed to produce e-h pairs so $I_{SC}$ increases. On the other hand the shortening of the band gap decreases $V_{OC}$. The formed effect is much smaller than the latter as illustrated in figure 3.6(b).

### 3.2.3 Cell Efficiency

The efficiency parameter is used to compare PV cell performances. It is the ration between maximum power it can generate and total incident electromagnetic power. If $P_{in}$ is given by the solar irradiance $G_i$ times the cell's surface area $A$, then efficiency is

$$\eta = \frac{I_{mp}V_{mp}}{G_i A} \tag{3.5}$$

The irradiance effect only shrinks or stretches the I-V curve by a multiplicative constant, it does not change its shape. Therefore the efficiency is maintained. On the contrary, temperature changes I-V curve shape. The increase in the current for a given temperature rise is proportionately lower than the decrease in voltage. Hence the efficiency of the cell is reduced by an increase in temperature. This effect is depicted in figure 3.6.

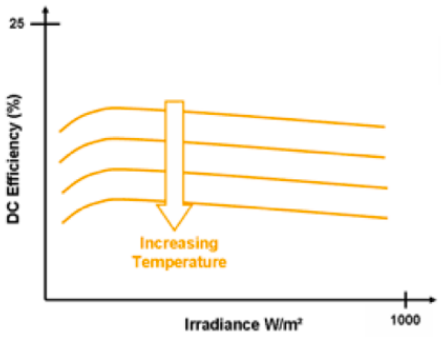


**Figure 3.6 – DC efficiency vs. Irradiance [34]**

### 3.2.4 Spectral Response

The performance of a solar cell also depends on the wavelength of the incident radiation. This behaviour is accounted for by another parameter called the *spectral response*. It is defined as the ratio of the photocurrent generated by a solar cell under, to the value of the spectral irradiance of monochromatic illumination of a given wavelength. It's a measure of the current produced by unit power at different wavelengths. This value is not constant because photons with different wavelengths have different probabilities of being absorbed. It is calculated by

$$SR(\lambda) = \frac{I_{SC}}{P_{in}(\lambda)} = \frac{q \times n_e}{hc/\lambda \times n_{ph}} = \frac{q\lambda}{hc} QE(\lambda) \qquad (3.6)$$

Where $QE$ is the *quantum efficiency*. As was described above, for a photon to generate current first it has to be absorbed by the material, and then the minority carrier it generates has to reach the depletion zone without recombining. This series of events only happens with a limited probability. Quantum efficiency is a measure of this probability. It also depends on the wavelength of the incident photon. A comparison of the spectral response of different PV technologies is presented in figure 3.7

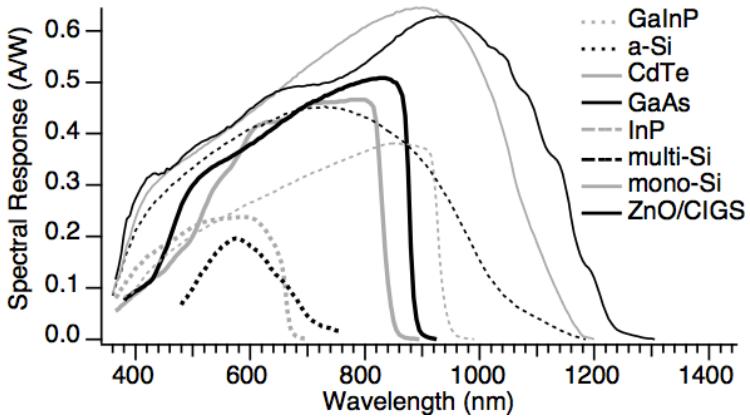


**Figure 3.7 – Spectral Responses of different PV Cell types [35]**

# 4 SCALED POWER PLANT DESIGN

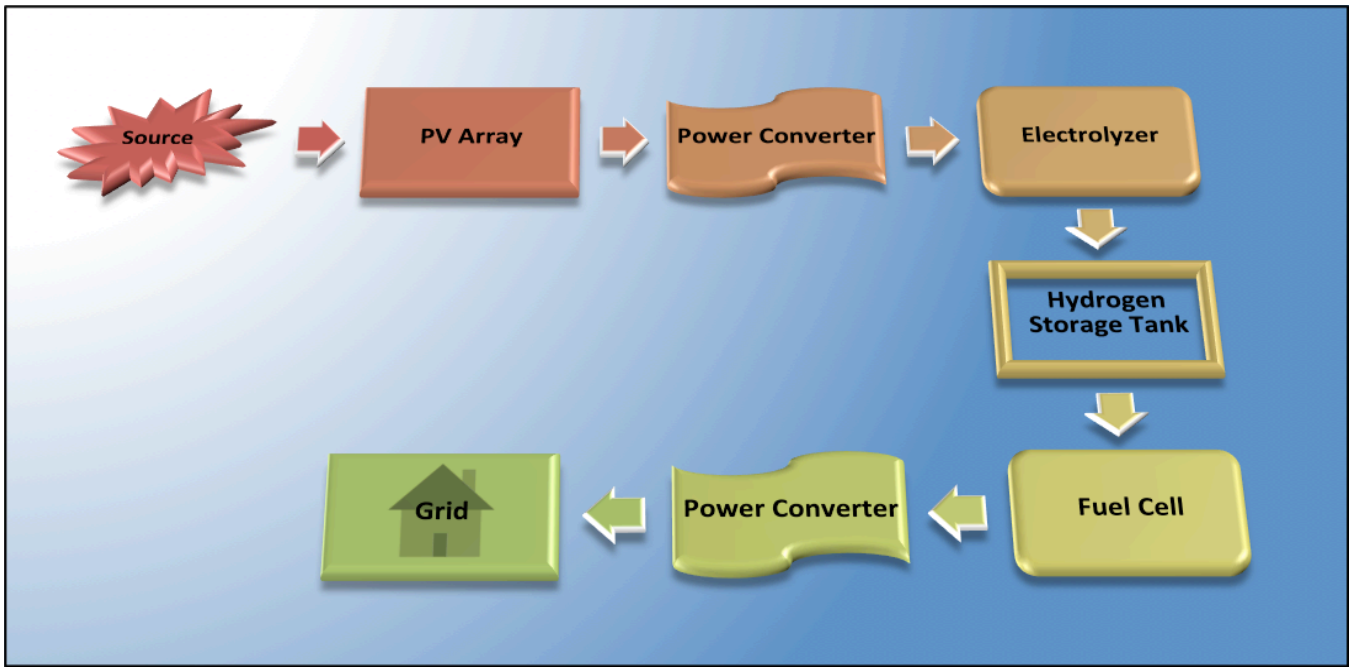


**Figure 4.1 – Block Diagram of a PV Power Plant that stores energy in the form of Hydrogen**

In the previous chapters I have introduced and described the most important theoretical concepts surrounding the experimental setup. In this chapter I will compare the operation of the prototype with a real scale plant. The Block diagram in figure 4.1 represents the flow of energy, from production to storage, to final consumption. The design of each of these stages will now be described.

## 4.1 Light Source

As this work has educational purposes, the prototype has to be prepared for usage at any time of day with any weather condition. These requirements would not be met if the Sun had been used as the light source for the setup. The answer to this problem was to create a panel of high brightness LEDs of three different colours – Red, Green and Blue. This panel offers some useful functionalities. It not only solves the problem of availability of the source, but it also grants the user the possibility to test the spectral response by changing the wavelengths and the intensity of incident radiation. In order to achieve a better stability of irradiance, an algorithm was developed to equidistribute the power in time, so as to reduce LED flickering. This algorithms is described in Chapter 5 and it's implementation is in the code of Appendix A.

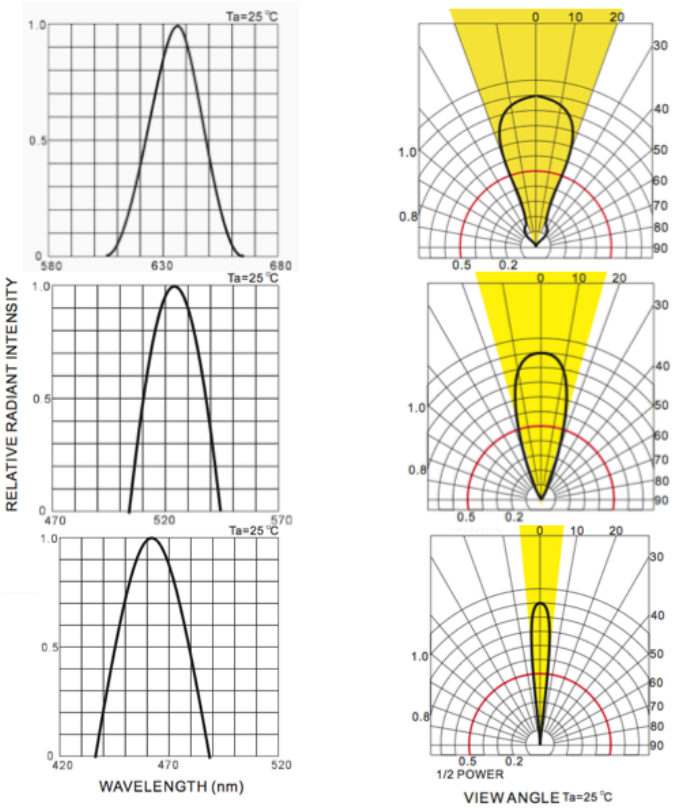


**Figure 4.2 – Intensity spectrum and look angle of high brightness (a) Red – 629nm (b) Green – 525nm (c) Blue – 465nm LEDs. [Taken from the specification sheets of the LEDs]**

## 4.2 PV Array

The energy produced in real plants has to be transported over long distances in order to reach its final destiny. This long-range transfer of energy is called *transmission*. However, just like any electrical conductor, transmission lines have some resistance associated with their finite conductivity, which means there will be ohmic losses. . These losses are given by the equation

$$P_{diss} = \Delta V \cdot I = R \cdot I^2 \qquad (4.1)$$

Where R is the line resistance, not the load resistance. Notice the quadratic dependence on current means that higher currents produce bigger losses. Also, for transmission cables to handle high currents they need to be thicker. Since they are very long, a change in thickness would amount to a huge increase of transmission line costs. The costs associated with handling high voltages are much lower. So, in order to minimize the losses and costs of transmission lines, utilities use transformers at both ends of the line to scale voltage from low to very high levels and vice versa. This allows power to be transmitted at lower currents, consequently with thinner cables.

Typically, doubling the voltage quadruples the power transfer capability. Therefore, the evolution of grids in most countries is characterized by the addition of network layers of higher and higher voltages. In Portugal, this tendency is confirmed by the data provided in [7] and [8]. The Portuguese transmission lines are operated at 150kV, 220kV or 400kV. The total length of the lines has grown 18,3% since 2006, which demonstrates the growth of energy demand. By the end of this year, these lines represented 34.3%, 43.5% and 22.2% of the total length

respectively. As of August 2012, the proportion is now 31.6%, 41.7%, 26.7%. Clearly, in order to deal with the increase of demand, the national electrical system has invested in 400kV lines at expense of the lower voltage ones. And for heavily populated and industrialized energy systems, demanding higher amounts of power, there are transmission lines operating at extra high voltages (EHV) reaching 800kV. Ultra high voltage (UHV) transmission lines of 1000kV have been constructed in Russia (USSR) and Japan, [24]. However these are presently operated at 500kV. A massive demonstration project in China is operating a 640km long 1000kV transmission line, [25].

In a real PV Plant, the PV modules are connected in parallel and series. As a series connection increases voltage, for the reasons presented above, the design of the plants consists of more series that parallel.

The specifications of the solar cell used in the experimental setup indicate a maximum power rating of 200mA and 1V. To mimic the design of a real plant, the three solar panels where connected in series, for a total of 200mA and 3V, yielding 600mW of installed power. As was concluded in chapter one, in Portugal, in order to be able to deal with peak demand, a power plant must have an installed power in the order of 1000MW. This means we have a scaling factor of roughly $1{:}10^9$.

## 4.3 Power Converter

The voltage and current characteristics of the PV array are determined by external factors (e.g. irradiance, temperature). We need to have a unit that is able to transform the their output power to a form that is usable for our applications. For example, the grid used alternate current (AC) because it is easier and cheaper to transform, and because the power produced by turbines is AC, which are responsible for the majority of the energy delivered to the grid. But the output of a PV array is direct current (DC), so in order to feed the grid, there has to be a power converter unit that transforms DC to AC – this is called an *inverter*. In our prototype the load does not require AC current so we do not need this. But we do have an Electrolyzer that is fed by the PV cells and works at a different DC voltage. So we need to step the voltage down while preserving the total power. To do this a *Buck Converter* was used. The operation of these devices will be explained next and its dimensioning equations derived.

Over the years, as the portable electronics industry evolved, new requirements arose concerning power consumption. With the massification of products such as cellular phones, laptop computers, digital cameras and mp3 readers, an ever increasing demand for better energy performances and battery lifetimes from power systems has placed power consumption as one of the industry's most important issues. In order to respond to these demands, engineers have worked towards developing efficient power conversion techniques. A Power Converter is an electrical or electro-mechanical device that converts electrical energy from one form to another. This discussion will be focusing on one type of these: the DC-to-DC converter. The simplest and cheapest member of this family is the Linear Regulator.

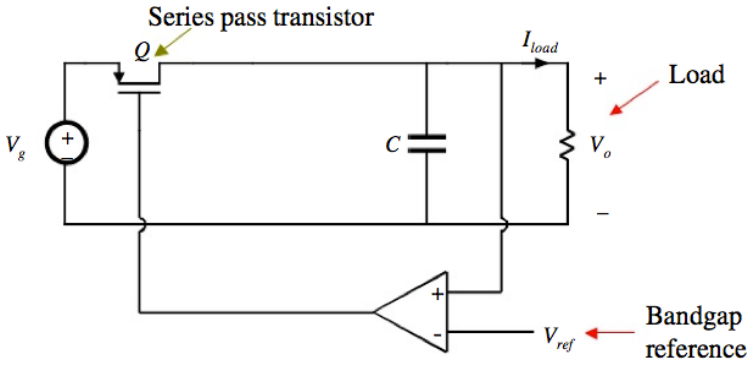


**Figure 4.3 – Linear Regulator. The transistor Q is in the linear region, thus acting as a variable resistor, controlled by gate-to-source voltage. [5]**

Linear Regulators are systems used to maintain a constant output voltage, always lower than the input one. It consists of a voltage divider with a variable resistor that changes in accordance with the load through a negative feedback, as shown in figure 4.3. The device is continuously adjusting the voltage divider network in order to maintain a constant output voltage, and continuously dissipates the difference between the input regulated voltages as ohmic losses, in the form of heat. As discussed above, this dissipation is proportional to the current and the voltage difference across the resistors and it is described by equation (4.1). This raises obvious issues of power efficiency but also of temperature limitation. Another limitation is that its efficiency is always smaller the ratio of the output and input voltages, so the bigger the difference between input and output voltages, the lower its efficiency. On the upside this device is much simpler than its counterparts, has low noise levels, no ripple and requires a small footprint area (assuming the power dissipation is not big enough in order for the device to need a heat sink). This being said, the Linear Regulator is usually only used in low power, noise sensitive systems, where the input and output voltages are not very different.

Conventionally voltage regulation has been done by Linear Regulators, but they are slowly being replaced by Switching Regulators. A Switching Regulator uses an active device that switches storage elements, inductor and capacitor, on and off at a fixed rate. The energy stored in these elements can then be transformed to output voltages that can now be greater than the input. Thus one can say that switching power supplies can step-up the input voltage, which is called a *Boost Converter*, or step-down, which is called a *Buck Converter*. The switching mechanism is typically a transistor oscillating between off-state and saturation mode. An ideal device would have no losses as an ideal switch would have no current flowing in the off-state and zero resistance in the on-state. As the transistor is not an ideal switch, there will be some losses, but very few when comparing to the Linear device. The ratio of on time to switching period is called the Duty Cycle,

$$D = \frac{t_{on}}{T_s} = \frac{t_{on}}{t_{on} + t_{off}} \tag{4.2}$$

In this case, the output voltage is regulated by a feedback loop that varies the Duty Cycle in order to maintain a constant average value. Switching regulators achieve efficiencies as high as 80%-95%, whereas its Linear counterpart only manages 50%-60% efficiencies. Figure 4.4 shows this comparison. Note that for very low output

currents the linear regulator can have smaller losses. This happens because for low currents, buck converter's transistor switch mode quiescent currents are higher, resulting in bigger losses.

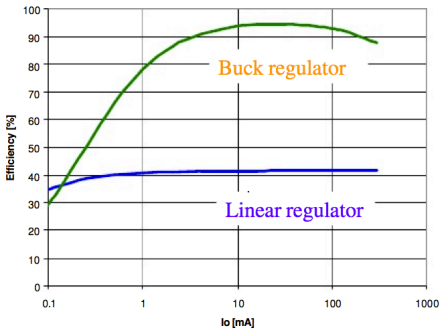


**Figure 4.4 – Comparison of efficiencies of Switch and Linear regulators as a function of output current for conditions $V_{in} = 3.6\,V$ and $V_{out} = 1.5\,V$. [5]**

I this work I will use a Buck Converter to step-down the dsPic's power source voltage, so that it can feed the electrolyser's membrane in an adequate range. The output current and voltage will be read by the PIC's ADC module, and the PWM Duty Cycle will be varied in accordance with these values. Figure 4.5 represents the schematic view of a Buck Converter module.

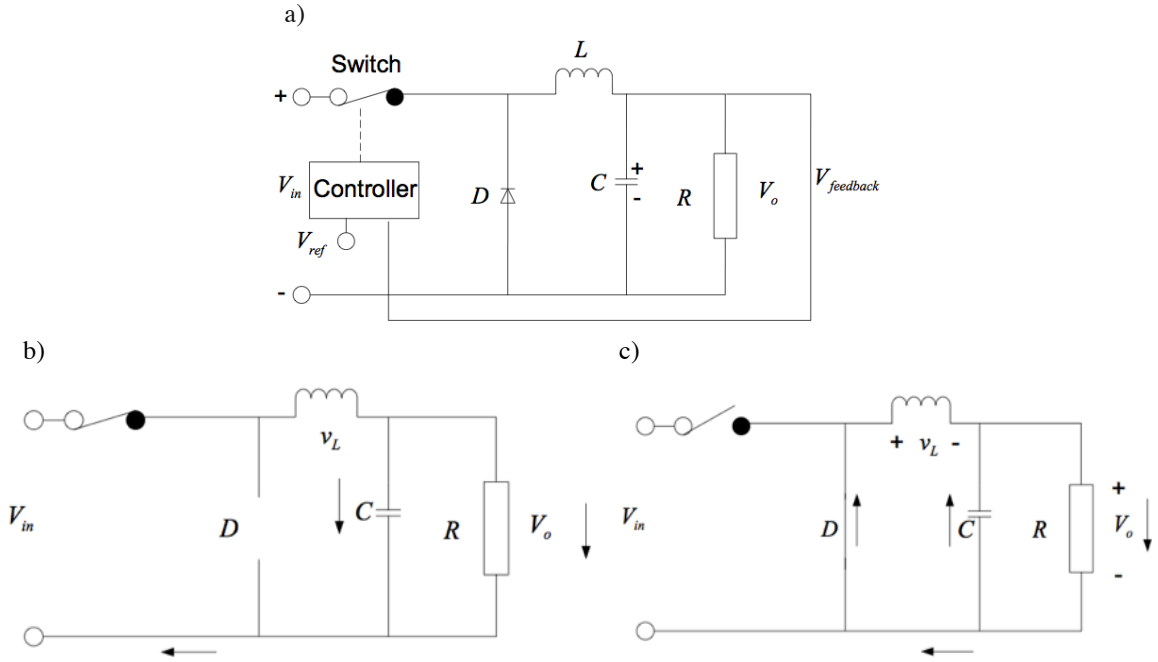


**Figure 4.5 – (a) Buck Converter schematic (b) ON state (c) OFF state [5]**

When the switch is in ON position (figure 4.5(b)), the inductor will have a voltage difference at its terminals, thus the current passing through it will increase, and so will the energy it stores

$$v_L = L\frac{di_L}{dt} \Rightarrow \frac{di_L}{dt} = \frac{v_L}{L} \qquad (4.3)$$

When the switch is in OFF position (figure 4.5(c)), the inductor acts as a source and maintains the current through the load. During this period the voltage drop across the inductor will be negative, resulting in a decrease of

stored energy and a fall in current. A very important aspect that results from this behaviour is that, although the switch introduces discontinuity, the inductor guaranties that there is continuous conduction through the load. The problem with this scheme is that the output voltage is not constant, it has a ripple associated with the switching frequency. From (4.3) we can conclude that by increasing $L$, current ripple is reduced, and consequently, as the current through the load is the same as that of the inductor, so is the ripple in output voltage. The next step to further reduce ripple is to add a capacitor across the load resistor. A capacitor soothes the voltage across it,

$$i_C = C\frac{dv_C}{dt} \Rightarrow \frac{dv_C}{dt} = \frac{i_C}{C} \tag{4.4}$$

The bigger the capacitance, the smaller the voltage ripple. The combined action of the LC filter reduces ripple in the output to a very low level. On the input side, the current is pulsating with large switching noise component. The final mandatory addition to our scheme would be a decoupling input capacitor to reduce input voltage noise and ensure proper operation of the device.

A DC-to-DC converter can have two different modes of operation: Continuous Conduction Mode (CCM) and Discontinuous Conduction Mode (DCM). The difference between the two being that for DCM the switching ripple of inductor current or capacitor voltage causes polarity to invert so, as this is an unidirectional circuit, the inductor current has to fall to zero. Both modes will now be described.

### 4.3.1 Continuous Conduction Mode (CCM)

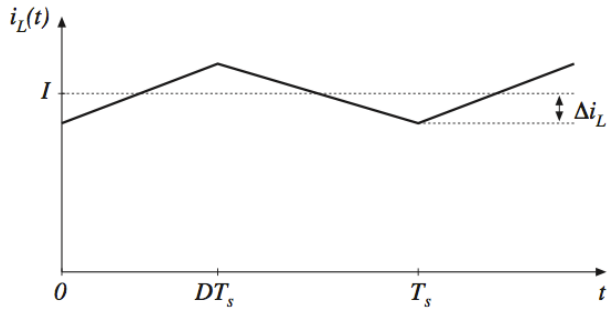


**Figure 4.6 – Continuous Conduction Mode [5]**

In an On-Time Event voltage across the inductor is

$$v_L = V_{in} - v_{out}(t) \tag{4.5}$$

If we assume small ripple, we can approximate the output voltage to a constant value

$$v_L = V_{in} - V_{out}$$

From equation (4.3) we can derive

$$\frac{di_L}{dt} = \frac{v_L}{L} \Rightarrow \Delta i_L = \frac{V_i - V_o}{L}\Delta t_{on} \tag{4.6}$$

Therefore, the inductor current increases in time with an approximately constant slope. In an Off-Time Event voltage across the inductor will be, assuming the same approximation

$$v_L = -v_o(t) \approx -V_o$$

And we can derive

$$\frac{di_L}{dt} = \frac{v_L}{L} \Rightarrow \Delta i_L = -\frac{V_o}{L}\Delta t_{off} \tag{4.7}$$

Summing equation (4.6) and (4.7) and knowing that the total current variation in on-state has to be equal in module to the current variation in the off state,

$$\frac{V_i - V_o}{L} t_{on} + \left(-\frac{V_o}{L} t_{off}\right) = 0$$
$$D(V_i - V_o)T_s + (1-D)(-V_o)T_s = 0$$
$$DV_i - DV_o - V_o + DV_o = 0$$
$$DV_i = V_o$$
$$\frac{V_o}{V_i} = D$$
$$\boxed{M = D} \tag{4.8}$$

Where M is the voltage gain. In this mode, the gain is equal to the duty cycle and independent of the load.

### 4.3.2 Discontinuous Conduction Mode (CCM)

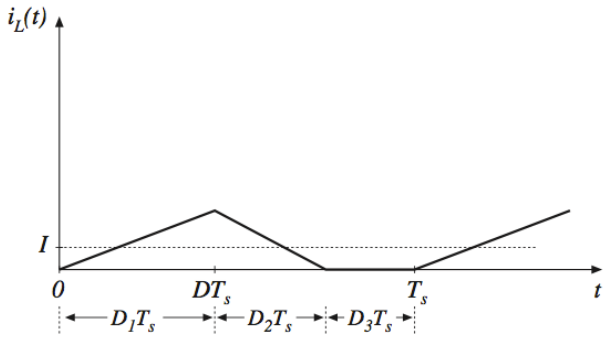


**Figure 4.7 – Discontinuous Conduction Mode [5]**

Here equations (4.6) and (4.7) still hold true. Assuming the steady state has been reached, the current gain during $D_1T_s$ has to be equal to the current drop during $D_2T_s$, we can write

$$\frac{V_i - V_o}{L} D_1 T_s + \left(-\frac{V_o}{L} D_2 T_s\right) = 0 \Leftrightarrow D_1(V_i - V_o)T_s + D_2(-V_o)T_s = 0$$

$$\frac{V_o}{V_i} = \frac{D_1}{D_1 + D_2} \tag{4.9}$$

Now we calculate $I_o$

$$I_o = \langle i_L \rangle = \frac{1}{T_s}\int_0^{T_s} i_L(t)\,dt = \frac{1}{t_s}\left[\frac{D_1 T_s I_{L,\max}}{2} + \frac{D_2 T_s I_{L,\max}}{2}\right]$$

$$\Rightarrow D_2 = \frac{2I_o}{I_{L,\max}} - D_1$$

We can determine $I_{max}$

$$I_{\max} = \frac{V_i - V_o}{L} D_1 T_s = \frac{V_o}{L} D_2 T_s$$

Now we substitute this equation in the previous, yielding

$$D_2 = \frac{2I_0}{V_0}\frac{L}{D_2 T_s} - D_1 \Leftrightarrow D_2^2 + D_1 D_2 - 2\tau_L = 0$$

Where $\tau_L = L/RT_s$ and $R = V_o/I_o$. Solving this second order equation, and substituting the result in equation (4.9) we obtain the expression for the gain in discontinuous conduction mode.

$$\boxed{M = \frac{2}{1+\sqrt{1+\frac{8\tau_L}{D^2}}}} \tag{4.10}$$

As we can see, the gain is now dependent on the load resistance, which in this application is an undesired effect, so we need to make sure our design always stays in CCM. To do this one must stay bellow the boundary between the two modes.

### 4.3.3 Mode boundary

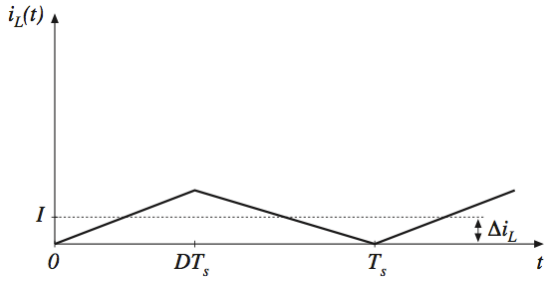


**Figure 4.8 – Boundary between CCM and DCM [5]**

The transition between the two modes is the point where $I_{o_{CCM}} = I_{o_{DCM}}$

$$\begin{cases} CCM: I_o = \dfrac{V_o}{R} = \dfrac{DV_i}{R} \\ DCM: I_o = \dfrac{V_i - V_o}{L}\dfrac{D}{2}T_s \end{cases}$$

Where we used the fact that in DCM boundary $D_1 = D_2 = D/2$. Now

$$I_{o_{CCM}} = I_{o_{DCM}} \Leftrightarrow \frac{V_i - V_o}{L}\frac{D}{2}T_s = \frac{DV_i}{R_c}$$

From this expression we can deduce the critical load resistance $R_c$

$$\boxed{R_c = 2\frac{f_s L}{1-D}} \tag{4.11}$$

If $R_{load} < R_c(D)$ then our system will always work in Continuous Conduction Mode.

### 4.3.4 Inductance and Capacitance

Now that we studied the theory on modes of operation of the converter, we can start trailing a more practical pathway by determine the right values for the components in order to build the converting unit. We start by determining the expression for dimensioning of the inductor.

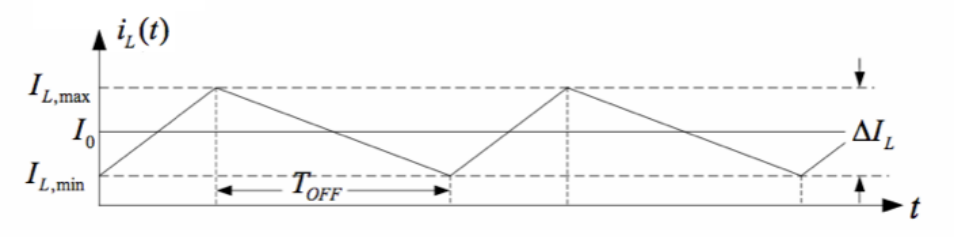


**Figure 4.9 – Current in the Inductor [5]**

Based upon the assumption that the voltage across the load is constant, we can derive a simplified differential equation in terms of the current through the inductor both in the on-state and the off-state

$$\begin{cases} ON \ : L\dfrac{di_L}{dt} = V_i - V_o \\ OFF : L\dfrac{di_L}{dt} = -V_i \end{cases}$$

$$\Leftrightarrow \begin{cases} i_{L_{ON}}(t) = \dfrac{V_i - V_o}{L}t + I_{L,\min} \\ i_{L_{OFF}}(t) = \dfrac{V_o}{L}t + I_{L,\min} \end{cases} \Leftrightarrow \begin{cases} I_{L,\max_{ON}} = \dfrac{V_i - V_o}{L}DT_s + I_{L,\min} \\ I_{L,\max_{OFF}} = \dfrac{V_o}{L}(1-D)T_s + I_{L,\min} \end{cases} \Leftrightarrow \begin{cases} \Delta i_{L_{ON}} = \dfrac{V_i - V_o}{L}DT_s \\ \Delta i_{L_{OFF}} = \dfrac{V_o}{L}(1-D)T_s \end{cases}$$

Where $\Delta i_{L_{ON}} = \Delta i_{L_{OFF}} = \Delta i_L$. So we can use

$$\Delta i_L = \frac{V_o}{L}(1-D)T_s \tag{4.12}$$

Notice that the current ripples are directly proportional to Duty Cycle and inversely proportional to the inductance. The average current in the inductor must be equal to the DC current through the load. That is,

$$\langle i_L \rangle = I_o = \frac{V_o}{R}$$

$$\begin{cases} I_{L,\max} = I_o + \dfrac{\Delta i_L}{2} \\ I_{L,\min} = I_o - \dfrac{\Delta i_L}{2} \end{cases} \Leftrightarrow \begin{cases} I_{L,\max} = \dfrac{V_o}{R} + \dfrac{V_o}{2L}(1-D)T_s \\ I_{L,\min} = \dfrac{V_o}{R} - \dfrac{V_o}{2L}(1-D)T_s \end{cases}$$

Now we determine the minimum inductance needed for the system to stay in CCM by making $I_{L,min} = 0$. This yields

$$L_{\min} = \frac{1}{2}\frac{1}{f_s}(1-D)R = \frac{1}{2}\frac{1}{f_s}\frac{V_i - V_o}{V_i}\frac{V_o}{I_o}$$

$$as \;\; I_o = I_{L,\min} + \frac{\Delta i_L}{2} \;\wedge\; I_{L,\min} = 0 \;\; \therefore \;\; I_o = \frac{\Delta i_L}{2}$$

$$\boxed{L_{\min} = \frac{1}{f_s}\frac{V_i - V_o}{V_i}\frac{V_o}{\Delta i_L}} \tag{4.13}$$

Next we determine the expression for dimensioning of the output capacitor. Capacitors pass AC but block DC signals. We can then approximately assume that the entire ripple component (AC) of $i_L$ flows through the capacitor, and its average component (DC) flows through the load resistor; that is – the capacitor is used to decouple AC form DC signal components. Thus $i_C$ is equal to $i_L$ minus its DC component. The shaded area in figure 4.10 represents an additional charge $\Delta Q$

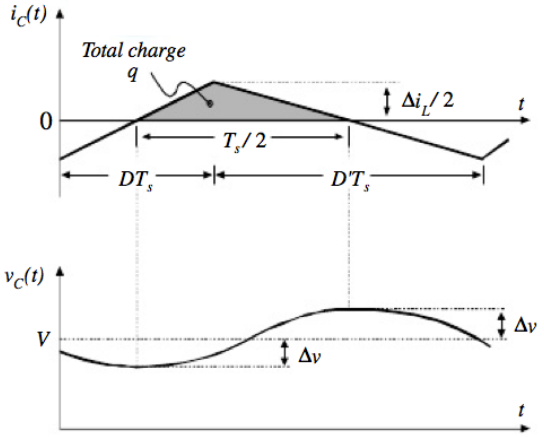


**Figure 4.10 – Output voltage ripple in a step-down converter. Note that $i_C = C\,dv_C/dt$ [5]**

So we can calculate the output voltage ripple $\Delta V_o$ with equation $\Delta Q = \mathrm{C} \cdot \Delta V$

$$\Delta V_o = \frac{1}{C}\left(\frac{1}{2}\cdot\frac{\Delta i_L}{2}\cdot\frac{T_s}{2}\right)$$

Using equation (4.12) we have,

$$\Delta V_o = \frac{1}{8C}\frac{V_o}{L}(1-D)T_s^2$$

$$C = \frac{1}{8}\frac{1}{\Delta V_o/V_o}\frac{1}{f_s^2}\frac{V_i - V_o}{V_i} \tag{4.14}$$

$$\boxed{\frac{\Delta V_{out}}{V_{out}} = \frac{\pi^2}{2}(1-D)\left(\frac{f_c}{f_s}\right)^2} \tag{4.15}$$

Which is the expression for the output voltage ripple, where $f_s$ is the switching frequency and $f_c$ is the corner frequency of the LC low pass filter

$$f_c = \frac{1}{2\pi\sqrt{LC}}$$

Equation 4.15 shows that the voltage ripple can be minimized if the corner frequency of the LC filter is chosen to be much smaller than the switching frequency, that is $f_c \ll f_s$.

### 4.3.5 Current and Voltage Measurement

As was described in the previous section, seeing that the components are not ideal, the output of the Buck Converter in practice will not be ripple free. There will be some noise associated with the switching, with the same frequency. In order to determine the power delivered to the membrane and to give the feedback information that changes the Duty Cycle of the switch to achieve a constant output current, we need to determine the values of current and voltage that the Buck Converter feeds. This task is performed by the microprocessor's 12-bit ADC module. But for this measurement to work flawlessly, we need to filter this switching noise and amplify the signal so the values to be read fall in the ADC reference voltages.

Keeping in mind the same hands on spirit, we need to determine the expressions that enable the dimensioning of the filters. Figure 4.11 shows the filter chosen for this purpose. It was developed using Sallen-Key topology, valued for its simplicity and has a non-inverted output. It is a second order filter for better attenuation, and it is Low-Pass in order to block the frequency of the noise introduced by the switching.

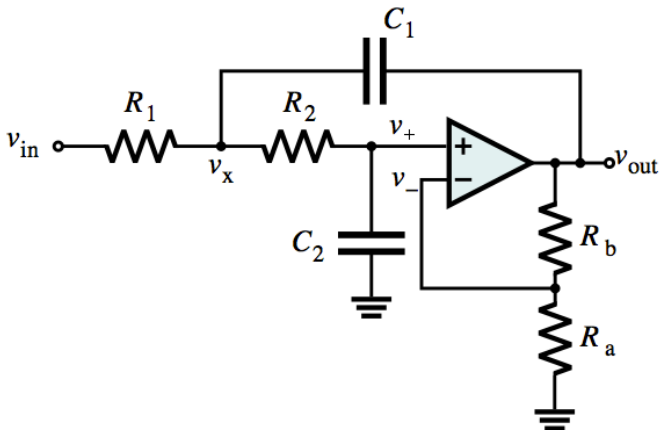


**Figure 4.11 – 2nd Order Low Pass Sallen-Key Filter**

Lets determine the transfer function for this filter. We can start by noticing that $R_a$ and $R_b$ constitute a voltage divider for $v_{out}$, so we can determine $v_-$ (as a function of $v_{out}$)

$$\frac{v_{out} - v_-}{R_b} = \frac{v_-}{R_a} \Leftrightarrow v_- = \frac{1/R_b}{1/R_a + 1/R_b} v_{out} \Leftrightarrow v_- = \frac{R_a}{R_a + R_b} v_{out}$$

We can further notice that $R_2$ and $C_2$ constitute a low pass filter for $v_X$, so we can determine $v_+$ (as a function of $v_X$)

$$\frac{v_X - v_+}{R_2} = \frac{v_+}{1/sC_2} \Leftrightarrow v_+ = \frac{1/R_2}{1/R_2 + \frac{1}{1/sC_2}} v_X \Leftrightarrow v_+ = \frac{1/sC_2}{R_2 + 1/sC_2} v_X \Leftrightarrow v_+ = \frac{1}{1 + sR_2C_2} v_X$$

If we consider the operational amplifier to be ideal, then $v_+ = v_-$, both these equations can be equalled, yielding $v_X$ as a function of $v_{out}$

$$\frac{1}{1+sR_2C_2}v_X = \frac{R_a}{R_a+R_b}v_{out} \Leftrightarrow v_X = \left(1+sR_2C_2\right)\frac{R_a}{R_a+R_b}v_{out}$$

Now we can apply Kirchhoff's current law to $v_X$ node

$$\frac{v_{in}-v_X}{R_1} = \frac{v_X - v_{out}}{1/sC_1} + \frac{v_X - v_+}{R_2}$$

$$\Leftrightarrow \frac{1}{R_1}v_{in} + sC_1v_{out} = \left(\frac{1}{R_1}+\frac{1}{R_2}+sC_1\right)v_X - \frac{1}{R_2}v_+$$

If we substitute here the equations above, this equation becomes

$$\frac{1}{R_1}v_{in} + sC_1v_{out} = \left(\frac{1}{R_1}+\frac{1}{R_2}+sC_1-\frac{1}{R_2}\frac{1}{1+sR_2C_2}\right)v_X$$

$$\Leftrightarrow \frac{1}{R_1}v_{in} + sC_1v_{out} = \left(\frac{1}{R_1}+\frac{1}{R_2}+sC_1-\frac{1}{R_2}\frac{1}{1+sR_2C_2}\right)\left(1+sR_2C_2\right)\frac{R_a}{R_a+R_b}v_{out}$$

$$\Leftrightarrow \frac{1}{R_1}v_{in} = \left[\left(\frac{1}{R_1}+\frac{1}{R_2}+sC_1+\frac{1}{R_2}\frac{1}{1+sR_2C_2}\right)\left(1+sR_2C_2\right)\frac{R_a}{R_a+R_b}-sC_1\right]v_{out}$$

$$\Leftrightarrow \frac{v_{in}}{v_{out}} = \left(1+\frac{R_1}{R_2}+sR_1C_1-\frac{R_1}{R_2}\frac{1}{1+sR_2C_2}\right)\left(1+sR_2C_2\right)\frac{R_a}{R_a+R_b}-sR_1C_1$$

$$\Leftrightarrow \frac{v_{in}}{v_{out}} = \left(1+sR_2C_2+\frac{R_1}{R_2}+sR_1C_2+sR_1C_1+s^2R_1R_2C_1C_2-\frac{R_1}{R_2}\right)\frac{R_a}{R_a+R_b}-sR_1C_1$$

$$\Leftrightarrow \frac{v_{out}}{v_{in}} = \frac{\frac{R_a+R_b}{R_a}}{1+sR_2C_2+sR_1C_2+s^2R_1R_2C_1C_2-sR_1C_1\left(1-\frac{R_a+R_b}{R_a}\right)}$$

$$\Leftrightarrow \boxed{H(s) = \frac{\frac{R_a+R_b}{R_a}}{s^2R_1R_2C_1C_2+s\left[R_1C_2+R_2C_2+R_1C_1\left(-\frac{R_b}{R_a}\right)\right]+1}} \qquad (4.16)$$

Which is the transfer function for the filter in figure 4.11. The standard form of a second-order, low-pass filter is given as

$$H_{LP}(s) = \frac{A_0}{\left(\frac{s}{\omega_0}\right)^2+\frac{1}{Q}\frac{s}{\omega_0}+1}$$

Where $\omega_0 = FSF(2\pi f_c)$ is the normal frequency and FSF is the frequency scaling factor. From this we can determine the DC gain $A_0$, the corner frequency $f_c$ (defined as the frequency that corresponds to a -3dB attenuation – approximately half the power) and the quality factor $Q$. We finally arrive to the expressions that give us the possibility to perform the dimensioning of the filters:

$$A_0 = \frac{R_a + R_b}{R_a} \tag{4.17}$$

$$f_c = \frac{1}{FSF}\frac{1}{2\pi\sqrt{R_1 R_2 C_1 C_2}} \tag{4.18}$$

$$Q = \frac{\sqrt{R_1 R_2 C_1 C_2}}{C_2\left(R_1 + R_2\right) - R_1 C_1\left(R_b / R_a\right)} \tag{4.19}$$

Where the quality factor $Q$ determines the amount of damping of the oscillations. If

- $Q < 1/2$ the system is *Overdamped* – the system does not oscillate. It tends asymptotically to a final value. The smaller the $Q$ the slower it reaches this value.
- $Q > 1/2$ the system is *Underdamped* – the system oscillates with a decay of amplitude, towards a stable final value. The bigger the $Q$ the slower it reaches this value.
- $Q = 1/2$ the system is *Critically damped* – it's the limit between the two situations above. Corresponds to the fastest response.

This dimensionless parameter defines the filter type. For this implementation I chose the Bessel type, which is the implementation that is optimized for flattest group delay. This means that the filter has almost linear phase response and excellent transient response to a step function, which is the input of our Buck Converter. This response is shown in figure 4.12. As one can se, there is no overshooting, nor nay oscillation

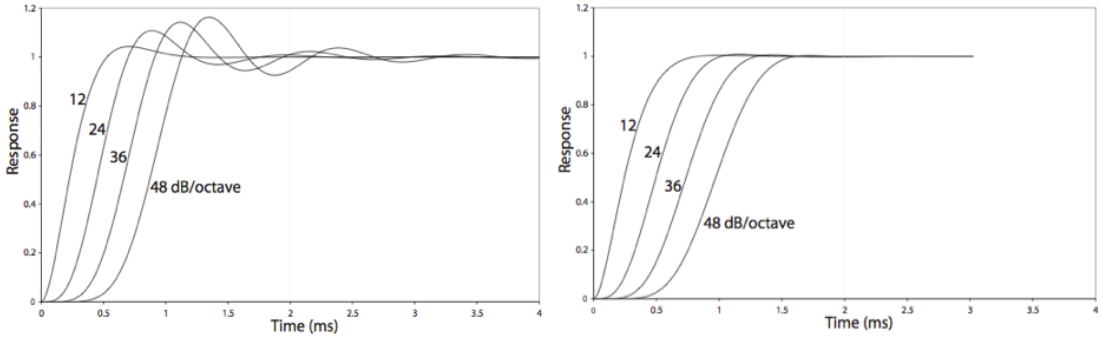


**Figure 4.12 – (a) Butterworth step response (b) Bessel step response**

For second order Bessel type filters the quality factor and frequency scaling factor are

$$Q = \frac{1}{\sqrt{3}} = 0.57735$$

$$FSF = 1.2736$$

Now we have all we need to build the DC-DC converter.

### 4.3.6 Power Converter Dimensioning

The Power from the PV array turned out to be very small, and was not enough to polarize the Electrolyzer with the desired current densities. The solution was to use an additional power source, capable of delivering the appropriate currents. With it, one can measure the current delivered to a constant load by the PV array, multiply it by a factor and use this value as the desired output in the feedback system of the buck converter. This factor is chosen so that when the PV array is delivering maximum power (maximum irradiance of the LED panel), the output of the buck converter is feeding the Electrolyzer with the maximum current of the new power source – 2A.

For the 2A current the electrolyzer imposes a 1.7V voltage but the source is rated at 9V. So $V_i = 9\,V$ and $V_o = 1.7\,V$. Choosing a maximum current ripple $\Delta i_L = 0.6\,A$ (30% of the maximum value); and a switching frequency of $f_s = 50kHz$, we can use equation (4.13) to get the value $L_{min} = 46\,\mu H$. In the lab the closest inductance value was $\boldsymbol{L = 74\,\mu H}$, that corresponded to a 19% ripple, so this was the inductor used in the setup. Now what we need to get the capacitance value, as was established above when analysing equation (4.15), is choose a corner frequency much smaller than $f_s$. The capacitance needed for $f_c = 5\,kHz$, a factor of 10 (it should not be a lot smaller because the time constant of the LC filter would then be very large and we want a system with fast responses so that the feedback loop works flawlessly), is $C_{min} = 13.7\,\mu F$. If we use the value $\boldsymbol{C = 10\,\mu F}$, which is not much smaller, the voltage ripple, according to equation (4.15) is approximately 5.7%, which is perfectly acceptable.

For the dimensioning of the filters, equations (4.17), (4.18) and (4.19) where used. The gains were selected so that both filters had an output voltage range equal to the microprocessors ADC input range. This way the measurement's precision is maximized. As we are dealing with DC power, both filters were dimensioned to have a 10Hz cut frequency, in order to attenuate most of the noise. The values obtained are shown in figure 4.13.

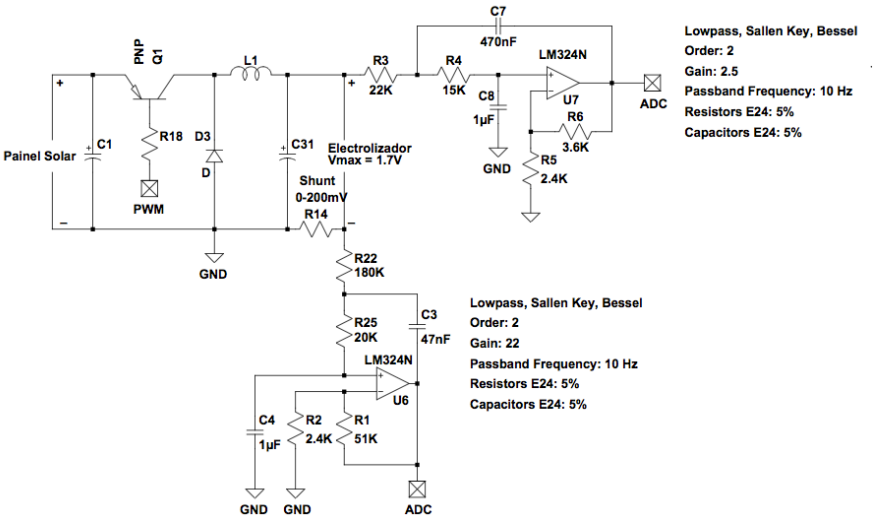


**Figure 4.13 – Design and dimensioning of the Power Conversion Unit**

This circuit was tested in PSpice, and the results will be presented in chapter 5.

Actually, in a more advanced stage of the project, this filter arquitecture was deemed not useful for differential measurements, so it was substituted by a simpler differential arquitecture with the same gain. Filter calibration is performed in chapter 6.

### 4.3.7 Control Algorithm

As was previously discussed, the buck converter measures the output current, which is called the *controlled variable*; compares it with a desired value, called the *set point* (defined the current delivered by the PV array to a fixed load); and the manipulates the duty cycle in a way that will hold the controlled variable at its set point when the set point changes or when a disturbance changes the process. The duty cycle is therefore called the *manipulated variable*. In order to decide what change to inflict on the manipulated variable, based on the controlled variable, the system needs a control algorithm. There are many such algorithms, but the most common is known as the *PID algorithm* (Proportional, Integral and Derivative), so this was the one used in the buck converter.

## 4.4 Hydrogen Storage

To measure the volume of Hydrogen stored in the column a sensor was built, composed of an oscillator whose frequency of oscillation depends on a variable capacitor. If a covering of a conducting material is applied on the outside of the cylindrical tank and a copper wire is introduced on the inside by the axis, with the proper connections we have a capacitor. As hydrogen is formed and makes its way to the top the tank, the column of water is 'pushed' down. As liquid water and gaseous hydrogen have very different dielectric constants, the capacitance of our hand-made capacitor changes with the height of the water column. Now the period of oscillation also varies, and if we measure it with the microprocessor's Input Capture mode, by choice of a calibration constant we can determine the height. To indicate when the tank is full of water, a simple mechanism uses the conducting properties of water to close a circuit, flaring an interruption in the microprocessor. This will be useful for calibration.

The circuit shown in figure 4.14 represents the Astable mode of operation of the oscillator NE555. The corresponding graph demonstrates its operation in the same mode.

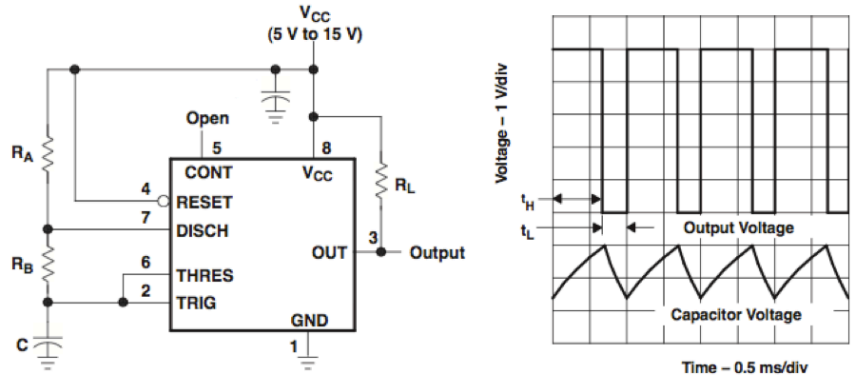


**Figure 4.14 – NE555 oscillator its Astable mode of operation and its typical output [Taken from the specification sheet of the NE555]**

We begin with the general equation for capacitors

$$v_C(t) = v_C(\infty) = \left[v_C(\infty) - v_C\left(0^+\right)\right]e^{-\frac{t}{\tau}}$$

The equations corresponding to a charging and discharging of the capacitor are given by,

$$v_{C_{char}}(t) = V_{CC}\left(1 - \frac{2}{3}e^{-\frac{t}{(R_A - R_B)C}}\right)$$

$$v_{C_{dis}}(t) = \frac{2V_{CC}}{3}e^{-\frac{t}{R_B C}}$$

By default, when there is no external voltage applied in pin CONT, the trigger and threshold voltages are $v_{trig} = 1/3\,V_{CC}$ and $v_{thres} = 2/3\,V_{CC}$. So now we can calculate the time needed for charging and discharging the capacitor,

$t_{char}$ :

$$v_{C_{char}} = v_{thres} \Leftrightarrow V_{CC}\left(1 - \frac{2}{3}e^{-\frac{t}{(R_A - R_B)C}}\right) = \frac{2}{3}V_{CC}$$

$$\Leftrightarrow e^{-\frac{t}{(R_A - R_B)C}} = \frac{1}{2}$$

$$\Leftrightarrow t_{char} = (R_A - R_B)C\ln 2$$

$t_{dis}$ :

$$v_{C_{dis}} = v_{trig} \Leftrightarrow \frac{2}{3}V_{CC}e^{-\frac{t}{R_B C}} = \frac{1}{3}V_{CC}$$

$$\Leftrightarrow e^{-\frac{t}{R_B C}} = \frac{1}{2}$$

$$\Leftrightarrow t_{dis} = R_B C\ln 2$$

Finally we can determine the Duty Cycle (D) of the square wave produced by the NE555 oscillator.

$$D = \frac{t_{chat}}{t_{chat} + t_{dis}} = \frac{(R_A + R_B)C\ln 2}{(R_A + 2R_B)C\ln 2} \Leftrightarrow D = 1 - \frac{R_B}{R_A + 2R_B}$$

As well as its oscillation period given be the sum of the charging and discharging times,

$$T_{osc} = (R_A + 2R_B)C\ln 2 \qquad (4.20)$$

One can deduct form (4.19) that if the value of C varies, the period and frequency of oscillation of the NE555 will also vary. So now, in order to establish the relation between the oscillation period and the height of the water

column, we still need to deduce the dependence of the column's capacitance on the latter parameter. To do this lets start by calculating the capacitance of a cylindrical capacitor in vacuum, as the one shown in figure 4.15

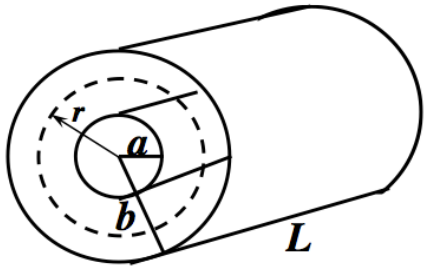


**Figure 4.15 – Cylindrical Capacitor**

Lets start by applying the Gauss Law in the space $a < r < b$

$$\oint_{GS} \vec{E} \cdot \vec{n} = \frac{\sum q_{\text{int}}}{\varepsilon_0} \Leftrightarrow \left|\vec{E}\right| 2\pi r L = \frac{Q}{\varepsilon_0} \Leftrightarrow \left|\vec{E}\right| = \frac{Q}{2\pi r L \varepsilon_0}$$

Next, we determine the potential difference,

$$V_a - V_b = -\int_b^a \vec{E} \cdot \vec{dl}\, dr = -\int_b^a \left|\vec{E}\right| dr = -\int_b^a \frac{Q}{2\pi r L \varepsilon_0} dr = -\frac{Q}{2\pi L \varepsilon_0} \left[\ln r\right]_b^a = \frac{Q}{2\pi L \varepsilon_0} \ln\left(\frac{b}{a}\right)$$

Now I use the relation between capacitor's charge and the potential difference at its terminals and deduce the final relation

$$C = \frac{Q}{V_a - V_b} = \frac{Q}{\frac{Q}{2\pi L \varepsilon_0} \ln(b/a)} = \frac{2\pi\varepsilon_0}{\ln(b/a)} L$$

In my experimental setup the capacitor is filled with water, which means there are two capacitors: one with the dielectric constant of water, the other with the dielectric constant of air (approximately equal to vacuum). They share the anode and the cathode, so, they are in parallel. The capacitance of the parallel of two capacitors is the sum of their capacitances, so, if $d_{water}$ is the height of the water column, and $d_{air} = L - d_{water}$ the height of the air column, then we have

$$\begin{aligned} C &= C_{air} + C_{water} \\ &= \frac{2\pi\varepsilon_{air}}{\ln(b/a)} d_{air} + \frac{2\pi\varepsilon_{water}}{\ln(b/a)} d_{water} \\ &= \frac{2\pi\varepsilon_0}{\ln(b/a)} (L - d_{water}) + \frac{2\pi\varepsilon_0 \varepsilon_{r_{water}}}{\ln(b/a)} d_{water} \\ &= \frac{2\pi\varepsilon_0}{\ln(b/a)} \left[L + (\varepsilon_{r_{water}} - 1) d_{water}\right] \\ &= X_1 + X_2 \cdot d_{water} \end{aligned} \qquad (4.21)$$

Where $X_1$ and $X_2$ are constants. Equation (4.21) shows that there is a linear relation between water height and capacitance. Equation (4.20) shows that there is a linear relation between capacitance and the oscillation period. By substituting (4.21) on (4.20) we can finally conclude that **there is a linear correspondence between the height of the water in the cylinder and the period of oscillation of the NE555 circuit**, which allows us to measure the level of the water with the Input Capture feature of the microprocessor by a simple multiplicative calibration constant.

## 4.5 Grid

As discussed in the first chapter, energy consumption is not constant. It is constantly changing within the hours in a day, and the days in a year. From the viewpoint of the Power Plant this means the load resistance is continuously changing. Well, the final consumer in the prototype will be represented by a light bulb, which has a constant I-V characteristic, so for a given output of the fuel cell, its resistance is constant. But as current rises, so does the temperature in the radiating filament, and consequently the resistance increases. This means the I-V characteristics of the bulb is not linear so the grid's load fluctuations can be mimicked in the prototype by the introduction of another power converter between the fuel cell and the load. This converter will change the operation point of the bulb by stepping down the voltage that leaves the fuel cell.

The operation of the prototype will be controlled by the user through a programed microcontroller that sends and receives signals and variable values. Well, for this we will use a generic controller board called *PICNODE* (described in chapter 5), as will be explained in the following chapter. But as the name suggests, this board does not have the controlling components specific to this particular project. So I designed and manufactured the Prototype Controller Board (also described in the next chapter) that connects to *PICNODE*.

# 5 ENGINEERING DEVELOPMENT TOOLS

The design of the prototype was made possible by the help of various development tools. These were used in throughout various stages of the work and will be shortly described in this chapter.

## 5.1 3D Mechanical Modelling

The need for a 3D representation of the prototype arose right from the beginning. To make it, I used a 3D mechanical Computer-Aided Design (CAD) program called *SolidWorks 2012*. A model of the prototype is depicted in figure 5.1.

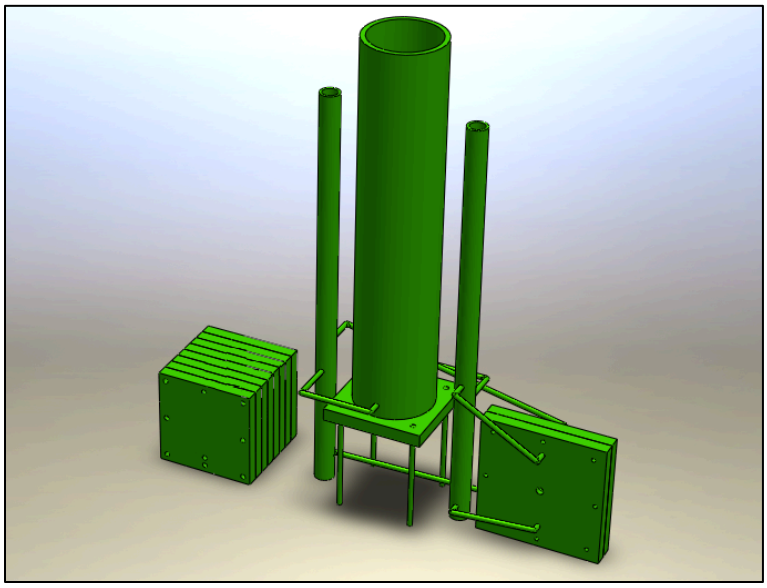

**Figure 5.1 – *SolidWorks 2012* 3D representation of the prototype**

The electrolyzer had to be built from scratch. The membrane was purchased online, but the casing had to be designed in with this program because of its high specificity. The material chosen was Acrylic because it does not react with hydrogen, it is easy to work and transparent (which is required for the user to be able to see the bubbles of hydrogen so as to get a better idea of what is going on). The eight holes close to the outside rim are destined for placement of the screws that attach this Acrylic plate to another one to form the casing of the membrane. An opening was carved in the middle for the membrane and the metal lattice (that helps deliver the electric power to the membrane) to fit in. Around this central area a very thin trench was opened where a rubber ring can be introduced to seal the interior. The hexagonal form carved in the centre is destined for a brass screw that transports the electric power from the exterior to the interior of the electrolyzer. Finally hydrogen will leave by the other two holes (one above and one below the hexagonal screw). To manufacture this part I contacted 'FabLab EDP', a fabrication laboratory, equipped with digital fabrication tools for rapid prototyping supported by open source software [26]. It is completely free and opened for the general public. The electrolyzer casing was manufactured by a CNC miller. The design is shown in figure 5.2.

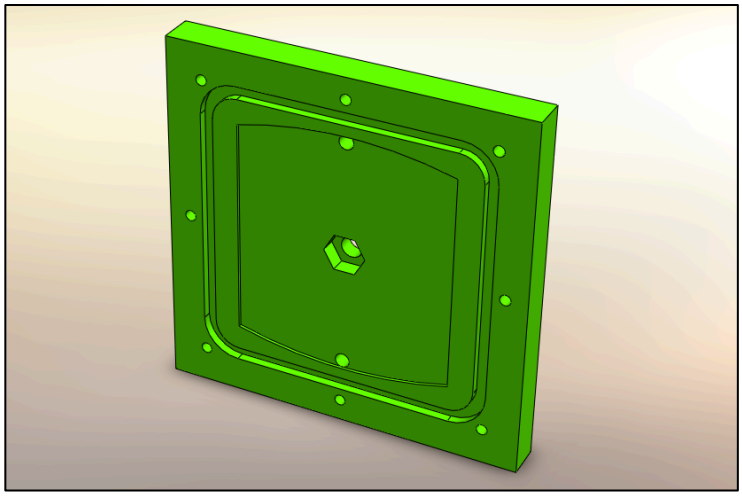

**Figure 5.2 – *SolidWorks 2012* design of the acrylic casing for the electrolyzer membrane**

## 5.2 Software Development

As was referenced numerous times in preceding chapters, in order for the prototype to be autonomous, it needs a central processing unit that performs all kinds of electrical and mechanical operations required. In other words, it needs a microcontroller. For controlling and acquisition purposes I used the *PICNODE* board, developed by researchers at CNF (Nuclear Fusion Centre at Instituto Superior Técnico) [27]. This board is a generic controller based on Microchip's dsPIC30F4013 microcontroller, suitable for real-time control and data acquisition. In order to program this microcontroller, *MPLAB IDE v8.84* was the elected choice. It is a software program to develop applications for Microchip microcontrollers. The complete C program is presented in Appendix A. In order for the user to control the prototype, he has to be able to command instructions (e.g. start/end electrolysis, start/end reconversion) and to introduce the values of some variables (e.g. LED intensity, storage time). For this purpose the RS232 serial port of the board is connected a computer. This connection is managed by the serial console client *PuTTY*. Some of the most important features of the microcontroller program will now be presented:

- **Multiple input scan ADC** – five of the board's IO pins are simultaneously being read by the 12bit ADC. Two of them are measuring the current and voltage values delivered to the electrolyzer to determine the total power and to send feedback to the buck converter, two others are doing the same for the light bulb and the final one measures the voltage delivered to a fixed load by the PV array.
- **Software PWM with bit equidistribution** – Three of the board's IO pins are sending PWM signals to control the intensity of each colour in the LED panel. These PWMs software programed so that it could be able to perform equidistribution – instead of incrementing the duty cycle continuously throughout the PWM period, the algorithm divides the period into 32 parts and every increment is placed so as to be optimally distributed. Let us use an example to better understand the algorithm. If the Duty Cycle is chose to be 50%, in a normal PWM implementation, the first half of the period would be set to digital one while the second to digital zero, which would mean the LED would shine and then turn of, producing a small flicker even with the relatively high frequencies used. With this algorithm the period would be filled of 16

sequences of digital one followed by digital zero. This feature is important in order to reduce the flickering of the LEDs, providing a more stable irradiance to the PV cells.

- **Output Compare Mode PWM** – Two of the board's IO pins are providing PWM signals that control the switching times of the buck converters. Duty cycles are determined by the comparison between the values being read by the ADC module and their desired output values.
- **Multiple Input Capture** – Two of the board's IO pins are determining the period of the oscillating signal that comes from the NE555 oscillators. As discussed above these periods are used to determine the height of the water level at each storage column.
- **External Interrupt** – One of the board's IO pins is programed to flare an interruption every time the water level in the storage columns reaches maximum capacity. As discusses above this is very useful for calibration purposes.
- **User commanded output** – One of the board's IO pins is programed to be set to VCC when the user demands it. This command will deliver power to both air valves that are keeping the hydrogen and oxigen stored and they will open so as to initiate fuel cell's activity.

## 5.3 Circuit Testing

After the theoretical designing and dimensioning of the electrical circuits, and before building it in its final real application, as their complexity increased, finding a way to test it became crucial. To perform this task *OrCAD Capture* and *PSpice* (both tools available in Cadence Design System's proprietary software tool suite *OrCAD Release 16.3*) were used. The former was used to create the schematic and choose component values, while the latter was used for the actual simulation of the aforementioned schematic. The Power Converter module was tested in this manner. Figure 5.3 one shows the circuit schematics edited on *OrCAD Capture* while figures 5.4 and 5.5 show the results of the simulation preformed by *PSpice*.

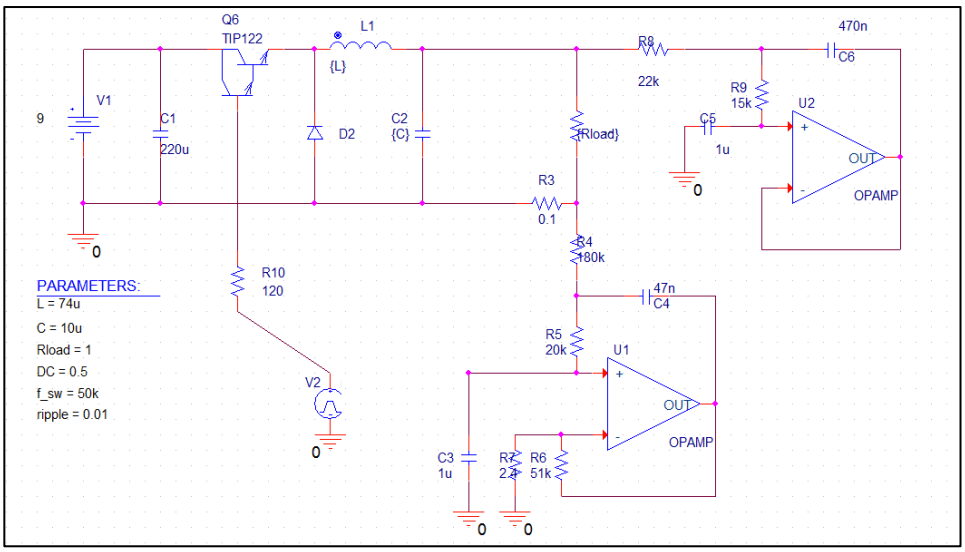


**Figure 5.3 – *OrCAD Capture* schematics of the Power Converter Module**

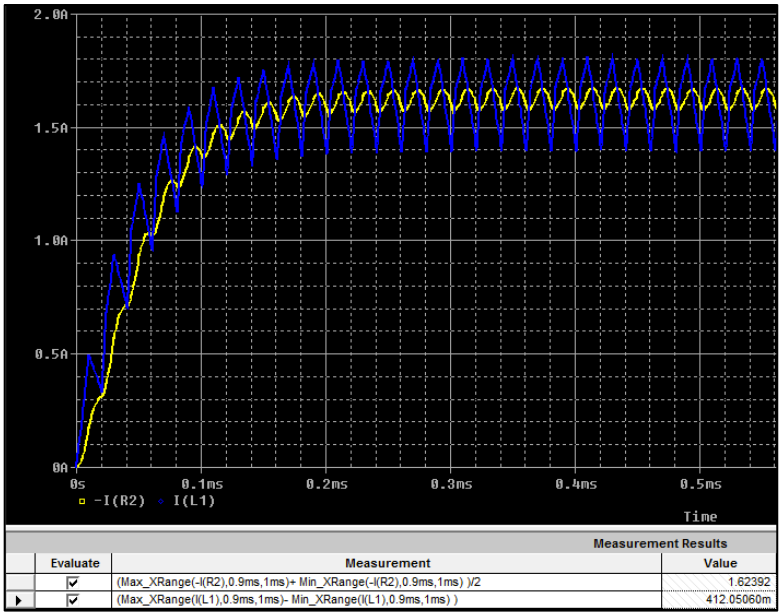


**Figure 5.4 – *PSpice* simulation result. The blue line is the current in the inductor and the yellow line is the current in the load.**

Notice that as predicted in the previous chapter, the current in the inductor (blue line) assumes a triangular and continuous form, even though its input is discontinuous. The smoothened shape of the current in the load (yellow line) evidences the work of the output capacitor. Notice the values in the bottom right corner of figure 5.4. They are the average current on the inductor and its ripple size. Dividing the latter by the former, we get $\Delta i_L / i_L = 25\%$ which is less that the 30% value we established in the previous chapter as the maximum current ripple in the inductor.

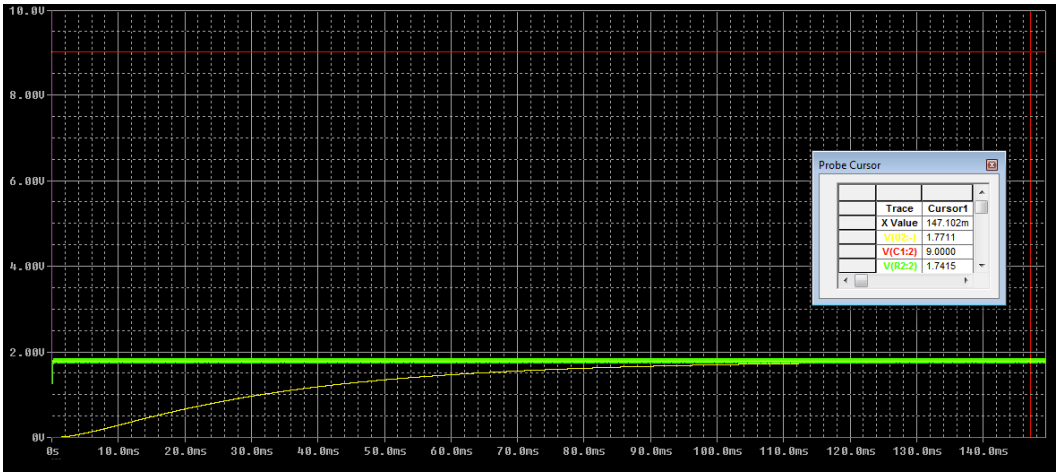


**Figure 5.5 – *PSpice* simulation result. Red is the input voltage, green is the load voltage and yellow is the voltage in the Sallen-Key Filter**

Notice that the input voltage (in red) is stepped down to the desired output value (in green). In order to obtain a low cut frequency filter, the time constant will have to be considerable. As shown in figure 5.5, the voltage at the output of the filter, which will be the input of the ADC, only stabilizes around 120ms (notice that for the purpose of

this simulation the filter does not have any gain). It's seems a long time, but for the time scale of this application it does not have any hazardous implications.

We can see that the Power Converter module is working as it was intended to. Now we need to fabricate it.

## 5.4 PCB Design

Finally, after successfully passing the initial phases of designing, dimensioning and testing, the electric circuit is ready for implementation in Printed Circuit Board (PCB) format. For this purposes, I chose the freeware program *EAGLE 5.11.0* that contains a schematic editor and a PCB layout editor that allows back annotation with the schematic editor, which means that every component that is placed or connection that is made in one of the sides, is updated to the other. The PCB layout editor has an auto-routing feature, but due to some bad experiences in the beginning, I chose to hand-route all the traces. After the layout is complete, the output file has to be converted to the industry standard file format, the *Gerber* format. These files describe the images of the various layers in a PCB (e.g. drills holes, board outline, copper layers). With the program *CircuitCAM 3.2* one can import these *Gerber* files and create the final usable format *.LMD*, which can then read by *Board Master,* the software that supports the PCB printer. Finally, the machine is run and the board is manufactured

For this work, three PCBs where manufactured with this process: the Height Sensor, the LED Panel and the Prototype Controller Board. Their layout schematics are presented in Appendix B. The Height Sensor is very simple, and apart from the extreme difficulty in soldering closely packed 252 LEDs (top and bottom), the LED Panel is not conceptually difficult. So the only design that requires a more detailed description is the Prototype Controller Board. Its purpose is to serve as intermediary between that microcontroller and the prototype. It receives/delivers and processes signals from/to the system. Its functionalities are described shortly:

- **Power Converter Unit** – This unit is composed of two buck-converters. One receives the power from the source, and the regulating PWM signal from the microcontroller, regulates the former according to the latter and supplies it to the electrolyzer. The other one does the same from fuel cell to load. Each of them has two second order filters for measuring current and voltage. Another filter is used to measure the power delivered by the PV array. The signals from the filters are routed to the ADC inputs of the microcontroller.
- **LED Panel control** – It receives the power from the 48V source that supplies power to the 252 LEDs and redirects it to the Panel along with the three intensity controlling software-programed PWM signals.
- **Height Sensor control** – It supplies power to the sensors and redirects their oscillating signals to the input capture of the microcontroller.
- **Hydrogen Valves control** – It provides power to the valves to open them, at the user's command.
- **Storage tank full capacity check** – A powers the circuit used to determine when the water column is at its maximum level in the storage tank. When this happens the circuit generates an interruption signal. The board receives it and redirects it to the external interrupt input of the microcontroller.

# 6 RESULTS AND DISCUSSION

In order to evaluate the performance of the PV array and determine the power that it could be deliver, a study on its I-V characteristics was performed. The array was illuminated by the Sun on a clear day and tested for various load values. The results are shown in figure 6.1 and 6.2

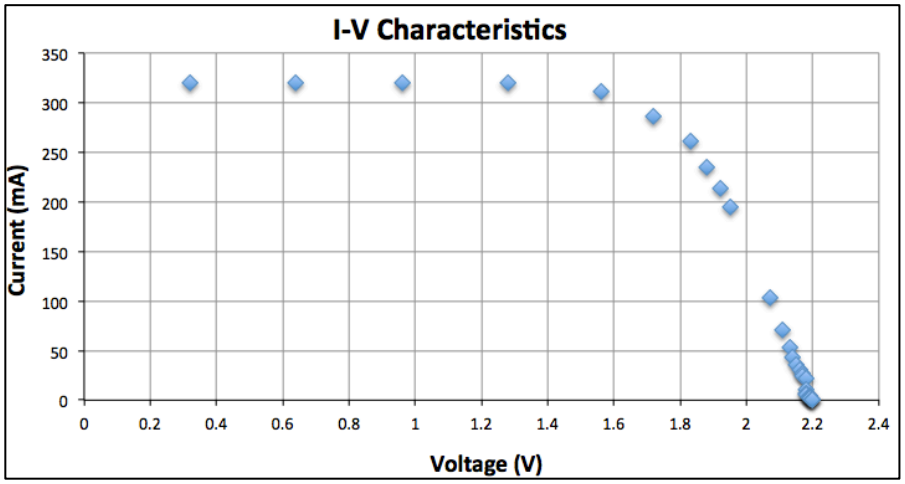


**Figure 6.1 – I-V Characteristics of the Solar Cell**

Theoretically, the characteristics should have yielded an open circuit voltage of $V_{oc} = 3V$ and a short circuit current of $I_{sc} = 200\,mA$. In fact, the values registered in figure 6.1 where $V_{oc} = 2.2\,V$ and $I_{sc} = 320\,mA$. The former was reduced and the later increased. According to the discussion in Chapter 3, this shows that the temperature effect affected the measurements. Figure 6.2 helps us determine the maximum power ratings.

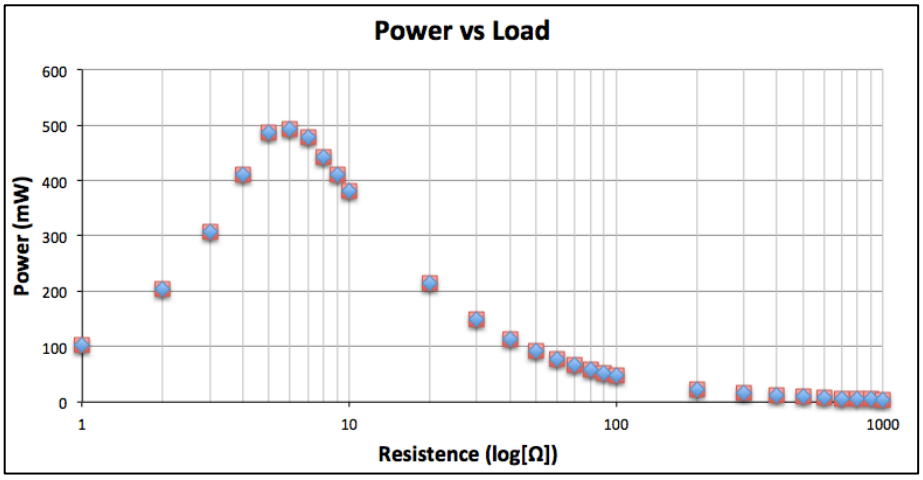


**Figure 6.2 – Total Power output of the PV array as a function of load resistance**

Figure 6.2 was derived from the I-V characteristics, and represents the power delivered to each load. It shows a distinctive maximum at $R_{load} = 6\,\Omega$. This corresponds to $I_{max} = 287\,mA$ and $V_{max} = 1.72\,V$. With these values

one can now evaluate the Fill Factor of the array – $FF = 0.287 \times 1.72 / 0.320 \times 2.20 = 0.70$. The standard value of resistance closest to this is 4.7 Ω, which is the value chose for the load of the PV panel in the setup.

To better understand the efficiency characteristics of the array, another experiment was performed. By varying the duty cycle applied to each colour of the LED panel, we can observe that the difference in the efficiency of conversion of the panel depends on the wavelength of the incident light,

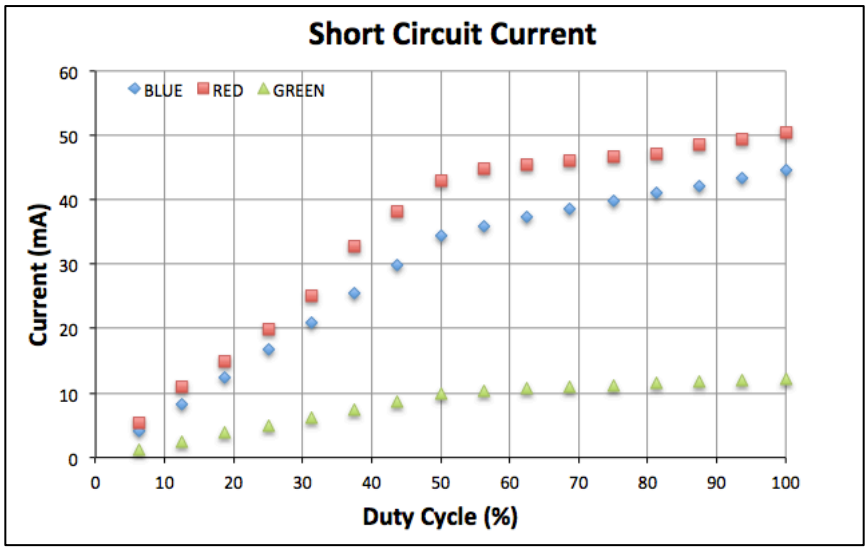


**Figure 6.3 – Short circuit current in the PV array produced by three different wavelengths delivered by the LED panel**

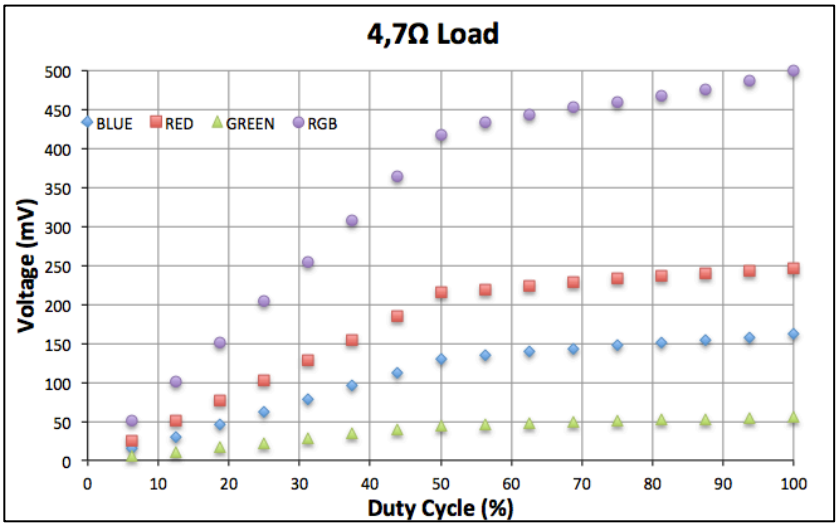


**Figure 6.4 – Voltage delivered to a 4,7 Ohm load by the PV array when illuminated by the LED panel**

The power delivered to each LED was calculated by measuring the current in each branch of the parallel arrangement for each colour. For the red LEDs (629 nm) the power was $P_R = 67{,}4\ mW$, for the green ones (525 nm) $P_G = 92{,}1\ mW$ and for the blue (465 nm) $P_B = 88{,}0\ mW$. As shown in figure 3.7, the spectral response of a typical amorphous silicon cell has a maximum at around 700-800 nm. And in the visible region it decreases with

the shortening of the wavelength. This means that blue should have a lower efficiency that green, but these results do not follow that pattern. Green LEDs have more power delivered to them when compared to the blue ones and, even so, they produce less power. But there is another factor that is not being taken into account and was not measured. The LEDs have different quantum efficiencies. This difference should explain this discrepancy.

In order to understand the range of voltages and currents I was going to work with, the I-V characteristics of the electrolyzer was also studied. Figure 6.5 shows its polarization curve.

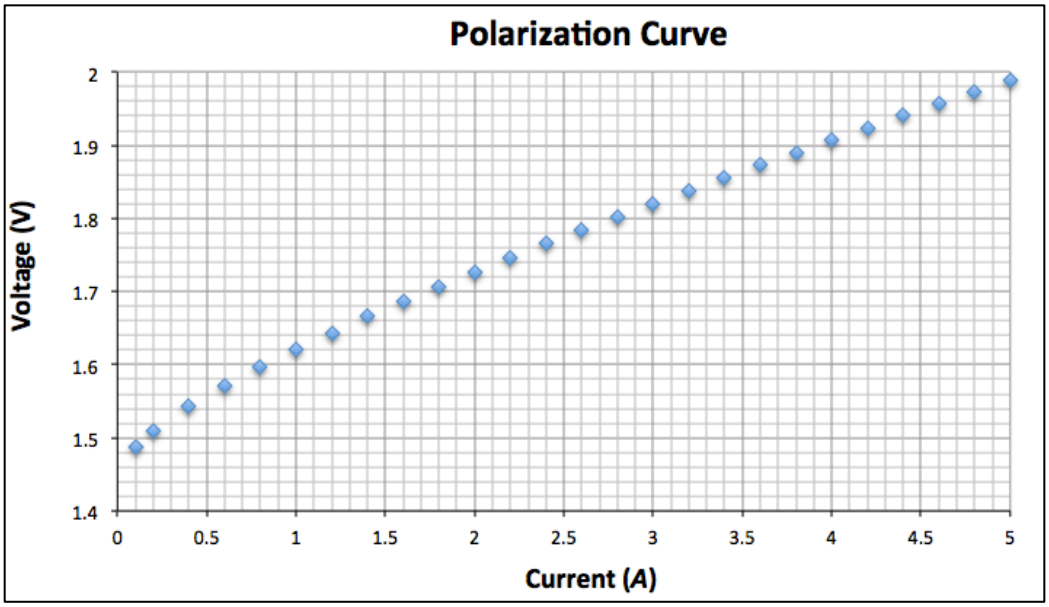


**Figure 6.5 – I-V Characteristics of the Electrolyzer**

Notice that in this range of current densities, the most important effect is the Ohmic effect, described in Chapter 3. This is evidenced by the approximately constant slope of the polarization curve. We can conclude from the picture 6.5 that the range of operation is $1.5 - 2.0\ V$ and $0.0 - 5.0\ A$.

## 6.1 Calibrations

In order for our PID algorithm to be able to manipulate the output variable (current or voltage), the relationship between duty cycle and this variable has to be known. These curves are presented next. The duty cycle is not in percentage but in actual period register units. The total period was set to 1500, but the values only included the range up until 700 (out of 1500) because this was the active range. The fitting curves where then used in the PID code to perform the conversion form Duty Cycle to Current.

a) b)

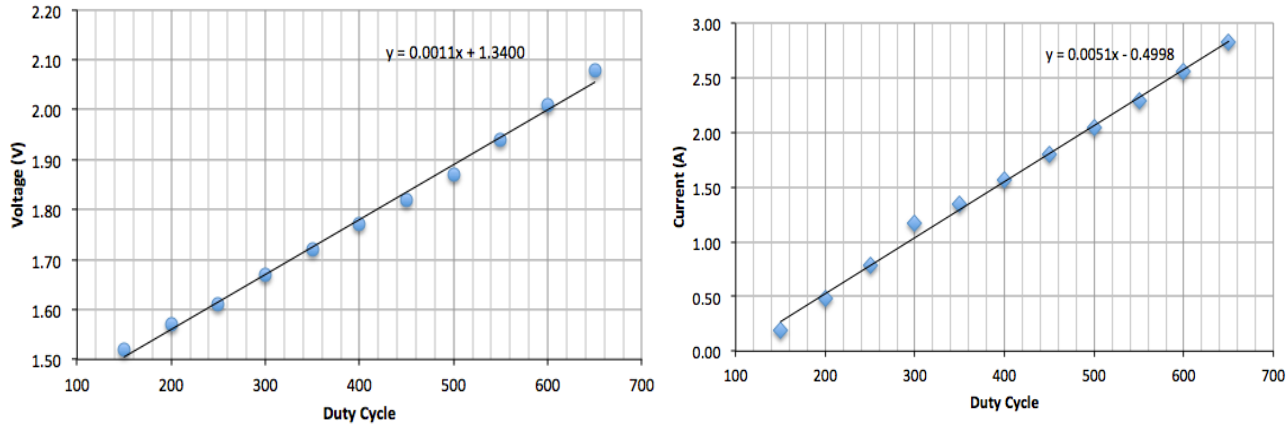


**Figure 6.7 – (a) Output Voltage and (b) Output Current as a function of duty cycle (in a 1500 scale). This is used by the controller algorithm to translate the controlled variable (current or voltage) into the manipulated variable (duty cycle) in order to reach the set point**

The filters that measured current and voltage had to be calibrated so that their precise gains could be measured. The calibration curves used to determine their actual gain are presented next.

a) b)

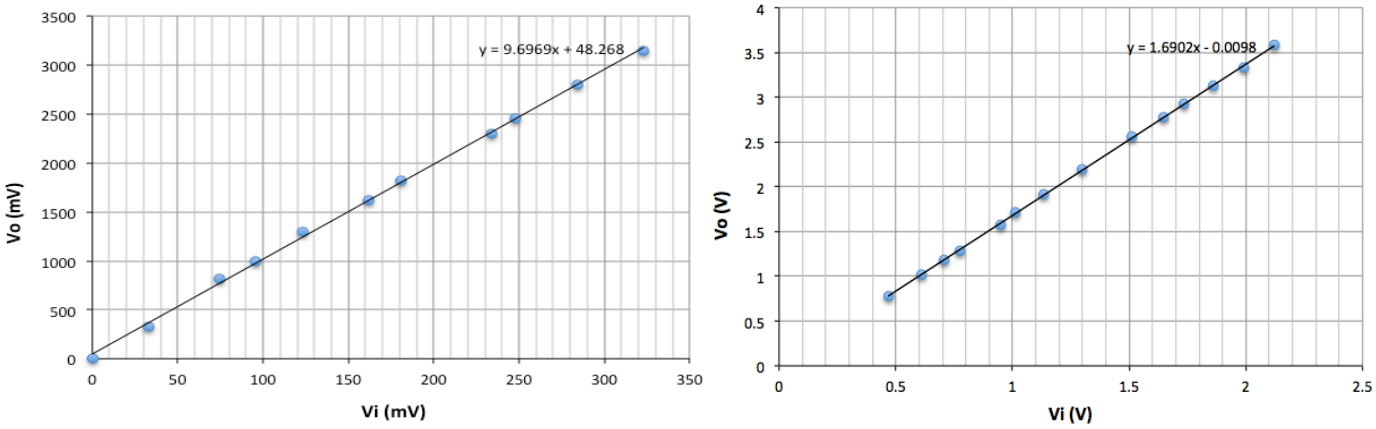


**Figure 6.8 – Calibration of the (a) current filter and (b) voltage filter that measure the power delivered to the electrolyzer by the buck converter**

The curves are very precisely defined, having small fitting errors. They show gains of 9.70 and 1.69 respectively.

Furthermore, the height of the water column had to be measured so another calibration was needed. Here an implementation problem arose. For practical reasons the inside electrode of the capacitor (the cathode) was made up of to different sections, so the capacitance changed at the boundary. To account for this problem, the height was calibrated in two separate curves. The result was as follows,

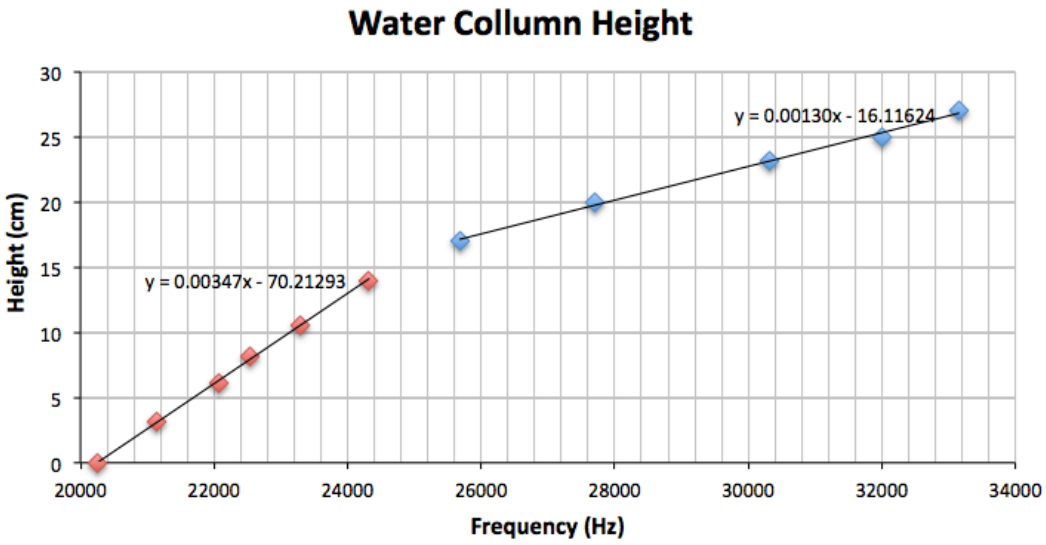


**Figure 6.9 – Water column height calibration curves**

## 6.2 Measurements

With all the filters and height sensors calibrated, finally measurements could be made. The ADC measured the current and voltage in order to calculate the total power delivered to the electrolyzer by our power source, while the height sensor measured the volume in real time and, consequently, the number of moles being stored. Figure 6.10 represents the filling up of the hydrogen storage tanks. The operation lasted for nearly two minutes.

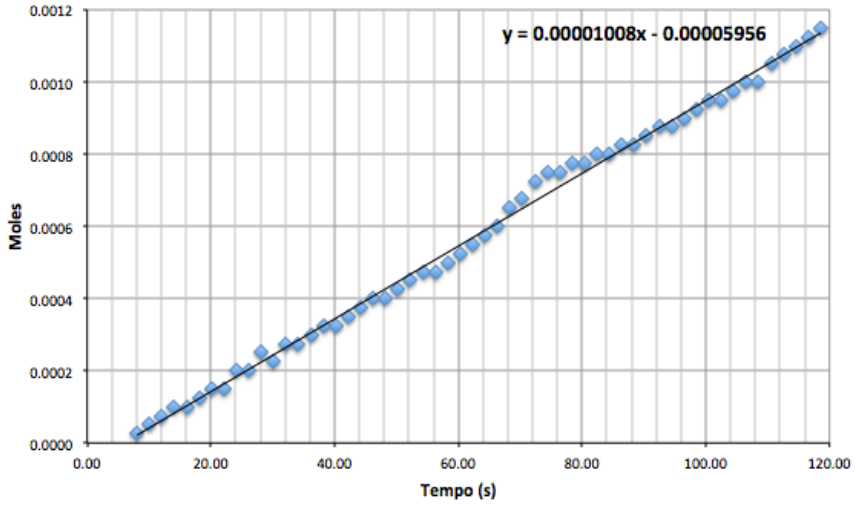


**Figure 6.10 – Real time measurement of the stored volume of the Hydrogen produced by electrolysis.**

The main goal of this measurement was to calculate the efficiency of the PEM electrolyzer. In section 2, the formulae needed to calculate the efficiency of a fuel cell were presented, but in fact the ones needed for the electrolyzer are closely related but not the same, mainly because it's the inverse process. As shown in [18], the current efficiency for relatively large current densities is almost 100% because the effects of diffusion of hydrogen

are dwindled. Thus we need not take in to account this effect. So the analysis will be centred on thermal and voltage efficiencies. The formula for the total efficiency of the electrolyzer is thusly

$$\eta_E \approx \eta_u$$

$$\eta_E = \frac{E_H}{u} = \frac{-\Delta\bar{h}_f / 2F}{u} = \frac{1.48}{u}$$

The efficiency was measured during the filling of the tanks, and the results are shown in figure 6.11,

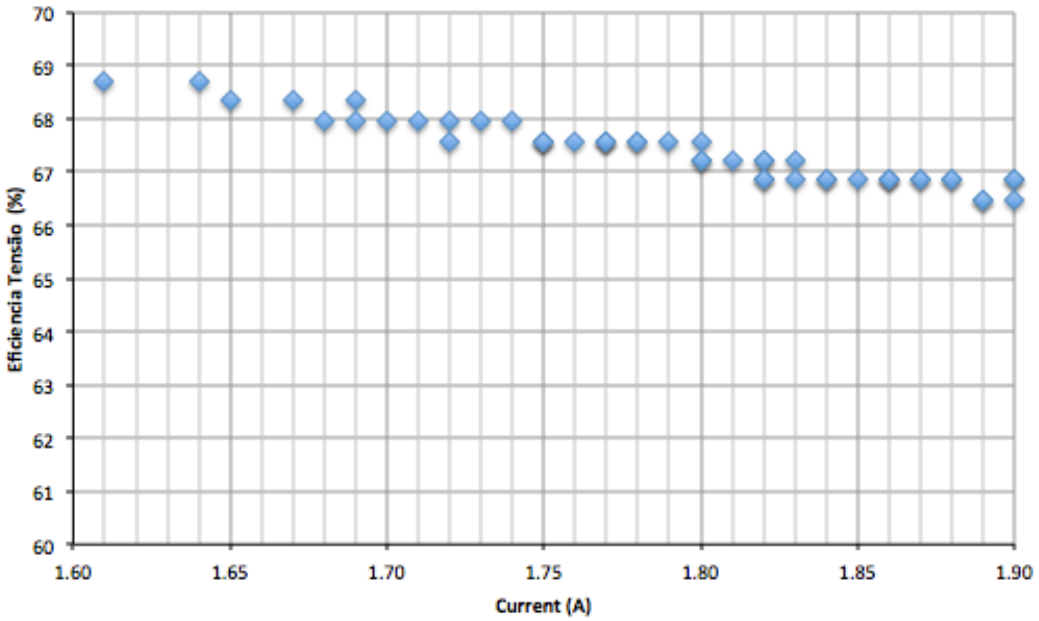


**Figure 6.11 – Real-time measurement of the total efficiency of the Electrolyzer**

The result is consistent with the expected values discussed in section 2. The small oscillations in the end are related to the variations in the delivered power introduced by the buck converter. One last remark will be made on the behaviour of the voltage efficiency. As the membrane is fed by the buck converter, its temperature varies and its demand for current grows larger. As more current is drawn, more losses start to occur so, to overcome them, the source has to deliver higher voltages. This has obvious repercussions on the efficiency as the operating voltage increases in reference to the reversible operating voltage. So as current increases the voltage efficiency decreases. This behaviour is illustrated in figure 6.12

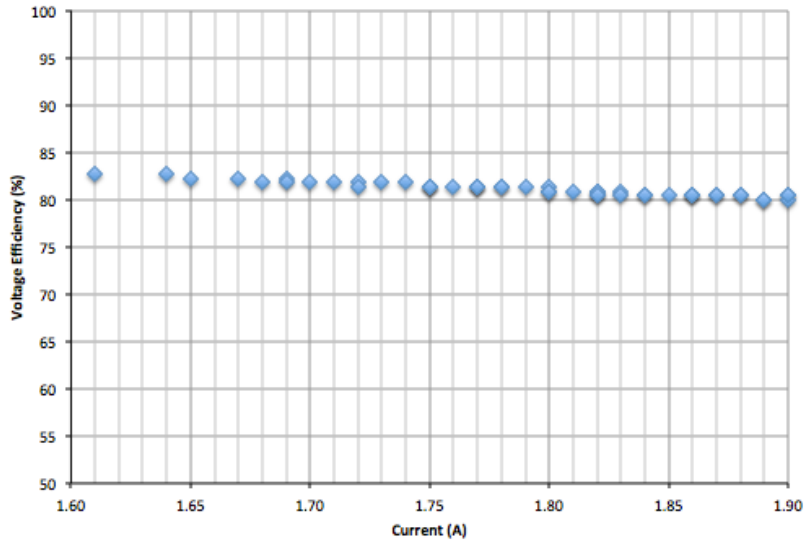


**Figure 6.12 – Decrease of voltage efficiency with the increase or current**

After storing the hydrogen, the next step was to use it to supply power to a load (a small motor that moves a fan) by means of the inverse process of electrolysis – the fuel cell. But there was a problem with this part of the measurement. The only available fuel cell was designed to work at much higher power ratings that those needed for our small-scale prototype. As was studied in [18], very small current densities lead to very low current efficiencies. A big part of the hydrogen supply passes through the membrane without reacting – low consumption rate. Thus the efficiencies managed in this low power regime were very small. Never the less, the study on its efficiency was made, but, for future work, a different fuel cell needs to be used.

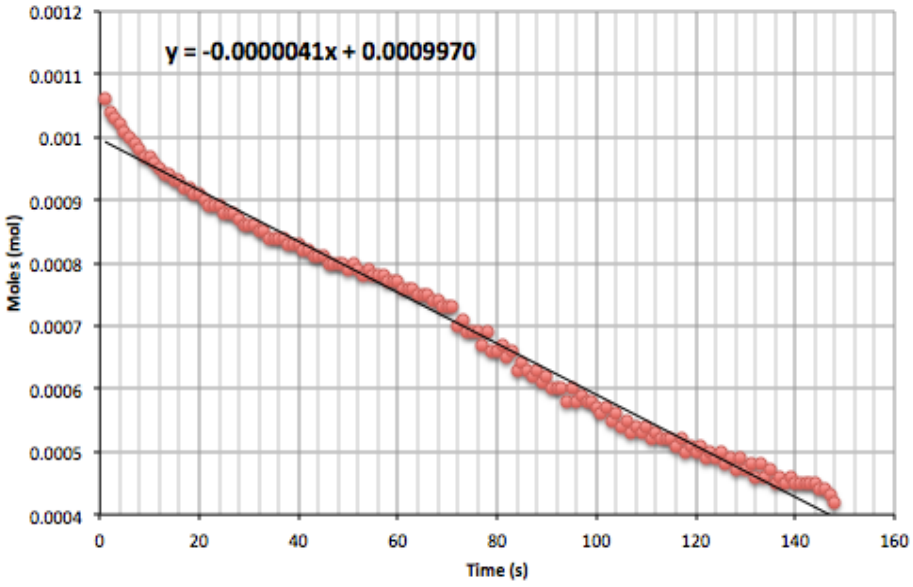


**Figure 6.13 – Real time measurement of the delivered volume of the Hydrogen, consumed by the fuel cell**

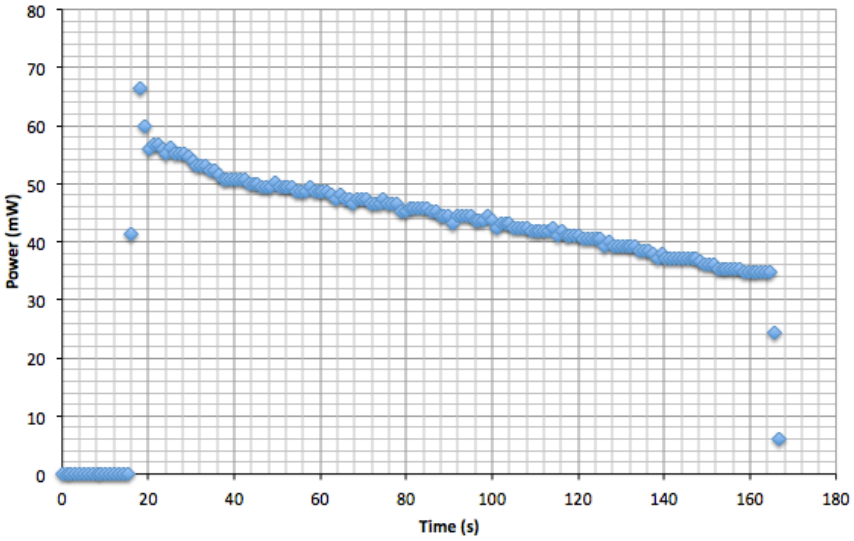


**Figure 6.14 – Power delivered by the fuel cell to the motor**

One can see that the process takes a little while to kick off, but at about 15-20 s it finally starts, showing an peak in the transient region. Thereafter the delivered voltage decreases with time until the supply runs out and there is a final transition to zero right about 165-170 s. During these 167 seconds of operation, the fuel cell consumed 0.00074 $mol$ of hydrogen. The efficiency can be calculated as follows

$$\eta_{FC} = \eta_{th} \times \eta_U \times \eta_I$$

$$\eta_{FC} = \frac{\Delta \bar{g}_f}{\Delta \bar{h}_f} \times \frac{U}{E_{rev}} \times \frac{I}{2F\nu_{total}} \qquad \left( \nu_{total} = \frac{\nu_{consumido}}{\mu_F} \right)$$

$$\eta_{FC} = \frac{-237.2\,kJ/mol}{-285.8\,kJ/mol} \times \frac{0.73V}{12 \times 1.23V} \times \frac{0.061A}{2 \times 96485\,s{\cdot}A/mol \times 0.000004\,mol/s}$$

$$\eta_{FC} = 0.32\%$$

The final value for electrical efficiency is very small. The causes for this strange value are relatively straightforward. The fuel cell was operated in an open circuit mode, so, the bulk of the hydrogen passed through the cell without ever reacting. This problem is reflected in a small consumption factor. Had the fuel cell been operated in a closed circuit, then a closed circuit, then the cell would only consume the hydrogen that it needed. Another problem arises from the fact that very few current is consumed by the load, so the cell is in Activation Mode, where the losses due to diffusion of hydrogen are significant.

# 7 CONCLUSIONS

Power Plant incorporated Hydrogen storage shows good prospects as a solution for intermittency of renewable sources in the near future. But in order to become a standard and matured procedure, it still requires a lot of research and development in problems like hydrogen storage and overall process efficiency.

This experiment is suitable for the e-Lab because it encompasses a great number of very interesting concepts like PV electricity generation and hydrogen production and electricity generation. It would thus be a helpful tool to better understand these concepts.

This prototype is intended to incorporate the remote laboratory e-Lab. An experience in the e-Lab platform is composed of three parts: the experimental setup, the microprocessor and the driver. The driver connects the platform (high level) to the hardware (low level). It receives instructions from the user and sends them to the microprocessor, and received data from the microprocessor, interprets it and shows them to the user in the graphical user interface. The present work is focused on the setup and microprocessor. The driver will need to be developed in future work in order to enable remote control.

As for the project per say, a lot was accomplished. Even so, some of the initial objectives where not met. The biggest achievements were the measurement of the electrolyzer efficiency (close to 65%) and the measurement of the fuel cell efficiency. Also the spectral response of the solar panel was studied but in a more qualitative fashion. Here I present a list of suggestions for possible future work directions:

- The LEDs should be balanced in actual radiating power with direct measurements, and not by delivered power because LEDs have different quantum efficiencies. For future work some sensors should be acquired in order to perform this calibration.
- The filter pair (current + voltage) responsible for measuring the power delivered to the electrolyzer was very well calibrated as shown in figure 6.8. They where extensively tested so their results are very much reliable. On the other hand, due to time constraints, the filter pair responsible for the measurement of the power delivered by the fuel cell to the load was not that well tested or calibrated. Further work will have to be done to refine these measurements.
- This works results deemed the fuel cell not apt to work at the power ratings used in this prototype. Future work should further test this hypothesis and, if it is confirmed, a better-fitted cell should be acquired.
- The PID algorithm implemented but not optimized. In order to achieve lower ripples in the set point, the algorithm constants have to be tuned, for example with Ziegler-Nichols Method.
- The electrolyzer that was used for these measurements where borrowed, so a new electrolyzer membrane will have to be acquired.

- This setup is capable of measuring only the volume of stored hydrogen. For educational purposes, it would be interesting to measure the volume of oxygen n order to acknowledge that it is half the volume of hydrogen. This should not be difficult to do seeing the software and schematics of the sensor have already been developed.
- In order to prevent water from running to the valves and consequently to the fuel cell, a simple circuit was supposed to trigger an interruption whenever water reached the maximum level and connected to conductors electrically. These conductors are place and the software interruption is implemented. The only thing missing is the simple circuit

# BIBLIOGRAPHY


[1] BP (2012) "*Statistical Review of World Energy*"

[2] <http://en.wikipedia.org/wiki/Heat_of_combustion> , 05/09/12

[3] <http://en.wikipedia.org/wiki/Image:Solar_Spectrum.png>, 05/09/12

[4] Castorena J., Schelle D. (2006) "*Buck-Converter Design Demystified*" in Power Electronics Technology

[5] Saad M. R. (2007) "*Buck Converter Design Issues*" at Linkoping Institute of Technology

[6] Rodrigues C. N. (2008) "*Centrais Solares Fotovoltaicas Ligadas à Rede Electrica*" at INETI

[7] REN (2011) "*Dados Tecnicos 2011 – Sistema Electrico Nacional*"

[8] <http://www.centrodeinformacao.ren.pt/PT/publicacoes/InformacaoMensal/Forms/VistaPadrao.aspx>, 10/09/12

[9] DGEG (2011) "*Renovaveis – Estatísticas Rápidas*"

[10] Ministério de Economia, da Investigação e do Desenvolvimento (2010) "*ENE2020"*

[11] IEC (2011) "*Electrical Energy Storage – White Paper*"

[12] Steward D. et al. (2009) "*Lifecycle Cost Analysis of Hydrogen Versus Other Technologies for Electrical Energy Storage*" National Renewable Energy Laboratory

[13] Moldrik P., Hradilek Z. (2010) "*Hydrogen Production for Solar Energy Storage*" at Technical University of Ostrava

[14] Ulleberg Ø. (2003) "*Modeling of advanced alkaline electrolyzers: a system simulation approach*." Hydrogen Energy; 28(1):21–33

[15] Zhang H. et al. (2012) "*Efficiency Calculation and Configuration Design of a PEM Electrolyzer System for Hydrogen Production*", Int. J. Electrochem. Sci., 7, 4143 – 4157

[16] Barbir F. (2005) "*PEM electrolysis for production of hydrogen from renewable energy sources*", Elsevier, Amsterdam, pp. 661–669.

[17] EG&G Services (2000) "Fuel Cell Handbook" 5th edition

[18] Teixeira J. (2009) "*Caracterização de pilha de combustível de hidrogénio"*, Master Thesis, IST

[19] Nunes G. (2010) "*Caracterização de pilha de combustível de hidrogénio e monitorização de célula individual*", Master Thesis, IST

[20] Miranda J. (2012) *"Caracterização de Célula e de Pilha de Combustível de Hidrogénio"*, Master Thesis, IST

[21] Shapiro D. et al. (2005) "*Solar-powered regenerative PEM electrolyzer/fuel cell system*", Solar Energy, 79, pp. 544-550

[22] Fujii H. et al. (2003) "*Recent developments on hydrogen storage systems*", Fuel Chemistry Division Preprints*, 48(1), 273*

[23] Kittel C. (2009) "*Introduction to Solid State Physics*", 7th ed., John Wiley and Sons

[24] *Kitajima T. (2008) "The Bulk Power Transmission System of Tokyo Electric Power Company – History and Future Prospects"* IEEJ Transactions on Fundamentals and Materials, Vol. 128, 3, pp. 153-157

[25] Badenhorst B. (2009) "*China unveils 1000kV AC transmission grid*" Energize, July, pp. 41-42

[26] <http://fablabedp.edp.pt/>, 21/09/12

[27] CNF (2007) "*CNF PICNODE board specs*"

[28] U.S. Department of Energy (2011) "*Fuel Cell Technologies Program*"

[29] Züttel , A. (2003) "*Materials for hydrogen storage*" Materials Today

[30] http://en.wikipedia.org/wiki/Fuel_cell

[31] Grove, William Robert (1842) "*On a Gaseous Voltaic Battery*", *Philosophical Magazine and Journal of Science* vol. XXI , pp. 417–420.

[32] <http://en.wikipedia.org/wiki/P–n_junction>, 20/10/12

[33] <http://www.mpoweruk.com/solar_power.htm>, 20/10/12

[34] <http://phys4030.blogspot.pt/2011/04/basic-concept-of-energy-bands.html>, 20/10/12

[35] H. Field (1997), "*Solar Cell Spectral Response Measurement Errors Related to Spectral Band Width and Chopped Light Waveform*" IEEE Photovoltaic Conf.

# Appendix A – The program for the Microcontroller

```
#include <stdio.h>
#include <p30f4013.h>
#include <libpic30.h>               //definicoes extra para as bibliotecas do C30
#include <math.h>


#define FCY ((long) 1843)           //instruction frequency in kHz
#define LED_R LATBbits.LATB8 //C9
#define LED_G LATBbits.LATB9 //C10
#define LED_B LATBbits.LATB10 //C11
#define VALVULAS LATBbits.LATB11 //C12
#define PERIODO2 587
#define PERIODO3 300
#define ENTER 13

#define VMAX 2.20
#define VMIN 0.00
#define AVCC 5.05

#define VOL_MOLAR 24.87 //26 graus

#define GANHO_I1 9.6969
#define GANHO_V1 1.69
#define GANHO_I2 14.5
#define GANHO_V2 1.0
#define GANHO_V3 2.5

#define R_SHUNT 0.1


//Configuration bits

//clock switching e fail safe monitor (detecta falhas do clock e toma medidas seguras) desactivados.
//XT_PLL16 e' a fonte do clock
_FOSC(CSW_FSCM_OFF & XT_PLL16);
_FWDT(WDT_OFF);  //watchdog timer off


//Definicao de variaveis globais
char RXbuffer[80];    //buffer used to store characters from serial port
int str_pos = 0;      //position in the RXbuffer
int flag=0;
int flag2=0;
int DC_R=0,DC_G=0,DC_B=0;
int timer1=0, buff1=0;              //contem a medida do periodo mais actual no IC1
int timer2=0, buff2=0;              //contem a medida do periodo mais actual no IC2
float Mol_Hid=0;
float V1,I1,V2,I2,V3;
typedef struct{
      double Vout; // Valor de V_out pretedido
      double Proportion; // Contante Proporcional
      double Integral; // Contante Integral Ki=[Kd*Periodo]/Ti
      double Derivative; // Contante Derivative Kd=[Kd*Td]/Periodo
      double LastError; // Erro na iterada anterior
      double PrevError; // Erro duas iteradas atras
       double SumError;
      double Control_Var;//Variavel de controlo
      } PID;


//------------------------------Declaracao de funcoes---------------------------------
```

```
void delay_ms(unsigned int delay); //delay in miliseconds
void teste();
void apaga_buff(char* RXbuffer, int* str_pos);
void recebe_int(int* val);
void adc_init();
void oc_init();
void ic_init();
void uart_init();
unsigned long equidist(int intensidade);
int PIDCalc( PID *pp, double Velocidade);//funcao que contem o algoritmo PID


//=====================================================================================================================
//*********************************************************************************************************************
//=====================================================================================================================

int main(){

     oc_init();
     adc_init();
     ic_init();
     uart_init();


     PID a;
     double i;
     float Vout,Kp,Ki,Kd;

     //recebe valores de intensidade dos leds
     printf("\rDiga a intensidade dos LEDs Vermelhos de 0 a 32..\n");
     recebe_int(&DC_R);
     printf("\rDiga a intensidade dos LEDs Verdes de 0 a 32..\n");
     recebe_int(&DC_G);
     printf("\rDiga a intensidade dos LEDs Azuis de 0 a 32..\n");
     recebe_int(&DC_B);

     //inicializa os elementos da estrutura PID
     while(RXbuffer[str_pos-1]!=ENTER ){sscanf(RXbuffer ,"%f %f %f %f", &Vout, &Kp, &Ki, &Kd);}
     a.Vout=Vout;
     a.Proportion=(double)Kp;
     a.Integral=(double)Ki;
     a.Derivative=(double)Kd;
     a.LastError=0;
     a.PrevError=0;
     a.Control_Var=0;

     //liga painel e comeca o armazenamento
     printf("\rPainel ligado");
     for (i=0;i<3;i++){printf(".");delay_ms(300);}
     printf("\n\rVai comecar o armazenamento de energia em forma de Hidrogenio");
     delay_ms(1000);
     printf("\n\rPara terminar a producao de hidrogenio carregue ENTER ou espere que atinja o volume maximo\n");
     while (RXbuffer[str_pos-1]!=ENTER ){
       OC1RS=PIDCalc(&a,V1);//algoritmo PID garante que a tensao a saida e contante
       printf("\r%.5f %.2f %.3f\n",Mol_Hid,V1,I1);//passa os valores pela porta serie para os calculos
     }

     //acaba o armazenamento e espera que seja dada ordem para iniciar o consumo do hidrogenio armazanado
     OC1RS=0;
     OC2RS=1499;
     printf("\n\rFim de Armazenamento",Mol_Hid);
     for (i=0;i<3;i++){printf(".");delay_ms(300);}
     printf("\n\rForam armazenados %.5f mol de Hidrogenio",Mol_Hid);
     delay_ms(2000);
     printf("\n\rPara abrir as valvulas carrege ENTER ");
     delay_ms(100);
     apaga_buff(RXbuffer,&str_pos);
     while (RXbuffer[str_pos-1]!=ENTER){
```

```
      printf("\rPara abrir as valvulas carrege ENTER ");
      for (i=0;i<7;i++){printf(".");delay_ms(100);}
      printf("\rPara abrir as valvulas carrege ENTER ");
      for (i=0;i<7;i++){printf(" ");}
    }
    apaga_buff(RXbuffer,&str_pos);
    delay_ms(100);

    //abra as valvulas e comeca o consumo
    VALVULAS=1; //Abre as valvulas
    printf("\n\rValvulas abertas...Para fechar valvulas carrege ENTER\n");
    while (RXbuffer[str_pos-1]!=ENTER){
      delay_ms(260);
      printf("\r%.5f %.2f %.3f\n",Mol_Hid,V2,I2);
      asm("btg LATB, #5");
    }
    OC2RS=0;
    VALVULAS=0; //Fecha as valvulas
    printf("\n\rValvulas fechadas...");


    return 0;
}

//=============================================================================================================================
//*****************************************************************************************************************************
//=============================================================================================================================




//=============================================================================================================================

void adc_init(){
    TRISBbits.TRISB12=1; //AN12(C1) pin de input
    TRISBbits.TRISB0=1;  //AN0 (C2)
    TRISBbits.TRISB1=1;  //AN1 (C3)
    TRISBbits.TRISB2=1;  //AN2 (C4)
    TRISBbits.TRISB3=1;  //AN3 (C5)
    TRISBbits.TRISB8=0;  //AN8 (C9) pin de output
    TRISBbits.TRISB9=0;  //AN9 (C10)
    TRISBbits.TRISB10=0; //AN10(C11)
    TRISBbits.TRISB11=0; //AN11(C12)

    TRISBbits.TRISB4 =0; //LED 1
    TRISBbits.TRISB5 =0; //LED 2

    ADCON1bits.ADSIDL = 1;   //1 = Discontinue module operation when device enters Idle mode
    ADCON1bits.FORM = 0b00;  //00 = Integer (DOUT = 0000 dddd dddd dddd)
    ADCON1bits.SSRC = 0b000; //000 = Clearing SAMP bit ends sampling and starts conversion
    ADCON1bits.ASAM = 1;     //1 = Sampling begins after last conversion completes. SAMP bit is auto set.
    ADCON1bits.SAMP = 0;     //0 = A/D sample/hold amplifiers are holding

    ADCON2bits.VCFG = 0b100;    //1xx AVDD-AVSS
    ADCON2bits.CSCNA = 1;       //1 = Scan inputs
    ADCON2bits.BUFS = 0;        //Buffer Status
    ADCON2bits.SMPI = 0b0100;   //0100 = Interrupts at the end of conversion each 5th sample/convert sequence
    ADCON2bits.BUFM = 0;        //0 = Buffer configured as one 16-word buffer ADCBUF(15...0)
    ADCON2bits.ALTS = 0;        //0 = Always use MUX A input multiplexer settings
    ADCON3bits.SAMC = 0b00001;  //00001 = 1 TAD
    ADCON3bits.ADRC = 0;        //0 = Clock derived from system clock
    ADCON3bits.ADCS = 0b100111; //100111 = TCY/2 (ADCS<5:0> + 1) = 39/2 TCY

    ADCHS =  0b0000000000000000; // quando CSCNA = 1 CH0SB e CHOSA sao ignorados
    ADPCFG = 0b0000111100000000;// Tudo analogico menos AN8-AN11 que sao digitais
    ADCSSL = 0b0001000000001111; //AN0-AN4 entram no scan

    ADCON1bits.ADON = 1;    //enable ad converter
```

```
     IFS0bits.ADIF = 0;      //clear adc interrupt flag
     IEC0bits.ADIE = 1;      //enable adc end of sampling/conversion interrupts

     T1CON= 0b1000000000000000;
    PR1 = 29410;//2353;                    //timer1 period
     IFS0bits.T1IF = 0;
    IEC0bits.T1IE = 1;              //enable interrupts from timer1
}

//=============================================================================================================

void oc_init(){

     TRISDbits.TRISD0=0; //pin de output do PWM
     TRISDbits.TRISD1=0;
     TRISDbits.TRISD2=0;
     TRISDbits.TRISD3=0;

     PR2=1500;
     T2CON= 0b1000000000000000; //Liga o timer -> TON=T2CON<15>=1  ||  pre scaler 1:1 -> T2CON<5:4>=00

     OC1RS =0; //dutycycle
     OC1CON=0b0000000000000110; //modo PWM (bits<2:0>=110) || timer 3 (bit3=0b0)
     OC2RS =0; //dutycycle
     OC2CON=0b0000000000000110; //modo PWM (bits<2:0>=110)

     PR4=100;
     T4CON= 0b1000000000000000;
     IFS1bits.T4IF = 0;
    IEC1bits.T4IE = 1;              //enable interrupts from timer1
}

//=============================================================================================================

void ic_init(){
     TRISDbits.TRISD8 = 1; //pin IC1 (C28) de input
     TRISAbits.TRISA11 = 1;//pin INT0(C29) de input
     TRISDbits.TRISD9 = 1; //pin IC2 (C30) de input

     //configura timer3
     T3CON = 0b1000000000010000 ; //TON=T3CON<15>=1 || Prescaler 1:8

     //configura os input captures
     IC1CON =0b0000000000000101; // captura todos os 16 rising edges (IC1CON<2:0>=101) | Timer3 (IC1CON<7>=0)
     IC2CON =0b0000000000000101;
     //activa as interrupcoes
     IEC0bits.IC1IE = 1;
     IEC0bits.IC2IE = 1;
     IEC0bits.INT0IE = 1;
}

//=============================================================================================================

void uart_init(){
     U2MODEbits.UARTEN=1;
     U2MODEbits.USIDL=0;
     U2MODEbits.LPBACK=0;
     U2MODEbits.ABAUD=0;
     U2MODEbits.PDSEL=0;

     U2STAbits.UTXISEL=0;
     U2STAbits.UTXBRK=0;
     U2STAbits.UTXEN=1;
     U2STAbits.URXISEL=1;

     _U2RXIE = 1;
     U2BRG=95;
     __C30_UART = 2;
}
```

```
//=============================================================================================================

void __attribute__((interrupt,no_auto_psv)) _INT0Interrupt (void) {
     IFS0bits.INT0IF = 0; //limpa a flag de interrupcao
     printf("\rINT0 INTERRUPT\n");
}

//=============================================================================================================

void __attribute__((interrupt,no_auto_psv)) _IC1Interrupt (void) {

     IFS0bits.IC1IF = 0; //limpa a flag de interrupcao
}

//=============================================================================================================

void __attribute__((interrupt,no_auto_psv)) _IC2Interrupt (void) {

     if(buff2<IC2BUF)timer2=IC2BUF-buff2;
     else if (buff2>IC2BUF)timer2=(65535-buff2)+IC2BUF;
     buff2=IC2BUF;

     float freq;
     freq=(7372800.0/8.0)*4.0*16.0/timer2;
     if(freq>24929.35) Mol_Hid = ((freq*0.00130-16.11624)*(0.6*0.6*3.141592)/(1000.0*VOL_MOLAR));
     else Mol_Hid = ((freq*0.00347-70.21293)*(0.6*0.6*3.141592)/(1000.0*VOL_MOLAR));
     if(Mol_Hid<0.0)Mol_Hid=0.0;

     IFS0bits.IC2IF = 0; //limpa a flag de interrupcao
}

//=============================================================================================================

void  __attribute__((__interrupt__, no_auto_psv)) _T1Interrupt (void) {
    IFS0bits.T1IF = 0;
    ADCON1bits.SAMP = 0;    //stops sampling and starts conversion
}

//=============================================================================================================

void  __attribute__((__interrupt__, no_auto_psv)) _T4Interrupt (void) {
     static int i;

     if(i<DC_R) LED_R=1;
     else LED_R=0;
     if(i<DC_G) LED_G=1;
     else LED_G=0;
     if(i<DC_B) LED_B=1;
     else LED_B=0;
     i++;
     if(i==100)i=0;

    IFS1bits.T4IF = 0;
}

//=============================================================================================================

void __attribute__((interrupt,no_auto_psv)) _ADCInterrupt (void) {
     IFS0bits.ADIF = 0; //limpa a flag de interrupcao
     flag=1;
     static int i,j;
     i++;
     if(i==200){ flag2=1; i=0; }


     static double V1sum,I1sum,V2sum,I2sum,V3sum;
     float V1out,I1out,V2out,I2out,V3out;
```

```
      I1sum = I1sum + (double)ADCBUF0*AVCC/4096.0;
      V1sum = V1sum + (double)ADCBUF1*AVCC/4096.0;
      I2sum = I2sum + (double)ADCBUF2*AVCC/4096.0;
      V2sum = V2sum + (double)ADCBUF3*AVCC/4096.0;
      V3sum = V3sum + (double)ADCBUFC*AVCC/4096.0;

      //medias de 100 em 100 valores para menos oscilacoes
      if (j==100){
        I1out=(float)I1sum/100.0;
        I1 = (I1out/GANHO_I1)/R_SHUNT;

        V1out=(float)V1sum/100.0;
        V1 = V1out/GANHO_V1;

        I2out=(float)I2sum/100.0;
        I2 = (I2out/GANHO_I2)/R_SHUNT;

        V2out=(float)V2sum/100.0;
        V2 = V2out/GANHO_V2;

        V3out=(float)V3sum/100.0;
        V3 = V3out/GANHO_V3;

        j=0;I1sum=0;V1sum=0;I2sum=0;V2sum=0;V3sum=0;
      }
      j++;


}

//=============================================================================================================================

void __attribute__((interrupt,auto_psv)) _U2RXInterrupt(void){
      IFS1bits.U2RXIF = 0;

      // Read the receive buffer until at least one or more character can be read
     while(U2STAbits.URXDA){
        RXbuffer[str_pos] = U2RXREG;
        str_pos++;
        if(str_pos >= 80){str_pos = 0;}
     }
}

//=============================================================================================================================

int PIDCalc( PID *pp, double V0 ) {
      double dError,Error;
      int duty;

      if (pp->Vout>2.0)pp->Vout=2.0;

      //Algoritmo
      Error = pp->Vout - V0;
      pp->SumError+= Error;
      dError = Error - 2*(pp->LastError) + pp->PrevError;
      pp->Control_Var=pp->Control_Var+(pp->Proportion*Error)+(pp->Integral*pp->SumError)+(pp->Derivative*dError);
      pp->PrevError = pp->LastError;
      pp->LastError = Error;

      if(pp->Control_Var>VMAX)pp->Control_Var=VMAX;//previne windup
      if(pp->Control_Var<VMIN)pp->Control_Var=VMIN;//previne que a var de controlo seja inferior ao valor min


      //equacao da recta que transforma a variavel de controlo num valor de Dutycyle
      duty = (pp->Control_Var-1.34)/0.0011;
      if (duty<0)duty=0;


      return duty;//retorna o valor de duty cicle a ser actualizado
```

```
}

//=============================================================================================================

void delay_ms(unsigned int delay){ //delay in miliseconds
     unsigned int cycles;    // numero de ciclos
     for(;delay;delay--)
       for(cycles=FCY*4;cycles;cycles--); //ciclo que demora 1 ms
}

//=============================================================================================================

void recebe_int(int* val){
     apaga_buff(RXbuffer,&str_pos);
     while(1){
       sscanf(RXbuffer,"%d",val);
       if(RXbuffer[str_pos-1]==13){
               delay_ms(500);
               apaga_buff(RXbuffer,&str_pos);
               break;
       }
     }
}

//=============================================================================================================

void apaga_buff(char* RXbuffer, int* str_pos ) {
     int i=0;
     (*str_pos) = 0;  //coloca o apontador da posicao a zero
     for(i=0;i<80;i++){RXbuffer[i] = '\0';}//apaga o conteudo do buffer }//end while(1)
}

//=============================================================================================================
```

# Appendix B – PCB layouts

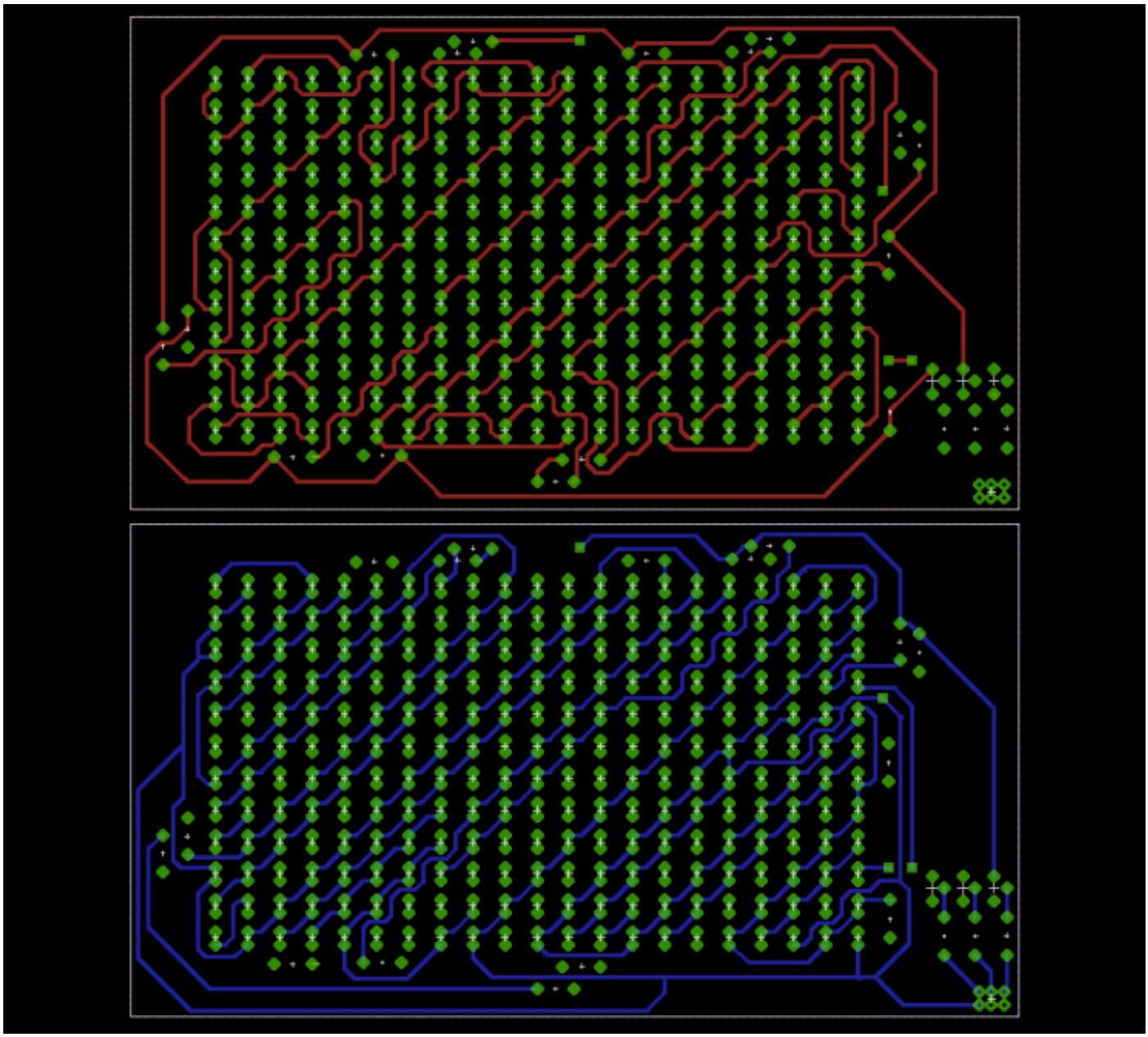

**Figure B.1 – The schematic layout of the three colored 252 High Brightness LED panel created with *EAGLE 5.11.0***

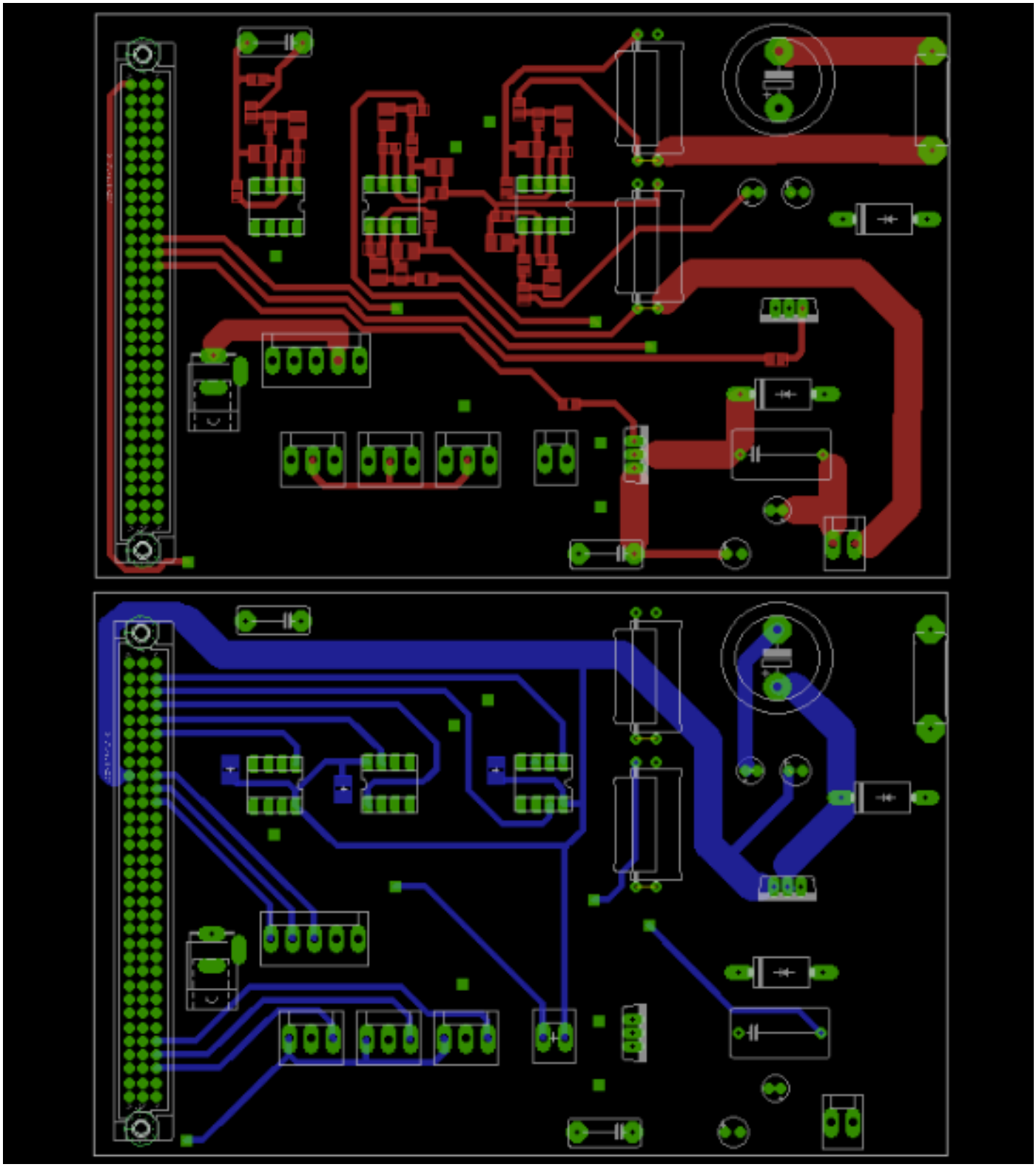

**Figure B.2 – The schematic layout of the Prototype Controller Board created with *EAGLE 5.11.0***

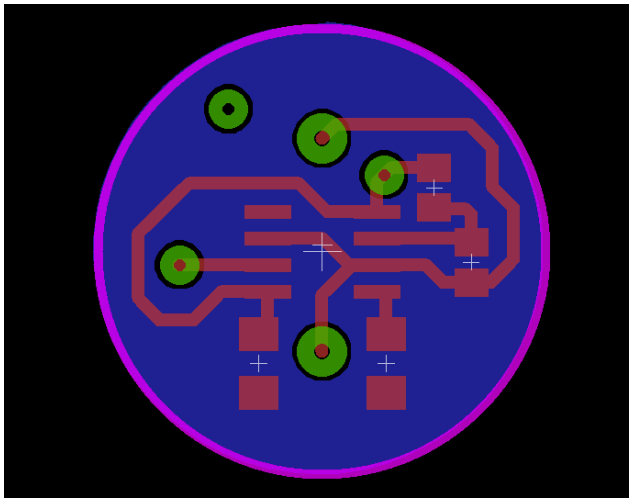

**Figure B.3 – The schematic layout of the Height Sensor created with *EAGLE 5.11.0***